

INFORMATION TO USERS

This dissertation was produced from a microfilm copy of the original document. While the most advanced technological means to photograph and reproduce this document have been used, the quality is heavily dependent upon the quality of the original submitted.

The following explanation of techniques is provided to help you understand markings or patterns which may appear on this reproduction.

1. The sign or "target" for pages apparently lacking from the document photographed is "Missing Page(s)". If it was possible to obtain the missing page(s) or section, they are spliced into the film along with adjacent pages. This may have necessitated cutting thru an image and duplicating adjacent pages to insure you complete continuity.
2. When an image on the film is obliterated with a large round black mark, it is an indication that the photographer suspected that the copy may have moved during exposure and thus cause a blurred image. You will find a good image of the page in the adjacent frame.
3. When a map, drawing or chart, etc., was part of the material being photographed the photographer followed a definite method in "sectioning" the material. It is customary to begin photoing at the upper left hand corner of a large sheet and to continue photoing from left to right in equal sections with a small overlap. If necessary, sectioning is continued again – beginning below the first row and continuing on until complete.
4. The majority of users indicate that the textual content is of greatest value, however, a somewhat higher quality reproduction could be made from "photographs" if essential to the understanding of the dissertation. Silver prints of "photographs" may be ordered at additional charge by writing the Order Department, giving the catalog number, title, author and specific pages you wish reproduced.

University Microfilms

300 North Zeeb Road
Ann Arbor, Michigan 48106
A Xerox Education Company

73-2090

NYCHAS, Stavros George, 1939--
A VISUAL STUDY OF TURBULENT SHEAR FLOW.

The Ohio State University, Ph.D., 1972
Engineering, chemical

University Microfilms, A XEROX Company, Ann Arbor, Michigan

A VISUAL STUDY OF TURBULENT SHEAR FLOW

DISSERTATION

Presented in Partial Fulfillment of the Requirements for
the Degree Doctor of Philosophy in the Graduate
School of The Ohio State University


By

Stavros George Nychas, Dipl. Eng., M.Sc.

* * * * *

The Ohio State University
1972

Approved by


Adviser
Department of Chemical
Engineering

PLEASE NOTE:

Some pages may have
indistinct print.

Filmed as received.

University Microfilms, A Xerox Education Company

ACKNOWLEDGMENTS

It is my pleasure to acknowledge my teachers and friends who contributed to this work. I wish to express my special thanks and appreciation to my adviser, Dr. Robert S. Brodkey, who suggested the subject of this dissertation, enthusiastically followed its progress, and was never tired to work with his student in the lab until the early hours in the morning. My special thanks are also extended to Dr. Harry C. Hershey for his continuous advice during the course of this investigation.

Acknowledgment is due to Dr. Joseph H. Koffolt, Dr. Aldrich Syverson, Chairman of the Department of Chemical Engineering and to the National Science Foundation for financial support. I wish also to express my special thanks to Miss Vasiliki Filippakopoulou for her invaluable assistance during the last stage of the experimental work. The technical assistance of Mike Kukla and Keldon Latham is acknowledged. Lastly thanks are extended to my friends Christine Dufala, Eric Grulke, Joe Taraba and Dan Wolf for helping in final preparation and to Mrs. Eleanor Sapp for typing this thesis.

VITA

- August 30, 1939 Born, Kalivia, Attica, Greece
- 1962 Dipl. Eng., National Technical
University, Athens, Greece
- 1962-1965 . . . Greek Air Force and Nuclear Research
Center "Democritos," Aghia Paraskevi,
Attica, Greece
- 1968 M.Sc., Virginia Polytechnic Institute,
Blacksburg, Virginia
- 1968-1970 . . . Roberts Memorial Fellow, The Ohio
State University, Columbus, Ohio
- 1970-1971 . . . National Science Foundation Graduate
Research Associate, The Ohio State
University, Columbus, Ohio

FIELDS OF STUDY

Major Field: Chemical Engineering

Studies in Momentum Transfer. Professor Robert S. Brodkey

Studies in Mass Transfer. Professor Christie J.
Geankoplis

Studies in Heat Transfer. Professor Thomas L. Sweeney

Studies in Thermodynamics. Professor Webster B. Kay

Studies in Chemical Kinetics. Professor Aldrich Syverson

CONTENTS

| | Page |
|---|------|
| ACKNOWLEDGMENTS | ii |
| VITA | iii |
| FIGURES | vi |
| TABLES | xi |
| SUMMARY | 1 |
| INTRODUCTION AND LITERATURE REVIEW | 4 |
| EQUIPMENT AND EXPERIMENTAL PROCEDURE | 16 |
| Purpose | 16 |
| Plan | 16 |
| Apparatus | 17 |
| Flow System | 21 |
| Flow Channel and Piping | 21 |
| Tripping of Boundary Layer | 30 |
| Fluid | 30 |
| Particles | 30 |
| Photo-optical System | 35 |
| Camera | 35 |
| Film | 36 |
| Lighting | 36 |
| Camera Lens | 37 |
| EXPERIMENTAL RESULTS | 41 |
| Velocity Measurements | 41 |
| General Description of the Flow Field | 43 |
| Detailed Description of Events | 54 |
| Deceleration (Low Speed Fluid) | 56 |
| High Speed Fluid (Acceleration) | 63 |
| Sweep Event | 78 |
| Ejection Event | 78 |
| Transverse Vortices | 83 |
| Large Scale Inflow | 105 |
| Large Scale Outflow | 117 |
| Connected Fluid Motions | 122 |

| | Page |
|---|------|
| Summary of Observations | 123 |
| DEDUCTIONS AND HYPOTHESIS FROM THE EXPERIMENTAL DATA | 129 |
| Wall Region ($0 < y^+ \leq 70$) | 130 |
| Outer Region ($y^+ > 70$) | 135 |
| DISCUSSION AND COMPARISON WITH OTHER WORK | 147 |
| Visual Studies | 147 |
| Other Studies | 161 |
| Summary | 167 |
| CONCLUSIONS | 169 |
| RECOMMENDATIONS | 172 |
| APPENDICES | 174 |
| BIBLIOGRAPHY | |

FIGURES

| Figure | Page |
|---|------|
| 1. Flow System with Flat Plate | 18 |
| 2. Photo Optical System | 20 |
| 3. Photograph of Experimental Equipment | 22 |
| 4. Photograph of Channel and Flat Plate | 23 |
| 5. Details of Flow Channel and Support | 24 |
| 6. Entrance Section | 26 |
| 7. (a) Leading Edge of Flat Plate; | 29 |
| (b) Positioning and Support of Flat Plate in the Channel | 29 |
| 8. Boundary Layer Tripping Device | 31 |
| 9. Camera Viewpoint and Field of View | 38 |
| 10. (a) Decelerated Region and Entering High Speed Fluid (Convected View) | 46 |
| (b) Decelerated Region, Progressing High Speed Fluid and Ejection (Convected View) . | 46 |
| 11. Forward Transverse Vortex and Its Relation to Low and High Speed Fluids (Convected View) . . | 49 |
| 12. Downstream Motion of a Forward Transverse Vortex (Convected View) | 50 |
| 13. (a) High Speed Fluid Entering at a Large Angle to the Wall (Convected View) | 52 |
| (b) Formation of a Reverse Transverse Vortex (Convected View) | 52 |
| 14. (a) Particle Paths During a Large Scale Inflow (Convected View) | 55 |
| (b) Particle Paths During a Large Scale Outflow (Convected View) | 55 |

| Figure | Page |
|---|------|
| 15. Velocity Profile of a Low Speed Fluid Region . . . | 58 |
| 16. Velocity Profile of a Low Speed Fluid Region . . | 59 |
| 17. Selected Particle Paths During a Deceleration Event (Convected View) | 60 |
| 18. Selected Particle Paths During a Deceleration Event (Convected View) | 61 |
| 19. Convected View of a Developing Acceleration Event | 65 |
| 20. Convected View of a Developing Acceleration Event | 66 |
| 21. Velocity Profile of a High Speed Fluid Moving Faster than the Mean \bar{U}_x | 72 |
| 22. Velocity Profile of a High Speed Fluid Moving Slower than the Mean | 73 |
| 23. Illustration of Sweep Event (Convected View) . . | 79 |
| 24. Illustration of a Complete Fluid Element Loop (Convected View) | 81 |
| 25. High Speed Fluid and Associate Forward Transverse Vortex (Convected View) | 85 |
| 26. Convected (Stationary Vortex) View of a Forward Transverse Vortex | 88 |
| 27. Individual Particle Paths During a Forward Transverse Vortex (Convected View) | 89 |
| 28. Convected (Stationary Vortex) View of a Forward Transverse Vortex | 91 |
| 29. Individual Particle Paths During a Forward Transverse Vortex (Convected View) | 93 |
| 30. Convected (Stationary Vortex) View of a Forward Transverse Vortex | 94 |

| Figure | Page |
|--|------|
| 31. Time Exposure Photograph Corresponding to the Transverse Vortex of Figure 30 | 97 |
| 32. Individual Particle Paths During a Forward Transverse Vortex (Convected View) | 98 |
| 33. Convected (Stationary Vortex) View of a Forward Transverse Vortex | 99 |
| 34. Forward Transverse Vortex Following the Vortex in Figure 26 (Convected View) | 101 |
| 35. Convected (Stationary Vortex) View of the Vortex Corresponding to Figure 34 | 102 |
| 36. Individual Particle Paths of a Reverse Transverse Vortex (Convected View) | 103 |
| 37. Convected (Stationary Vortex) View of a Reverse Transverse Vortex | 104 |
| 38. Particle Paths During a Large Scale Inflow (Convected View) | 112 |
| 39. Particle Paths During a Large Scale Inflow (Convected View) | 114 |
| 40. Particle Paths During a Large Scale Inflow (Convected View) | 115 |
| 41. Particle Paths During a Large Scale Outflow (Convected View) | 119 |
| 42. Particle Paths During a Large Scale Outflow (Convected View) | 120 |
| 43. Connected and Non-Connected Fluid Motions During Acceleration and Deceleration Events (Convected View) | 124 |
| 44. Connected and Non-Connected Fluid Motions During Inflow (a) and Outflow (b) Events (Convected View) | 125 |

| Figure | Page |
|--|------|
| 45. Interfaces of High and Low Speed Fluids Exhibiting High Velocity Gradients (Convected View) | 132 |
| 46. Pressure Field During a Forward Transverse Vortex | 142 |
| 47. Turbulent Energy Production, Dissipation and Exchange | 144 |
| 48. (a) A Streamwise Vortex Motion | 155 |
| (b) Formation of a Transverse Vortex | 155 |
| 49. Decelerated Fluid Region and Wall Ejection Considered as Lifted up "Low-Speed Streak" (Convected View) | 159 |
| 50. Analysis Grid | 174 |
| 51. Ejections and Acceleration (Convected View) . . . | 178 |
| 52. Acceleration (Convected View) | 179 |
| 53. Acceleration (Convected View) | 180 |
| 54. Ejections and Acceleration (Convected View) . . . | 181 |
| 55. Acceleration (Convected View) | 182 |
| 56. Acceleration (Convected View) | 183 |
| 57. Ejections and Acceleration (Convected View) . . . | 184 |
| 58. Ejections and Forward Transverse Vortex (Convected View) | 185 |
| 59. Acceleration and Forward Transverse Vortex (Convected View) | 186 |
| 60. Convected (Stationary Vortex) View of a Forward Transverse Vortex | 187 |
| 61. Individual Particle Paths During a Reverse Transverse Vortex (Convected View) | 188 |

| Figure | Page |
|---|------|
| 62. Convected (Stationary Vortex View) Corresponding to Figure 60 | 189 |
| 63. Acceleration and Reverse Transverse Vortex Convected View) | 190 |

TABLES

| Table | Page |
|---|------|
| 1. Study of High Speed Fluid Regions (Run M-132) . . . | 68 |
| 2. Study of High Speed Fluid Regions (Run M-132) . . . | 69 |
| 3. Study of High Speed Fluid Regions (Run M-104) . . . | 74 |
| 4. Study of High Speed Fluid Regions (Run M-132) . . . | 75 |
| 5. Study of High Speed Fluid Regions (Run M-134) . . . | 76 |
| 6. Wall Area Ejections | 82 |
| 7. Study of a Forward Transverse Vortex (Run M-132) | 106 |
| 8. Study of a Forward Transverse Vortex (Run M-133) | 107 |
| 9. Study of a Forward Transverse Vortex (Run M-134) | 108 |
| 10. Study of a Forward Transverse Vortex (Run M-132) | 109 |
| 11. Study of a Reverse Transverse Vortex (Run M-132) | 110 |
| 12. Study of a Large Scale Inflow (Run M-134) | 113 |
| 13. Study of Large Scale Inflows (Run M-132) | 116 |
| 14. Study of Large Scale Outflows | 121 |

NOMENCLATURE

| | |
|---------------|--|
| N_{Re} | Reynolds number based on average velocity-pipe flow |
| N_{Re} | Reynolds number based on x-distance-flat plate flow |
| p | pressure |
| \bar{U}_x | local mean average velocity, x-direction component |
| U_x | instantaneous velocity, x-component, $U_x = \bar{U}_x + u$ |
| U_c | camera carriage velocity |
| U_g | apparent ejection velocity |
| U_t | actual ejection velocity |
| U^* | $(\tau_w/\rho)^{1/2}$ |
| V | instantaneous velocity, y-direction component |
| d_p | particle diameter |
| e | apparent length of particle travel |
| g | constant of gravity |
| i, j | subscript index for component |
| t | time |
| u or $u(t)$ | instantaneous turbulent velocity fluctuation, x-direction |
| $v, v(t)$ | instantaneous turbulent velocity fluctuation, y-direction |
| x | streamwise coordinate in rectangular coordinate system |

| | |
|--------------------|---|
| x^+ | xU^*/ν |
| y | coordinate normal to flat plate in rectangular coordinate system |
| y^+ | yU^*/ν |
| \bar{y}^* | arithmetic average between two y^+ values |
| z | coordinate in the spanwise direction of flat plate in rectangular coordinate system |
| z^+ | zU^*/ν |
| α | apparent ejection angle measured from flat plate wall |
| δ | boundary layer thickness |
| λ | parameter for streak spacing |
| λ^* | correlation coefficient for streak spacing |
| μ | molecular viscosity coefficient |
| ν | kinematic viscosity |
| ρ_p | particle density |
| ρ_f or ρ | fluid density |
| τ | shear stress (τ_w for wall) |
| ϕ_e | actual ejection or outward angle measured from wall |
| ϕ_s | actual sweep or wallward angle measured from wall |

SUMMARY

A visual study was conducted of the outer region of a turbulent boundary layer along a flat plate; in addition, limited observations of the wall area was also made. The technique involved suspending very small solid particles in water and photographing their motions with a high speed camera moving with the flow (convected view). The method was basically the same as used by Corino and Brodkey to study the wall area of turbulent pipe flow. The emphasis of the study was on visual observations of individual motions occurring in the flow; some velocity measurements and estimations of Reynolds stresses were also made.

The single most important event observed in the outer region was a fluid motion which in the convected view of the travelling camera appeared as a transverse vortex. This was a large scale motion transported downstream almost parallel to the wall with an average velocity slightly smaller than the local mean \bar{U}_x . It was the result of an instability interaction between accelerated and decelerated fluid and it is believed to be closely associated with the wall region ejections.

To put the entire flow picture into proper perspective, the following idealized description is presented. A

deterministic sequence of events in the outer region was observed although they did occur randomly in space and time. The first of these events was a decelerated flow exhibiting velocities considerably smaller than the local mean. It was immediately followed by an accelerated flow. Both these events extended from near the wall to the far outer region. Their interaction resulted in the formation of one or more transverse vortices. Although decelerated fluid participated in the formation of the transverse vortex, it was the accelerated fluid that was responsible for its participation. While the transverse vortex was transported downstream, small scale fluid elements, originating in the wall area of the decelerated flow, were ejected outwards (ejection event). After travelling some outward distance, the ejected elements interacted with the oncoming accelerated fluid in the wall region and were subsequently swept downstream (sweep event). The sequence of events closed with two large scale motions. There were inflows (motions toward the wall) and outflows (motions away from the wall); they both extended from the far outer region up to an area adjacent to the wall region. Not all the events appear every time nor in exactly the same order; but for most of the cases they occurred as described. Estimated positive and negative contributions to the instantaneous Reynolds stress during the events were many times higher than the local mean averages.

the cases they occurred as described. Estimated positive and negative contributions to the instantaneous Reynolds stress during the events were many times higher than the local mean averages.

The visual observations and velocity measurements presented new insight to the puzzling questions concerning the connection and interaction of the wall and the outer regions in a turbulent boundary layer. They also provided a basic physical picture of the processes for further model studies.

INTRODUCTION AND LITERATURE REVIEW

Prandtl's (26) boundary layer hypothesis marked the beginning of a new era in fluid mechanics of non-ideal fluids; it was introduced as an approximation to the Navier-Stokes equations for the case of high Reynolds number laminar flow. According to this hypothesis, the viscous effects are confined to a region next to a solid wall, the boundary layer. Outside the boundary layer, the flow can be considered as potential. A great deal of effort has been devoted to the study of the flow phenomena inside the boundary layer, since its existence is enough to determine the development of a given flow configuration.

The boundary layer hypothesis is valid for both laminar and turbulent flows. The laminar boundary layer flow case is by no means simple and has the inherent mathematical difficulties associated with the non-linearity of the now-simplified Navier-Stokes equations. The turbulent flow case has all the mathematical complexity of the laminar case and, in addition, much of the geometrical simplifications cannot be made because of its inherent three-dimensional nature. Even in the simplest geometrical flow configuration, the solution of the time-dependent boundary layer equations for the instantaneous velocity

profile would be a very difficult task. By time-averaging of the equations a penalty is paid; namely, the introduction of additional terms called the Reynolds stresses (fluctuating velocity terms). One thus ends up having more unknowns than equations, in spite of the fact that the original system of equations was determinate. This is one aspect of the closure problem of turbulence. The so-called phenomenological theories are based on simple physically mechanistic models that relate the Reynolds stresses with the time-averaged velocity gradient in order to make the system of equations again determinate. The results all have one thing in common; no matter what the mechanistic assumption was, they all predict reasonably well the average turbulent velocity profile (29). It was soon realized that the chances of obtaining any understanding of the fundamental processes involved in the turbulent momentum mechanism by such methods were very small. However, the importance of phenomenological theories should not be underrated, because for many traditional engineering calculations, they are the only methods available.

Through this early work the importance of the Reynolds stresses and the role they play in turbulent shear flows were recognized. The need to obtain more physically sound relations between the Reynolds stresses and the mean flow, as well as the design of more meaningful experiments

for the measurements of fluctuating velocity terms, resulted in the formulation of the statistical theory of turbulent flow. It was Taylor (32) who first recognized that the velocity in a turbulent flow field could be pictured as a random continuous function of position and time. He then introduced the idea of the correlation of velocity fluctuations at two points as being an important quantity for the description of turbulence. There are several excellent reviews and treatments of the theory (2,5,15,35). The statistical theory of turbulence has contributed a great deal to our fundamental understanding of turbulence, and in several areas it has found direct applications (e.g., mixing). The theory, however, also suffers a closure problem but of a different form. The calculation of correlations of a given order requires the knowledge of the next higher order correlation. Several closure methods have been attempted and they are summarized elsewhere (5).

To proceed from this background of phenomenological and statistical turbulence, one must obtain a better understanding of the mechanisms that are actually operating in the flow and upon which improved phenomenological models can be built. Visual studies to be discussed and the subject of this work can provide the needed insight.

The importance of the wall region, regarding not only momentum transport but other transport phenomena as well,

has long been recognized. A realistic understanding of the processes inside this region would shed light on the nature of momentum transport and would permit the prediction of heat and mass transfer rates from measurements of only the turbulent field, i.e., correlations and cross-correlations, spectra and descriptive parameters from these (microscales and macroscales). The literature for quantitative measurements very close to the wall has been reviewed by Corino and Brodkey (8). Their direct visualization of the phenomena occurring in the wall region was a decisive contribution towards the understanding of the mechanism of the flow in this region. Such research efforts during the last fifteen years have given a fresh look at the whole subject. In what was considered to be a random phenomenon, a more or less coherent structure was uncovered. Moreover, a sequence of events in the wall area was observed. The events occur randomly in space and time but their sequence was found to be deterministic. A brief summary of these visual experimental findings will be given in this section. A detailed review of them can be found in Corino (7), Corino and Brodkey (8), and Kim et al. (18).

A combined dye injection and hydrogen bubble technique permitting quantitative measurements was developed by Kline and his coworkers (20,27,30). They applied this method to an artificially-tripped turbulent boundary layer.

In the region $0 \leq y^+ \leq 10$ they observed a regularly distributed spanwise structure composed of low-speed streaks lifting up from the wall and moving downstream. This low-speed streak is part of what Kline et al. (20) called "bursting," a sequence of events related to the production of turbulence. Kim et al. (18) described bursting as being composed of the "following three stages: (1) Slow lifting of a low-speed streak accumulates until a shift occurs involving more rapid outward motion of the low-speed streak; at this time, an inflexional instantaneous velocity profile is observed. (2) Downstream from the inflexional zone rapid growth of an oscillatory motion is observed; it continues for a few cycles. (3) The oscillation is terminated by the onset of a more chaotic fluctuation called 'breakup.' This completes the cycle, and the velocity profile returns to a form generally like the mean profile shape." They suggested that essentially all of the turbulence production in the area $0 < y^+ < 100$ occurs during bursting and that it is associated with a local dynamic intermittent instability.

Corino (7) studied the wall area of a fully-developed turbulent pipe flow. His technique was a visual method involving suspension of colloidal-size solid particles in a liquid as tracers. He photographed their motions with a high-speed motion picture camera moving with the flow. He

observed that the wall area showed a distinct pattern characterized by a deterministic sequence of events occurring randomly in space and time. This pattern was a function of the distance from the wall. The area of $0 \leq y^+ \leq 5$ sublayer region was found not to be laminar; it was characterized by velocity fluctuations of small magnitude and disturbed by fluid elements coming from the adjacent region. The area $0 \leq y^+ \leq 30$ was characterized by ejections of fluid elements away from the wall. These ejections were found to occur intermittently and randomly in both space and time; they were part of a sequence of events. The first event of this sequence was a deceleration of the axial velocity characterized by the essential disappearance of the velocity gradient, and by a velocity defect as great as 50 percent of the local mean velocity. The second event was an acceleration; i.e., a mass of fluid coming from upstream and entering at a y^+ of about 15 was directed towards the wall at angles 0 to 15 degrees, interacting with the fluid in the decelerated region. The third event was an ejection; i.e., an abrupt outward motion of fluid originating in the decelerated region and at the wall area. The fourth major event was the entry from upstream of a mass of fluid moving almost parallel to the wall, the sweep event. This latter higher speed fluid was often a part of the same mass of fluid giving rise to the acceleration stage. The above cycle was repeated randomly in space and time.

Corino estimated roughly that 70 percent of the $-\rho\overline{uv}$ Reynolds stress could be attributed to the ejections and that 30 percent (by difference) to the sweep events. More experimental findings, such as interactions between the events, frequency of occurrence and Reynolds number effects, can be found in Corino (7). Wallace, Eckelmann and Brodkey (37), by using hot-film anemometry techniques and by splitting the \overline{uv} signal into four parts, were able to measure approximately equal positive contributions to the Reynolds stress from ejections and sweeps, and negative contributions from their interactions (+70 percent from ejections, +70 percent from sweeps and -40 percent total from the interaction of ejections and sweeps). Those values are for a y^+ of 15, with the values being a weak function of position.

Willmarth and Lu (38), by using hot-wire anemometry and conditional sampling techniques, studied the structure of the Reynolds stress near the wall. They reported that 60 percent of the positive contribution to the Reynolds stress \overline{uv} occurred when the sublayer velocity was less than the local mean. Positive contributions to the instantaneous \overline{uv} , 62-times higher than the local mean average were measured. They concluded that the process of turbulent energy production in the wall region was intermittent and that 99 percent of the contribution to \overline{uv} occurred during

55 percent of the total time.

Grass (12), using the hydrogen bubble technique developed by the Stanford group, studied visually and quantitatively the turbulent boundary layer in a free surface channel flow. He mainly concentrated on surface roughness effects. Irrespective of wall roughness, he observed two well-defined flow events. These were ejections of low momentum fluid outwards and "inrushes" of high momentum fluid towards the wall. His measurements indicated that the process of turbulent energy production is intermittent and that it occurs by the contribution of both ejections and inrushes. He concluded that the contribution of the inrushes to the turbulent energy production was mainly confined to the wall region. The role of the ejections, though, extended to the outer region, where very large positive contributions to the \overline{uv} were measured.

Gupta, Laufer and Kaplan (13), using a ten hot-wire plug probe and by applying a conditional sampling technique, studied the spatial structure of the viscous sublayer. By keeping short averaging times, they measured the correlation coefficient R_{uu} . Their data strongly suggested a coherent structure for the sublayer. Measurements of the instantaneous velocity in the spanwise direction uncovered a structure of local peaks and valleys reminiscent of the ones in laminar-turbulent boundary layer transition. The

mean spacing of the peaks was found to be equal to about 10 sublayer thicknesses. The lifetime of this structure was estimated to be equal to $0.5\delta/U_0$ for the range of Reynolds numbers (2200-6500) studied.

The experimental verification that events in the wall area have a deterministic nature has strengthened the feeling among researchers that much information is lost in the averaging procedure. The long time averaging process tends to obscure the actual physical picture not only in the wall area but also in the outer region of turbulent shear flows. The first evidence of this was offered by Corrsin and Kistler (9), who observed the laminar-turbulent interface for the case of a shear flow having a free boundary; they found, by hot-wire measurements, that this interface sharply separated the laminar from the turbulent regions and was highly convoluted. They called this phenomenon "intermittency." Townsend (33) proposed to measure intermittency by an "intermittency factor" γ , which is the fraction of time during which the flow is truly turbulent. Two methods of measuring, γ , were proposed by Townsend; the first one (33) from the "Kurtosis" or "flattening factor" of the probability density of the intermittent signal. The second method (34) is based on obtaining an on-off square wave having the value of 1 when the sensing probe is in turbulent and zero when it is in

non-turbulent regions. In the latter method, the intermittency factor is equal to the mean square value of the on-off wave signal.

Corrsin and Kistler (9) proposed a theoretical analysis according to which the interface consists of a very thin fluid layer; within this layer viscous forces play the most important role and they are responsible for transmitting mean and fluctuating vorticity to the laminar regions. Their experimental results were in plausible agreement with this model for the three turbulent stress flows they studied, i.e., rough-wall boundary layer, plane wake, and round jet.

Klebanoff (19) measured accurately values of the intermittency factor γ for a flat plate turbulent boundary layer. Fiedler and Head (10) improved Corrsin and Kistler's method by introducing smoke into the boundary layer and using a photo-electric probe; they measured intermittency in a turbulent boundary layer with favorable and adverse pressure gradients. Their experimental results showed that in the case of adverse pressure gradients the width of the intermittent zone increased.

Townsend (36) suggested a viscoelastic model for the interface and pointed out the importance of visualization techniques in studying the development of such flow structures. Novel techniques have been applied in recent years

in order to obtain a better understanding of the behavior of the interface.

Kibens and Kovaszny (17) developed and applied a conditional sampling technique. They measured time averages of the streamwise and normal mean velocities in a flat plate turbulent boundary layer and extended their measurements to the streamwise fluctuating velocity component and spanwise vorticity component. They suggested that in the non-turbulent region the flow could be considered as an irrotational flow over a wavy displacement surface moving with a velocity equal to $0.93 U_0$.

Blackwelder and Kovaszny (4) and Kovaszny et al. (22) studied the large-scale motion in the intermittent region of a turbulent boundary layer. Conditionally averaged space-time correlations were measured; their interpretation suggested the appearance of a random sequence of "eruptions" or "bursts" near the free stream.

Kaplan and Laufer (16) studied intermittency in conjunction with the entrainment process associated with the nature and dynamics of the laminar-turbulent interface of a flat plate turbulent boundary layer. A ten hot-wire rake was mounted to traverse the intermittent zone; the conditional sampling of data from the wires was performed by a digital computer. Their results were in agreement with those of Kovaszny et al. (22).

Blackwelder and Kaplan (3) extended the work of Kaplan and Laufer (16) and Kovasznay et al. (22). They suggested a connection between the events close to the wall and the intermittent bursting of the outer region. The earlier and recent work on intermittency and the phenomena associated with the outer flow as well as their relation, if any, with the phenomena of the wall area have been reviewed in Hinze (15), Townsend (35), Brodkey (5), Kovasznay et al. (22) and Kovasznay (21).

The preceding discussion demonstrated the importance of the individual fluid motions occurring in the wall area and the outer region and emphasized the need for greater knowledge of their nature. A qualitative physical picture of the flow structure combined with quantitative measurements would be valuable in order to advance the picture of turbulent motions just presented. In this work, there was obtained visual information on fluid motions, both in the wall area and in the outer region of fully developed turbulent flow past a flat plate.

EQUIPMENT AND EXPERIMENTAL PROCEDURE

Purpose

The purpose of this investigation was to study visually the outer region of a turbulent boundary layer and to attempt to establish a connection between this region and the phenomena already known to occur in the wall area. The experimental technique used was directed, mainly, to the outer region, but it also permitted qualitative observations of those pertinent events of the wall region necessary to characterize this area.

Plan

Specifically, in this investigation, the visual-photographic study of a flat plate turbulent boundary layer was carried out. The technique involves suspending very small solid particles in water as tracers and requires no injection or the introduction of any measuring device into the flow field. The motions of the particles were photographed by a high speed motion picture camera which moved with the flow. The basic principle of the technique was the same as used by Corino (7) to study the wall area of a turbulent pipe flow. Although the principle was the same,

a considerable effort was devoted in development to make the technique suitable for the present investigation.

Apparatus

The equipment was composed of mainly three parts: the flow system, the flat plate and the photo-optical system. The flow system is depicted schematically in Figure 1. It was composed of a 200 gallon, rubber-coated tank (A) from which the water was pumped by either of the centrifugal pumps, (B) and (C). An aluminum flat plate (F) was placed as shown in the flow channel (E) which had dimensions 10 inches width, 13 inches depth and 16 feet length. The flow rate of water was controlled by the globe valve (P) and the water level in the channel by the perforated plate (H). Two expansion joints (K) and (L) were provided in order to minimize the transmission of pump vibrations to the flow channel. The water before reaching the flat plate (F) passed through the entrance section (D) which consisted of a deflecting plate, a tank of polyethylene straightening tubes and a series of screens. A glass window (G) was provided on one side of the channel for illuminating and photographing purposes. The flat plate (F) could be adjusted to various streamwise positions, thus allowing photographing different parts of its length. A dump tank (I), following the end of the channel,

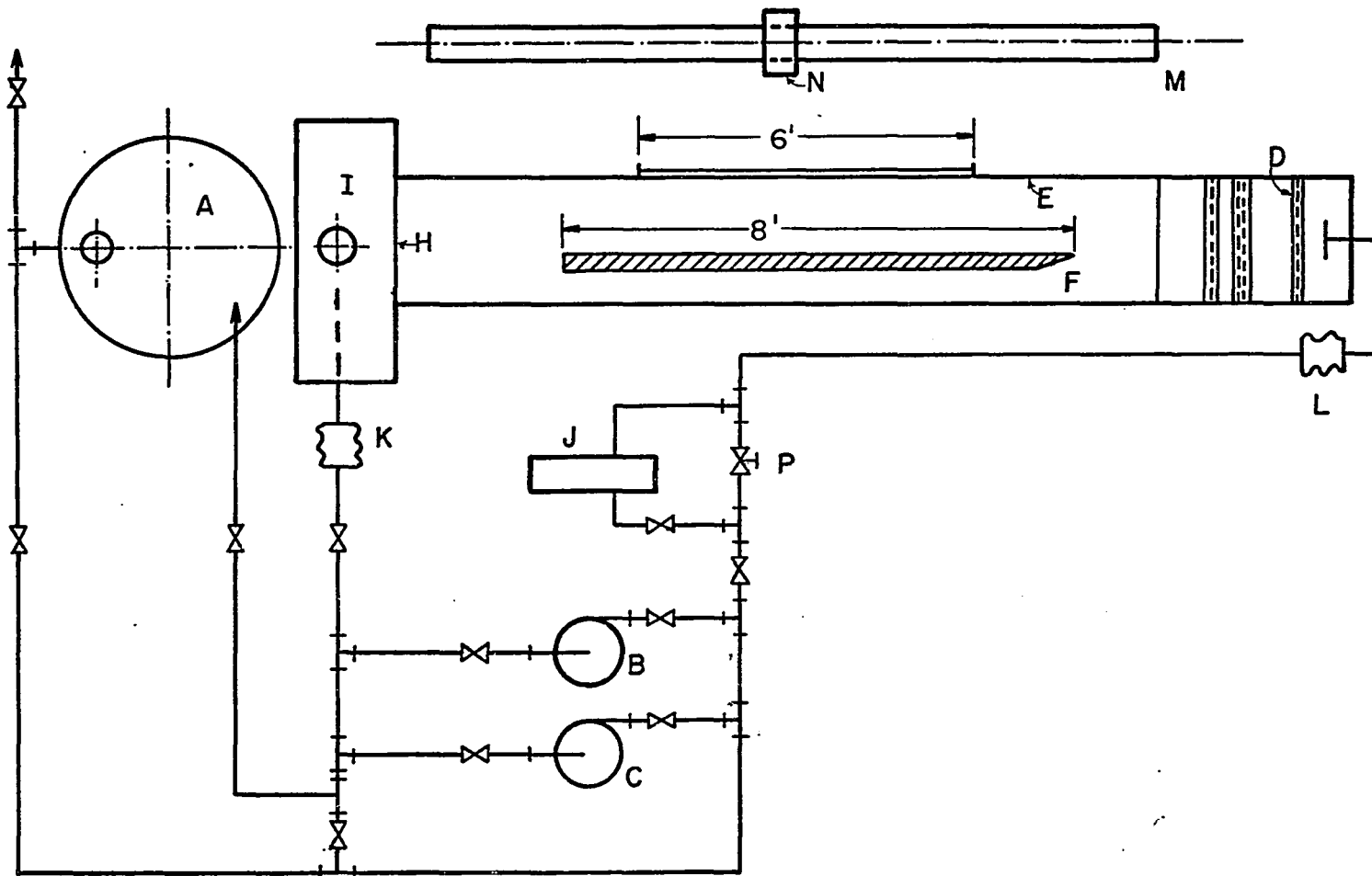


FIGURE 1. FLOW SYSTEM WITH FLAT PLATE

closed the flow loop, permitting continuous recirculation. On a bypass line, a 50 gpm capacity filter (J) retaining any particles larger than 5 microns was installed; this filter was used to clean the water before dispersion of the solid particles.

The tracer particles were dispersed in the water and stayed under suspension continuously. The particles were made visible only under dark field illumination, where the intensity of the scattered light was adequate for their photographing.

The photo-optical system consisted of the light source, the high speed "FASTAX" movie camera and the camera carriage equipment. The ability to transport the camera and the light source at preselected velocities relative to the mean flow allowed the continuous observation of the development of a given flow phenomenon. Figure 2 is a schematic representation of the photo-optical system. A high-intensity light source (B) was used, a narrow light beam was produced by means of two slits, (I_1) and (I_2). The light beam passing through the glass window was scattered by the tracer particles and the scattered beam was received at a 90 degree angle by the lens of the "FASTAX" camera (A). The camera lens was aligned parallel to the flat plate (F) surface so that the light reflected by it did not enter the camera lens. The flow channel (H)

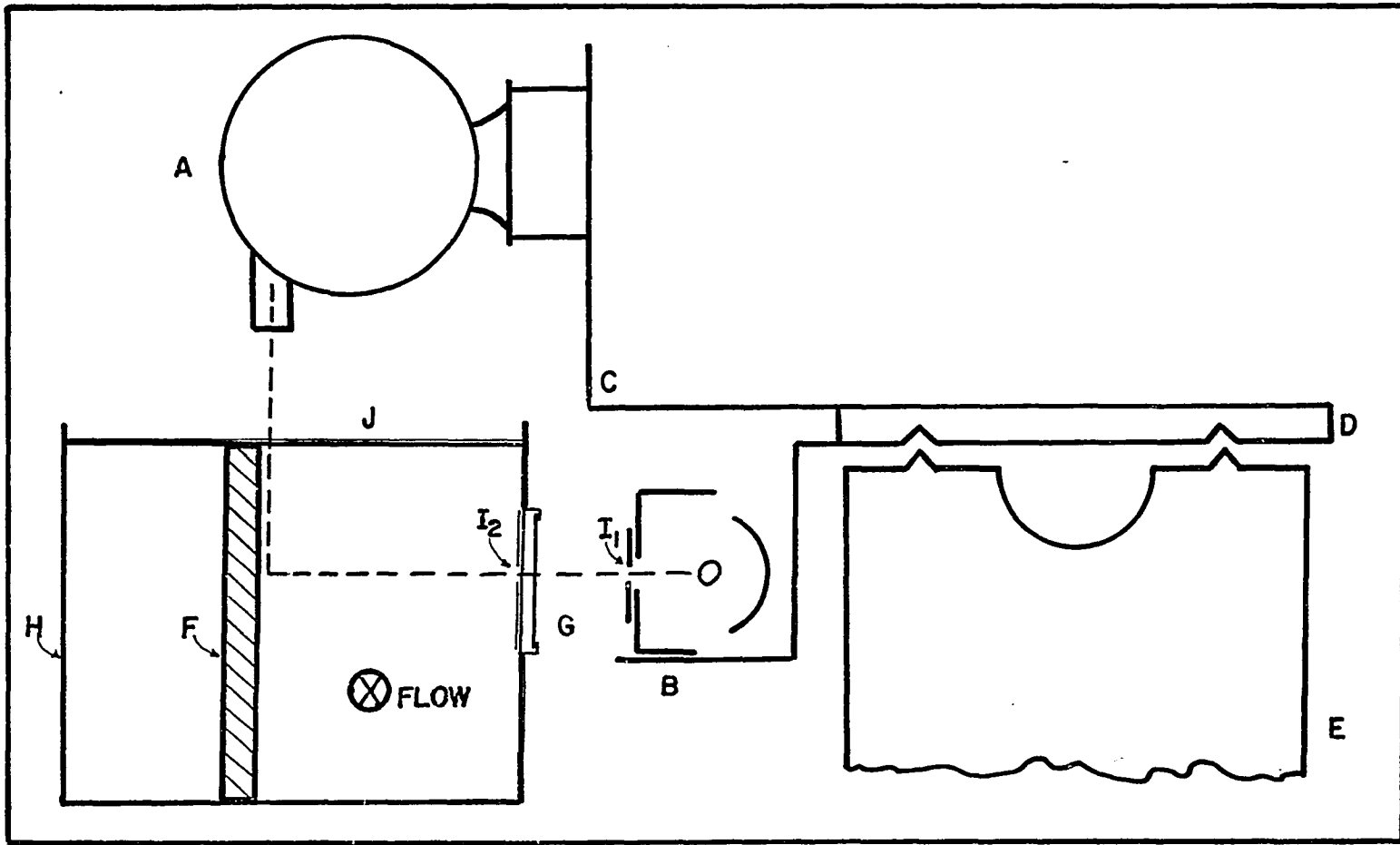


FIGURE 2. PHOTO OPTICAL SYSTEM

and the flat plate (F) were aligned in parallel to the already existing 8-foot lathe bed (E) bolted to the concrete floor. The camera (A) was supported by a 90 degree heavy steel frame (C), which in turn was attached to the lathe carriage (D). The lathe carriage was designed to slide along the lathe bed and it was driven by a hydraulic piston. The speed of the hydraulic drive could be preselected by means of a control valve setting. The entire camera light source system could be transported downstream at a preselected speed with respect to the mean velocity in the flow channel. Figures 3 and 4 are photographs of the equipment used.

Flow System

A detailed description of the various parts of the flow system will be now given.

Flow channel and piping. As is shown in Figure 5, the flow channel was composed of an entrance section (D), whose details of construction will be discussed in a subsequent section, followed by the main channel (E). In the main channel, a 6 feet by 6 inches glass window (G) was provided for illuminating and photographing purposes. Parallel to the glass window, a flat aluminum plate (F) 8 feet by 1 foot by 0.5 inches was positioned; the various boundary layer flows studied were developed along this flat

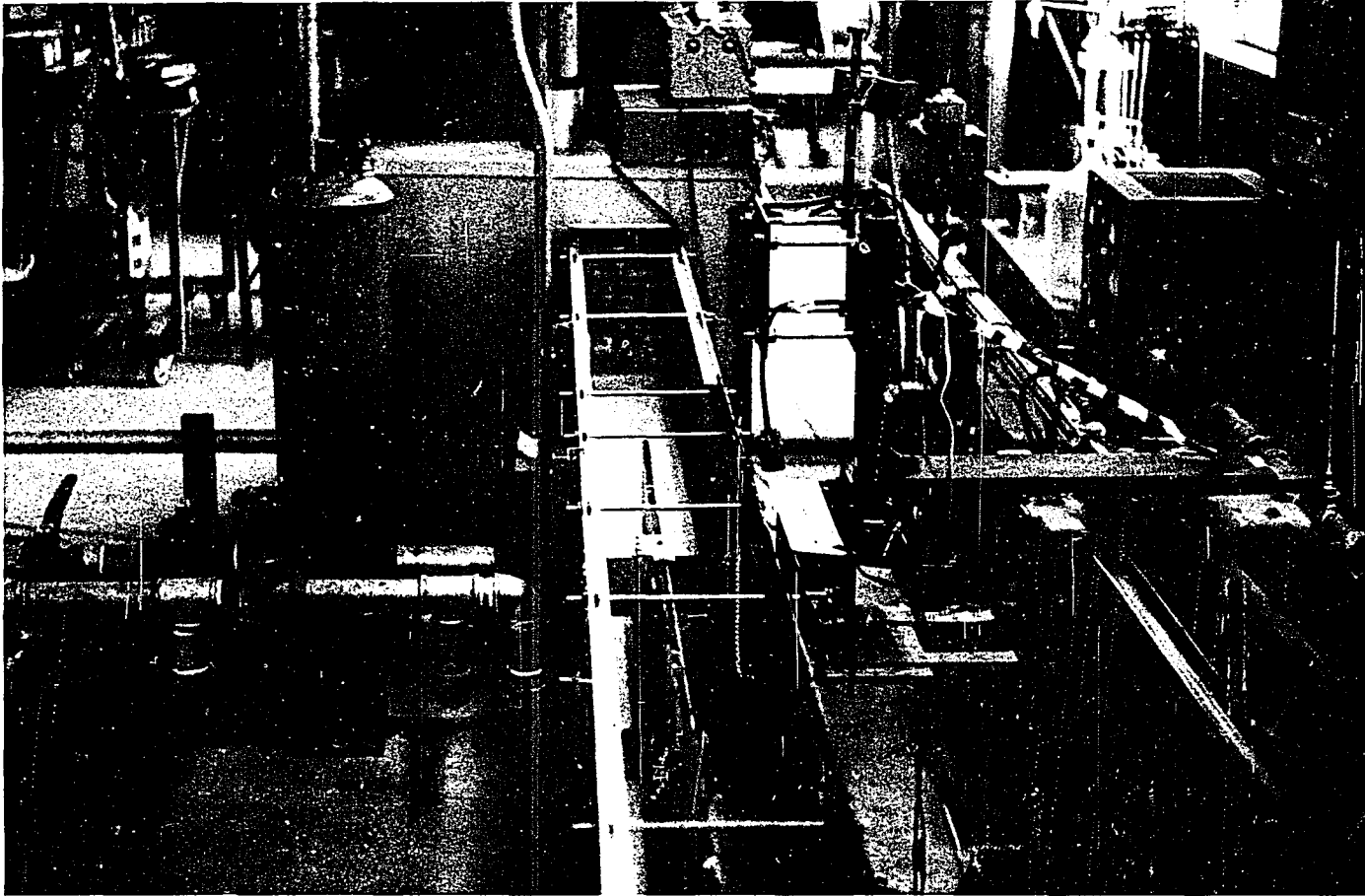


FIGURE 3. PHOTOGRAPH OF EXPERIMENTAL EQUIPMENT

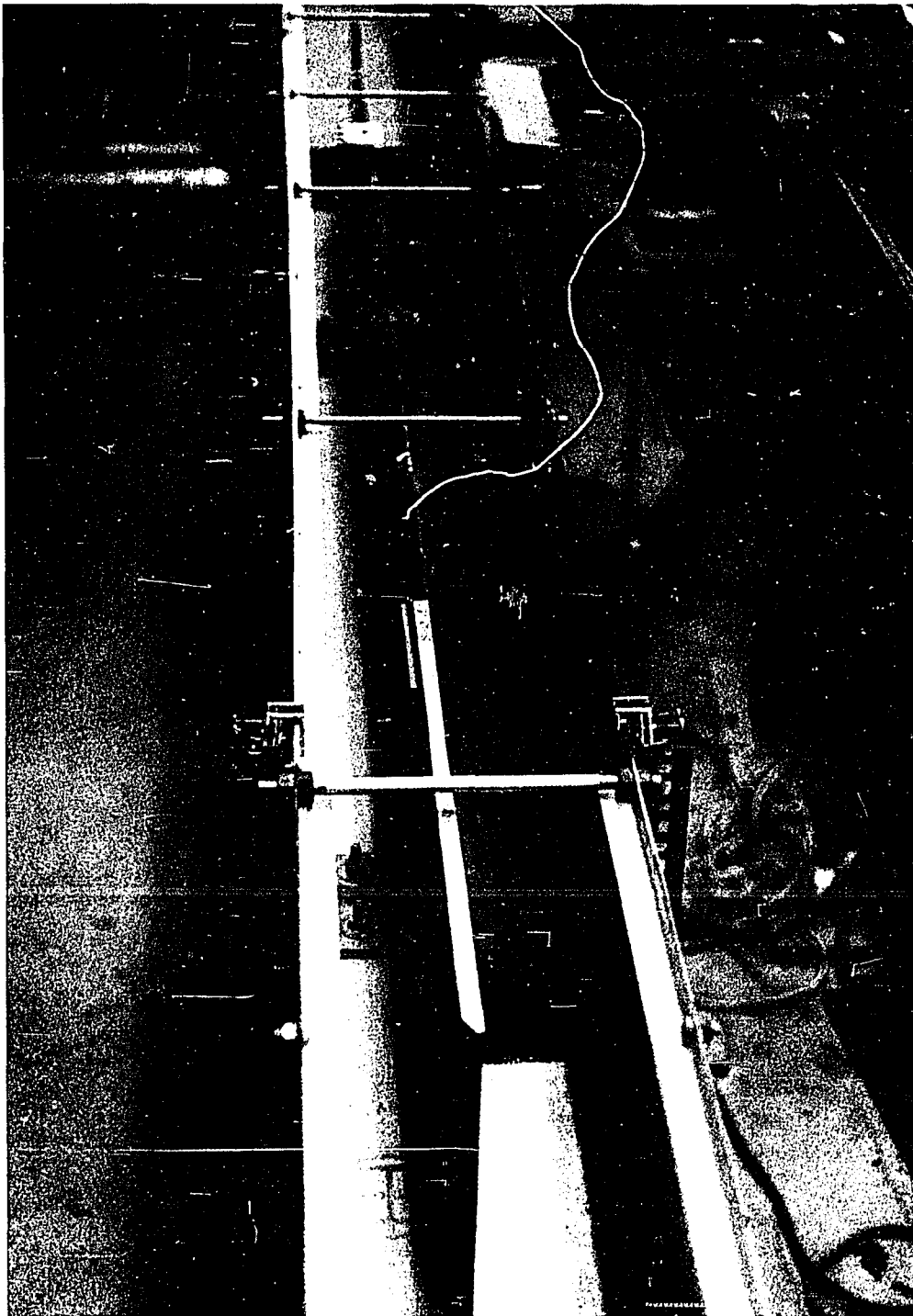


FIGURE 4. PHOTOGRAPH OF CHANNEL AND FLAT PLATE

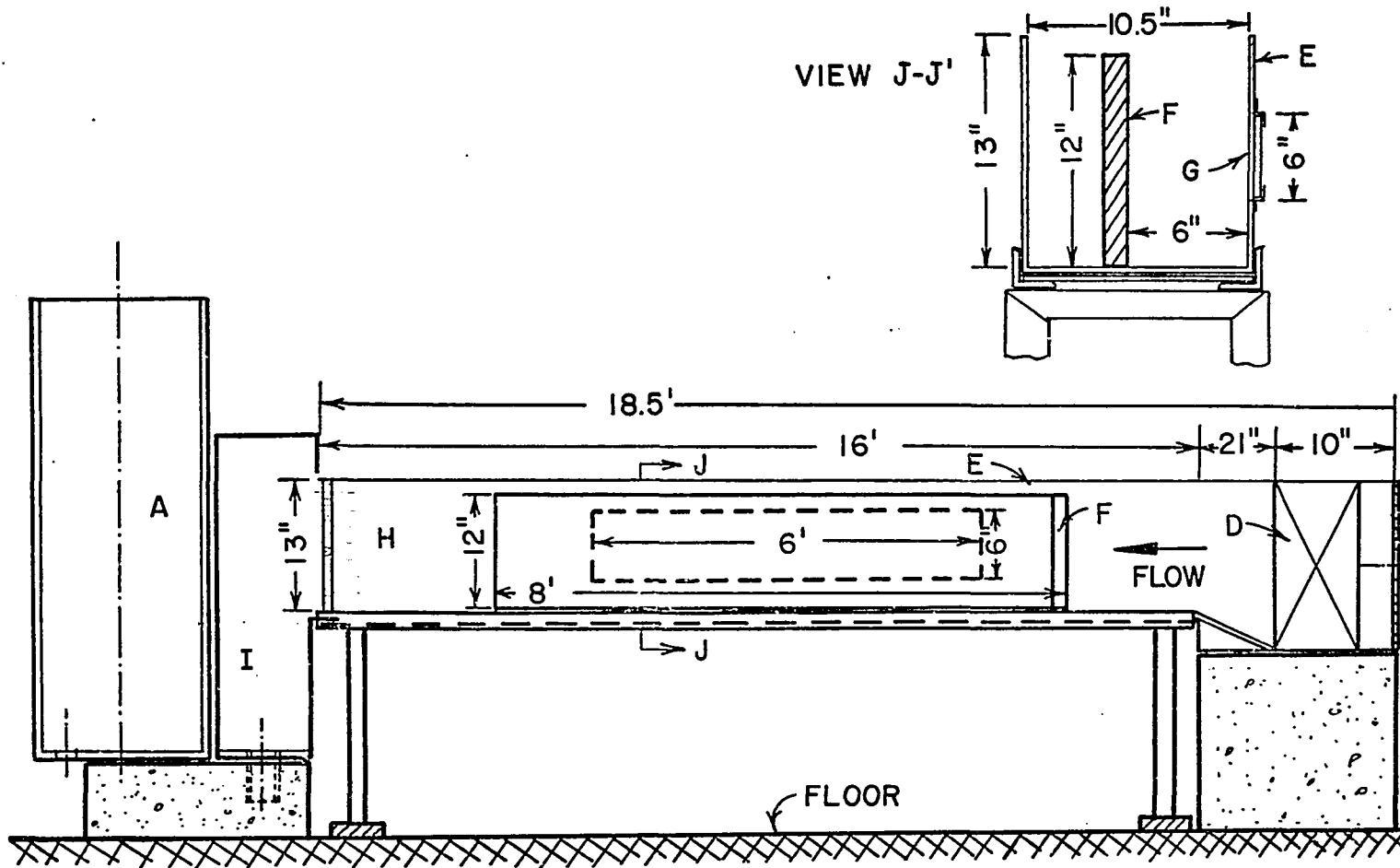


FIGURE 5. DETAILS OF FLOW CHANNEL AND SUPPORT

plate wall. The water level in the channel during the actual runs was kept at 12 inches; this level was adjusted by the perforated plate (H) at the end of the channel. The water flowed through the perforated plate and into the dump tank (I) from where it was pumped out and recirculated to the entrance section.

At the end of each series of runs, the water with the suspended solid particles was stored in the tank (A). The entrance section, dump and storage tanks were supported on concrete structures; the main channel was resting on heavy steel which was bolted on the concrete floor. To minimize vibrations transmitted by the recirculation pumps to the water channel, two expansion joints were provided; in this way a tight connection of the water channel and the piping of the system was eliminated.

Details of design and construction of the entrance section are shown in Figure 6. The jetting effect created by water coming out of the 2-inch feed line was eliminated by placing a baffle in front of it. Since the main task of the entrance section was to create a uniform, low, free-stream turbulence flow, every possible effort was made to reduce the degree of turbulence which was present in the 2-inch feed line. The baffle was preceded by a 3-inch long, 2-inch nipple which was filled with 1/4 inch I.D. copper tubing; at both ends of this nipple were placed

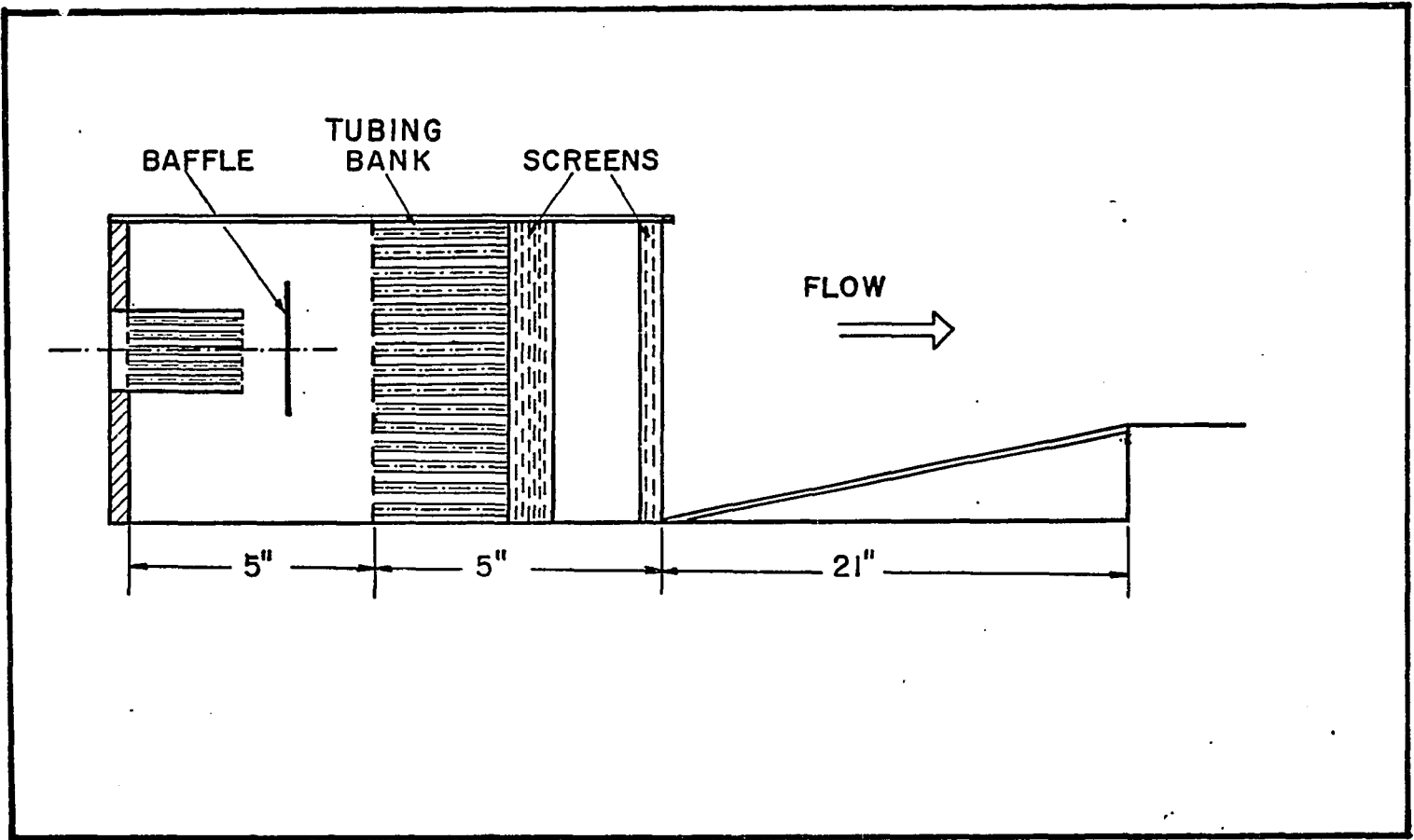


FIGURE 6. ENTRANCE SECTION

20 by 20 mesh stainless steel screens. The baffle was followed by a 20 by 20 mesh copper screen and after that followed a tank of 420 polyethylene pieces of tubing, 1/2-inch I.D., 1/16-inch wall thickness. These acted as a straightening vane. Next to this bank, a series of seven stainless steel screens was installed. This was a cascade of screen openings, the first six being 30 by 30 mesh and the last one 32 by 32 mesh.

In order to obtain a uniform flow out of the entrance section, it was necessary to provide a leak-tight top cover. This was accomplished by using a rubber gasket and a plexiglass plate. The pressure drop developed by the polyethylene tubes bank and the screens kept the entrance section filled; thus the fluid was forced to leave the entrance section uniformly across its total cross section. A polyethylene plastic film helped considerably in reducing water surface waves. As it will be discussed in a later section (photo-optical system), more drastic measures had to be taken to completely eliminate the effect of surface waves.

The entrance section, water channel and the dump tank were made out of 18-gauge galvanized steel sheets. A window was cut in one of the channel walls and a glass frame was attached to it by means of 1/16-inch diameter pop-rivets. All water leaks were sealed by silicon

rubber. Teflon gaskets were used in the pipe flanges of the entrance section and dump tank. The perforated plate at the end of the water channel was made out of plexiglass. Ten series of horizontal holes were drilled throughout its cross section; each series consisted of nine holes equally spaced. The diameter of the holes in each series was calculated such as to give the same water flow rate per hole regardless of its hydraulic head from the free water surface; thus the series closest to the bottom of the channel consisted of 5/32-inch diameter holes while those at the top were 5/16-inch diameter.

The steel water storage tank was rubber-coated on the inside and rated at 200 gallons capacity. All the piping, except the suction line of pump (B) shown in Figure 1, was 2-inch, schedule 40, galvanized steel; the suction line of pump (B), was 3-inch, schedule 40, galvanized steel. All valves, except the globe valve (P) used for flow control, were ball valves with teflon inserts. Pump (B) which was used for most of the actual runs was rated 200 gpm at 100 feet of head for water (3450 rpm); pump (C) was rated 50 gpm at 70 feet of head for water (1750 rpm).

An aluminum flat plate was positioned inside the water channel; its dimensions were 8 feet by 1 foot by 0.5 inches. Details of its construction are shown in Figures 7(a) and 7(b). The flat plate was fitted in such

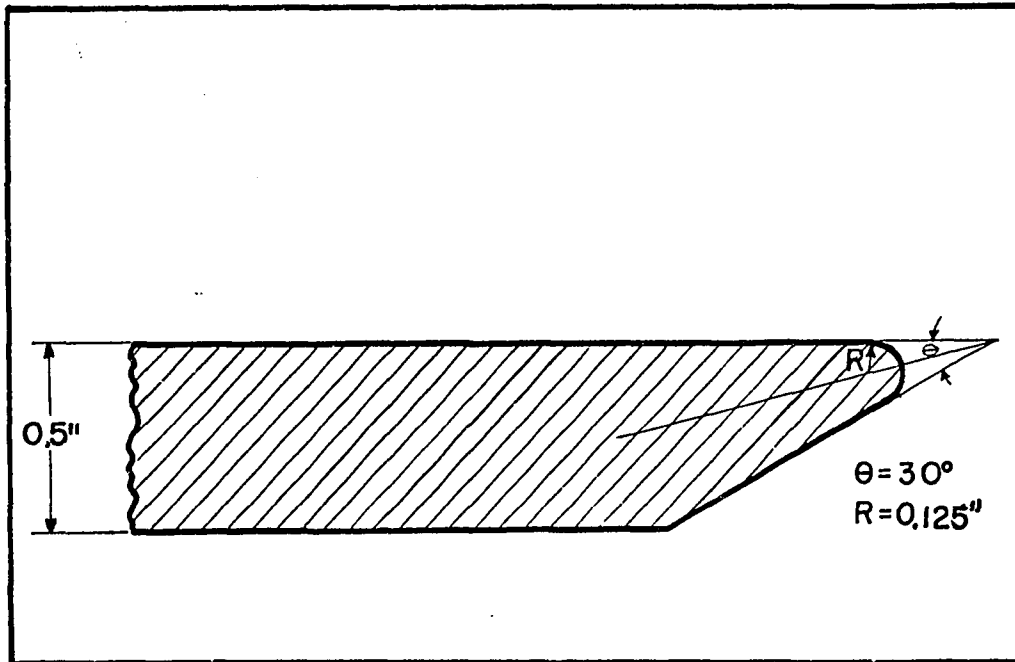


FIGURE 7(a). LEADING EDGE OF FLAT PLATE

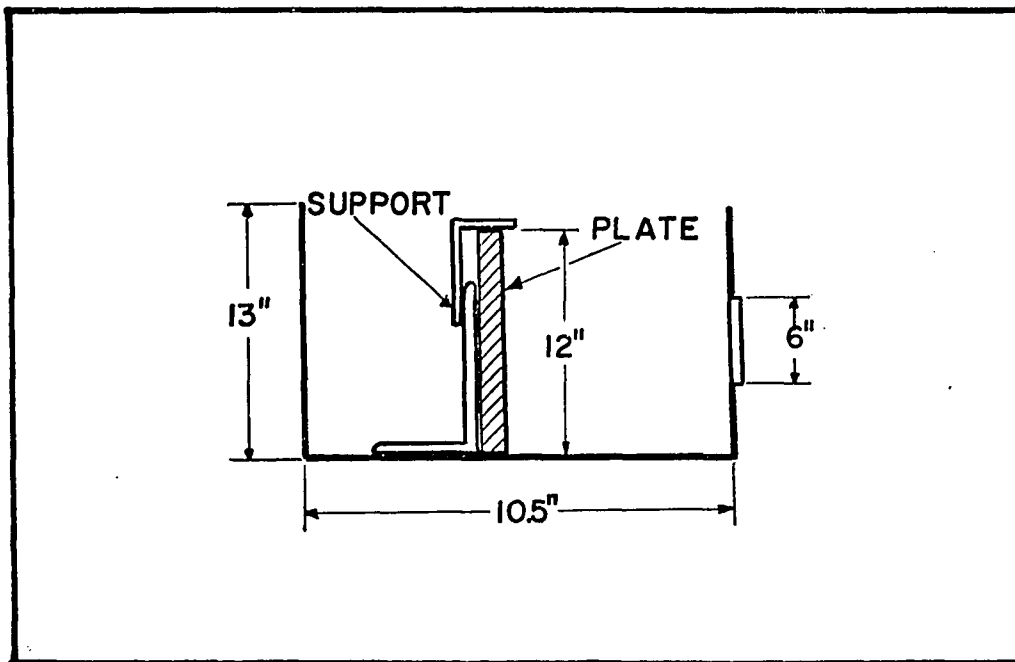


FIGURE 7(b). POSITIONING AND SUPPORT OF FLAT PLATE IN THE CHANNEL

a way as to allow repositioning of it along its length; this was found necessary for the various experimental runs as it will become apparent in a later section. Special attention was paid to the design of the flat plate's leading edge. It was machined as follows: first it was cut as a 30 degree angle wedge; next the wedge was machined to a cylindrical surface of 0.125-inch radius.

Tripping of boundary layer. In order to assure a fully developed turbulent flow, the boundary layer was tripped by a three-dimensional turbulence-stimulation device. It consisted of thin regular triangular elements placed side by side. Each triangle was made of five layers of insulating tape forming a tripping element of 1 mm. approximate thickness. They are shown in Figure 8. The characteristics and effectiveness of these tripping devices have been described by Hama (14).

Fluid. Water was selected as the test fluid. In this laboratory, there has been previous experience with trichlorethylene as the test fluid with "Seamag" magnesium oxide particles as fluid markers (9). In the present case of an open flow system, the toxicity of trichlorethylene vapors prohibited its use.

Particles. Considerable experimental effort was devoted to trying various types of solid particles to mark

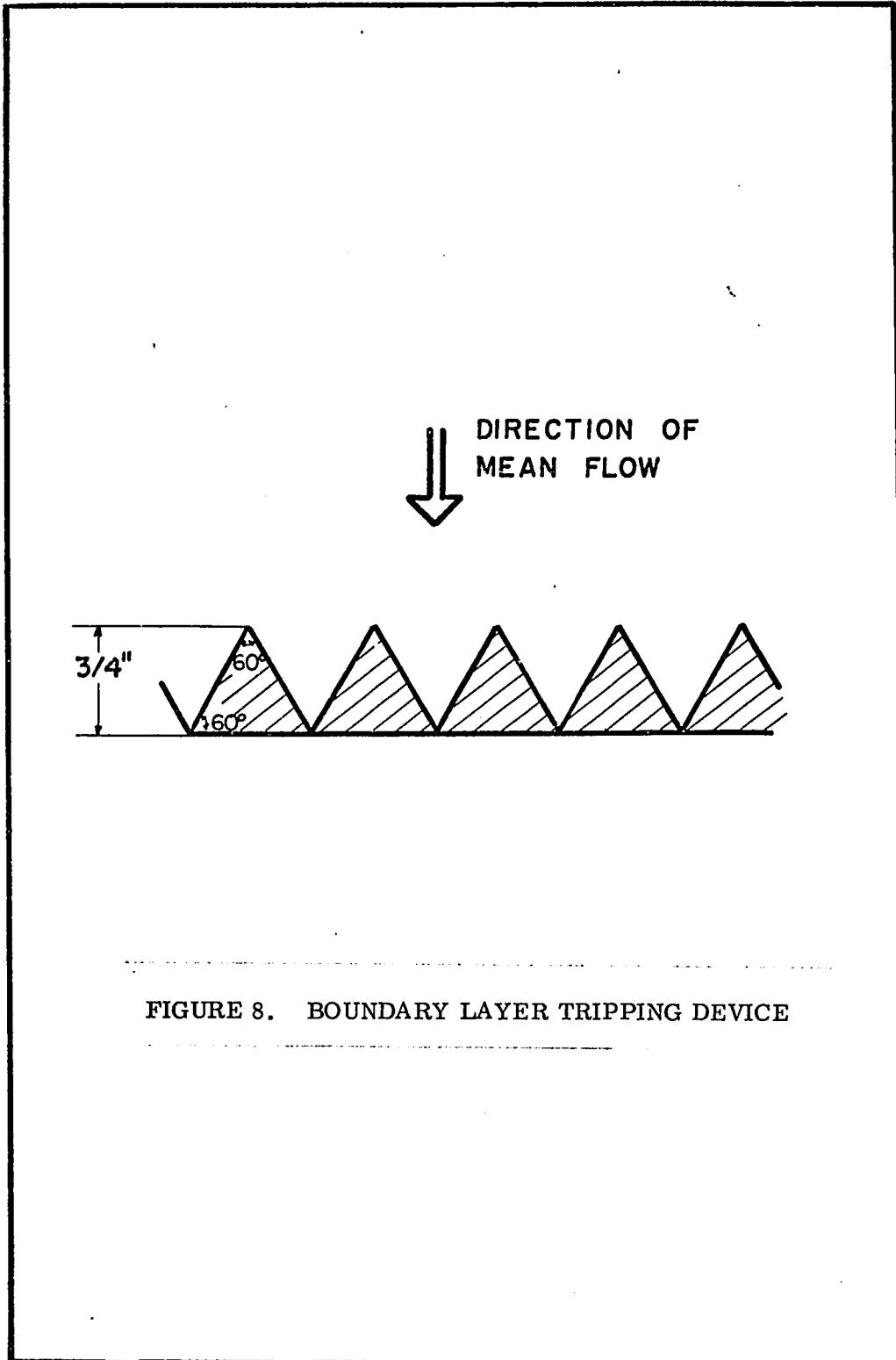


FIGURE 8. BOUNDARY LAYER TRIPPING DEVICE

the flow field. Pliolite* particles were finally selected; the density of pliolite is 1.026 g/cm^3 and its optical properties with respect to light scattering intensity are excellent. The geometrical dimensions of a typical particle are almost equal in all directions. It was found that particles in the form of flakes tended to align themselves in a preferred direction with the flow, and thus cannot be followed for the entire time while in the field of view. Preliminary experimentation with aluminum particles dispersed in water (with the help of a colloid mill) showed the effect of preferred orientation. While their light scattering properties were quite satisfactory, their projected image from the movies showed an "on and off" flashing effect. In contrast, the Pliolite particles were visible continuously as long as they were in the field of view. One of the most important properties of the Pliolite particles used was their size. Pliolite was received in the form of pellets; they were ground and screened and the fraction through 200 and on a 325 mesh screen was retained. This resulted in particles having a diameter range of 44-74 microns. The particle size, aside from other problems which will be mentioned in this section,

*Commercial name of Polyvinyltoluene butadiene.
Made by Goodyear Chemicals, Akron, Ohio.

dictated the lower limit for the scale of the flow motions observed.

Another aspect, closely related to the fineness of the above scale, was the particle concentration. The separation distance between particles should not be larger than this scale. Yet it should be large enough so that particle-to-particle interactions do not take place. This sort of optimum concentration was achieved by trial and error.

The particles did not settle out during time periods comparable to the runs. Nevertheless being subjected to gravitational forces an estimate of this effect can be made. The terminal velocity of a spherical particle suspended in a non-turbulent fluid is given by:

$$u_t = \frac{d^2}{18\mu} (\rho_f - \rho_p)g \quad (1)$$

Taking the worst case, i.e., $d = 74$ microns and $\mu = 0.7 \times 10^{-2}$ g. cm⁻¹ sec⁻¹, one obtains $u_t = 1.43 \times 10^{-2}$ cm/sec. This terminal velocity is very small compared with the individual instantaneous velocities of particles measured, as can be seen from the data given in the next section. A settling time important for consideration is the time during which the particle is viewed. With a filming speed of about 260 frame/sec rarely an event studied lasted for 1 second. This time would correspond to a distance of

1.43×10^{-2} cm, which is very small in comparison to the dimensions of the field of view and the scale of the motions studied.

The question as to how well the suspended solid particles follow the details of the turbulent motion has been considered by Brodkey et al. (6). The discussion of the pertinent literature is given by them and does not need to be repeated here. A calculation on a simple model suggested by Brodkey et al. will be given here to determine if it is reasonable to expect the particles to follow the fluid motions. The model assumes that a particle is surrounded by a fluid element initially at rest which suddenly undergoes an acceleration a_f . This is an extreme case because of the impulsive start of the motion. If the assumption is made that the fluid element accelerates from zero velocity to u_f in time t , then the relation

$$u_f = u_p \left(\frac{d^2 \rho_p}{18 \mu t} + 1 \right) \quad (2)$$

is obtained. Here u_p and ρ_p are the velocity and density of the solid particle respectively. An extreme case for the present system would correspond to $d = 74$ microns and $t = 3.50 \times 10^{-2}$ seconds (i.e., t equal to the time of 10 motion picture frames). The above relation then becomes

$$u_f = u_p (0.012 + 1). \quad (3)$$

For this extreme case the difference in fluid and particle velocity is negligible.

Photo-optical System

In this section the equipment and procedure used to photograph the flow will be described. The camera viewpoint will also be discussed.

Camera. A high speed motion picture camera is ideal for a detailed observation of the rapid fluid motions occurring in a turbulent flow. It provides a permanent record of the sequence of these motions, thus allowing a comparison to be made. In addition it permits a display of the photographs of the rapid motions at a reduced speed so that a detailed study can be conducted.

The camera used in the present study was a 16 mm Fastax WF 3 high-speed motion picture camera with a film capacity of 100 feet (4000 frames). It had a rated framing speed of from 150 to 8000 frames/sec., but was operated in this study at about 260 frames/sec. There were two reasons for this limitation. The first was that the amount of light available to expose the film without a reduction of the quality of the photograph was limited. The second reason was that the real time recorded on the 100 feet of film is short at high framing speeds; thus a developing sequence of fluid motions could have been missed by using a higher framing speed.

The camera had a timing light which imprints in the film margin timing marks at a rate of 120 marks/second. These timing marks permit the accurate calculation of the framing speed and, most important, the real time between given flow events. Duration of individual events and instantaneous velocities were measured in this way.

Film. After considerable preliminary testing it was found that Kodak #7278 Reversal film performed adequately under the conditions of the present experimental study. This film, after development, produced a black and white positive print in which the pliolite particles appeared as white spots on a dark background.

Lighting. In the present study dark field illumination was used; such a method requires that the direction of the light beam be at approximately right angles to the direction of view. Thus the only light reaching the camera lens is the light reflected or scattered by the suspended solid particles. The concentration of the particles was relatively small and a considerable amount of the light input passed through the clear fluid. The field of view in the present study was large and thus a light source of large dimensions was required. The lamp selected was a GE EKV Quartz Halogen lamp. It was operated by a D.C. power supply at 1100 watts and it had a rated luminous flux of 39000 lumens. The lamp was enclosed in a metal housing

and it was provided with a light reflector. Adjustable slits were fastened to the housing to control the width of light beam. During the runs, the light source moved with the flow by the same hydraulic mechanism which carried the camera.

Camera lens. The lens adapted to the Fastax Camera was an ELGEET model MF-142, 13 mm, f:1.5 wide angle lens. It produced a magnification of $(1/18)X$. The field of view available at $(1/18)X$ magnification was 18 cm measured in the streamwise direction, and 13.7 cm measured in the direction normal to the flat plate wall. The dimensions of the field of view were measured by photographing a scale which was placed at the downstream end of the flat plate.

To each magnification corresponds a depth of field. The depth of field is defined as the thickness of a plane perpendicular to the direction of view in which all objects are in focus. For very low magnifications, such as that used in the present study, the depth of field is very large. In the present work, this depth of field had to be kept as small as possible. Therefore it was dictated by the width of the light beam, which at the flat plate surface was about 0.74 inches. In Figure 9, the camera viewpoint and the dimensions of the field of view are given. Thus the field of view is seen to be a volume of

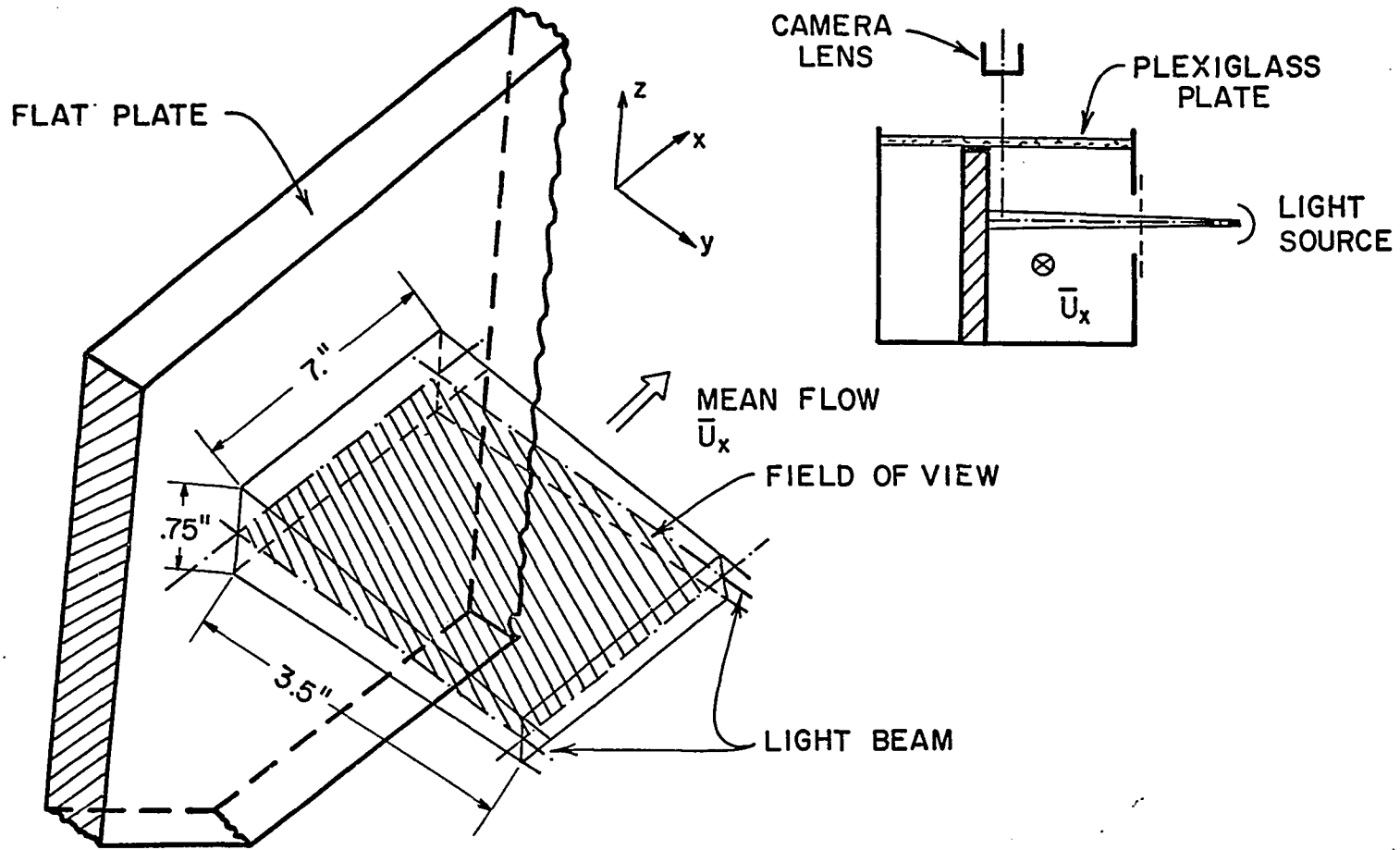


FIGURE 9. CAMERA VIEWPOINT AND FIELD OF VIEW

fluid which has dimensions 7.x3.5x0.75 inches in stream-wise, normal and spanwise directions respectively.

The photographing of the fluid motions was performed through a plexiglass plate, which was positioned perpendicular to the direction of view (see Figure 9). This was necessary in order to avoid image distortion which was caused by the water surface waves. In addition the plexiglass plate eliminated the meniscus effect in the interface of water and the aluminum flat plate; thus an accurate determination of the wall in the movies was made possible.

The experimental runs were carried out using the following procedure. The water was pumped out of the 200 gallon storage tank to the flow channel. The water level was adjusted to cover all of the aluminum flat plate; this was done by lowering or raising the perforated plate at the end of the channel. The flow rate was adjusted by the globe valve (P) (Figure 1). The desired area of view, y-position and filming speed were selected and the camera lens was focused at the center of the light beam. The plexiglass plates (J) (Figure 2) were positioned at the top of the flat plate and the free stream velocity was matched with the camera carriage speed by following certain particles through the camera viewer. Then the desired carriage velocity was selected on the hydraulic valve and

the camera was started after travelling about 6 inches from its rest position. A measuring scale was positioned towards the end of the flat plate in order to measure y-distances.

EXPERIMENTAL RESULTS

In this chapter it will be shown first how to obtain velocity measurements from the motion pictures. Next, in order to put the entire flow picture into proper context, a general description of the fluid motions observed will be presented. The nature and character of the various flow events will be given here in a sketchy, qualitative manner. Finally, after the events have been established, their detailed description and actual measurements will be presented.

Velocity Measurements

Instantaneous local velocity measurements were made by measuring the time required by a particle to travel a certain distance in the flow field. The trajectory of a particle was traced on graph paper when the movie was projected frame by frame. In every run, the scale placed at the end of the flat plate in order to measure the y-distance from the wall, was also photographed. Thus an exact correspondence between the projected dimensions of the movie frames and the actual values could be established. By counting the frames and knowing the filming speed, the time elapsed was calculated. No other probe or measuring

device was inserted in the flow. The obvious limitation of the above method was that for a given point in the flow field, a marker particle could not always be found. Nevertheless, for the purpose of this visual investigation, where exact average velocity measurements at a given time and position were not necessary, the measurements were satisfactory. Moreover this method offered the considerable advantage of not disturbing the flow by any external measuring device. Another important aspect of the present technique was that it permitted instantaneous velocity measurements during the times where certain flow events occurred. The velocities measured in this way were relative to the camera carriage speed; absolute velocities and angles of flow were calculated from the known carriage speed by applying simple trigonometric relations (see Appendix I).

To permit establishing a fully developed turbulent flow, an effective tripping of the boundary layer was used. It was described on the section on experimental equipment. Careful observation of the particle trajectories in the movies did not show signs of laminar flow; rather, violent particle ejections and interactions characteristic of turbulent flow were constantly observed. For further confirmation of the turbulent nature of the flow, the mean average velocity profile for the runs analyzed was measured.

Results of such measurements will be given later. For every y-distance from the wall, particles were randomly selected for the whole length of the movie and their streamwise instantaneous velocity was measured; an average of these velocities was established for a given distance from the wall. In spite of the fact that the length of time for the averages was rather small (about 18 sec.), a good agreement was observed with the logarithmic velocity profile.

General Description of the Flow Field

An overall view and presentation of the phenomena observed will be given in the present section. Sketches will be used to illustrate the various events. In the next section, a detailed description of the fluid motions and experimental data supporting the arguments will be given. A very detailed examination of a large number of movie runs was conducted. The identification, study and interconnection of the flow events was a painstaking task due to the complexity of the overall phenomenon. Each flow event, once identified and its existence established in more than one run, was carefully analyzed. Everything described here and in later sections is much clearer in the motion pictures. A selection of the most representative ones has been compiled and will be available for loan. The most important feature of both the wall and the outer regions of

a turbulent boundary layer is the existence of a number of discrete events occurring in sequence randomly in space and time. The nature and scale of these events are different for the wall area and the outer flow.

In the wall area ($0 \leq y^+ \leq 70$), the single most important event is the ejection of fluid elements; these ejections are very localized in nature and they disturb the surrounding fluid. They are part of a more or less deterministic sequence of events; it is the sequence of events which occurs randomly in both space and time. Sometimes variations of the sequence were observed. Not in all the runs studied was the whole sequence observed nor was it always observed in the same exact order. But for most of the runs and for most of the times, the general picture was as follows:

The first event observed was the appearance in the flow field of a decelerated region moving with a streamwise velocity lower than the mean. Most of the time, this region extended from the area very near the wall up to and including the outer region. Within this decelerated region the flow characteristics were regular; not very chaotic motions or violent interactions were observed. Following this event and while the decelerated region was still in view, a very large mass of fluid entered from upstream. Most of the time this mass of fluid was moving with a

velocity higher than the local mean \bar{U}_x , and first appeared in the field of view as a high speed fluid front covering a region of approximately $150 \leq y^+ \leq 400$. It should be emphasized that a real sharp distinct interface between the decelerated region (low speed fluid) and the entering higher speed mass of fluid did not exist; moreover, in some cases the higher speed fluid had a velocity lower than the local mean. Nevertheless, the established fact was that two regions could be distinguished, one of which (high speed fluid) was moving downstream with a velocity higher than that in front of it decelerated flow region. A sketch of these two events is presented in Figures 10(a) and 10(b).

As the mass of the high speed fluid moves downstream it looks like "expanding" toward the wall and at the same time expands faster toward the outer region. The meaning of an "expanding" accelerated flow region can be best clarified in the Figure 10(b). In this convected view, the decelerated fluid appears as being gradually displaced by the accelerated one. This is shown by the change in the shape of the interface as it moves downstream. The field of view is covered more and more by the accelerated flow. It is in this context that the word "expands" should be understood. A region of high shear is formed between the low speed fluid adjacent to the solid wall and the high speed fluid just next to it (in the positive y-direction).

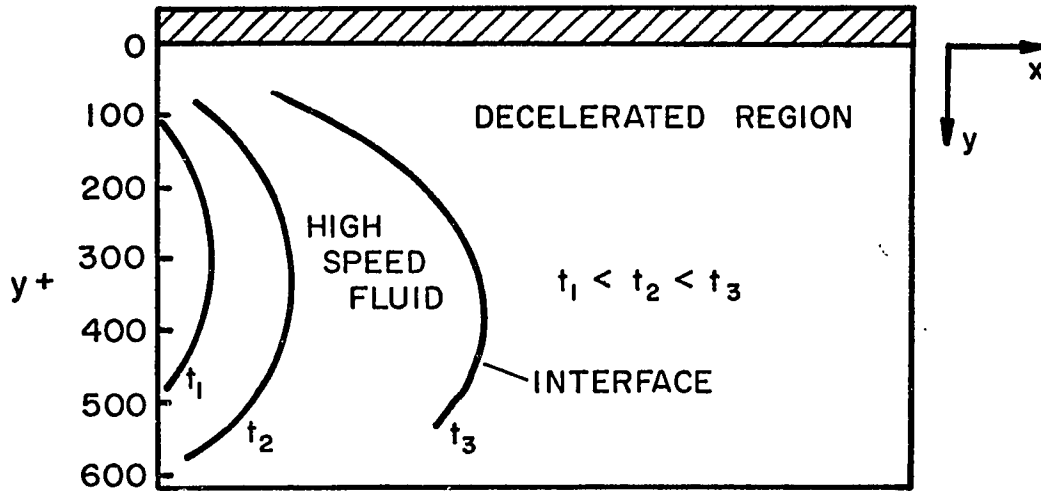


FIGURE 10(a). DECELERATED REGION AND ENTERING HIGH SPEED FLUID (CONVECTED VIEW)

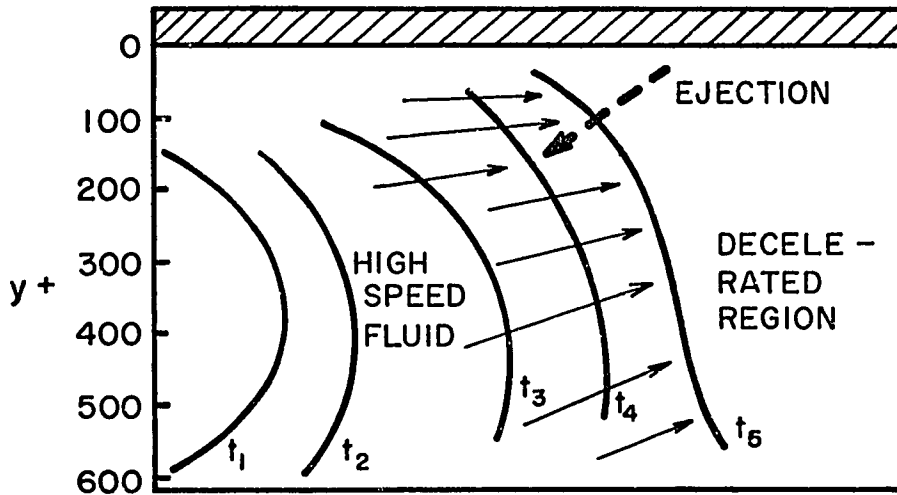


FIGURE 10(b). DECELERATED REGION, PROGRESSING HIGH SPEED FLUID AND EJECTION (CONVECTED VIEW)

The next event, immediately following, is a very small scale ejection (just one single particle or two at the most). The ejected fluid originates in the low speed fluid region and from an area of approximately $0 < y^+ < 50$; as it is ejected on an angle it violently interacts with the surrounding lower speed fluid and moving outward it enters the high speed fluid area. In some cases it was observed that ejected particles reached a y^+ of about 200 inside the high speed fluid region. Most of the ejected particles observed reached y^+ of 80 to 100 and then were swept downstream by the incoming high speed fluid. The development of the high speed fluid moving downstream and the ejection event are sketched in Figure 10(b). The flow inside the high speed fluid was directed along an angle towards the wall; this angle was observed to decrease in the region closer to the wall and become almost zero for the part of the acceleration in the wall area. Again it is to be emphasized that the interface between high and low speed fluid regions is not a sharp dividing line as it is sketched in Figures 10(a) and 10(b). Beyond a y^+ of about 100, the localized and violent nature of the flow events and their small scale tends to disappear. The outer region was observed to exhibit different type of events characterized by a much larger scale.

The single most important event of the outer region was a transverse vortex type of motion. In almost all the cases observed this transverse vortex was formed as follows. It will be recalled [Figure 10(b)] that the interface of the advancing high speed fluid was stretched along an angle towards the wall. This resulted in a region being composed of two large scale streams of fluid moving almost parallel to each other and having different velocities. Immediately after such a flow configuration was established, it was observed that a rotational large scale motion developed. This transverse vortex was the result of a Helmholtz type of flow instability; the interface between the high and low speed fluid regions, being unstable, gives rise to such a vortex formation.

Figure 11 presents a sketch of the transverse vortex and its relation to the regions of high and low speed fluids. It will be referred to as a Forward Transverse Vortex (FTV). As soon as this vortex was formed, it was transported downstream with a velocity slightly less than the local mean \bar{U}_x . Its center of rotation was observed to move on a line at a slight angle with respect to the flat plate wall (see Figure 12). Most of the time during its downstream movement, the vortex moved away from the wall; there were some cases, though, where it moved towards the wall.

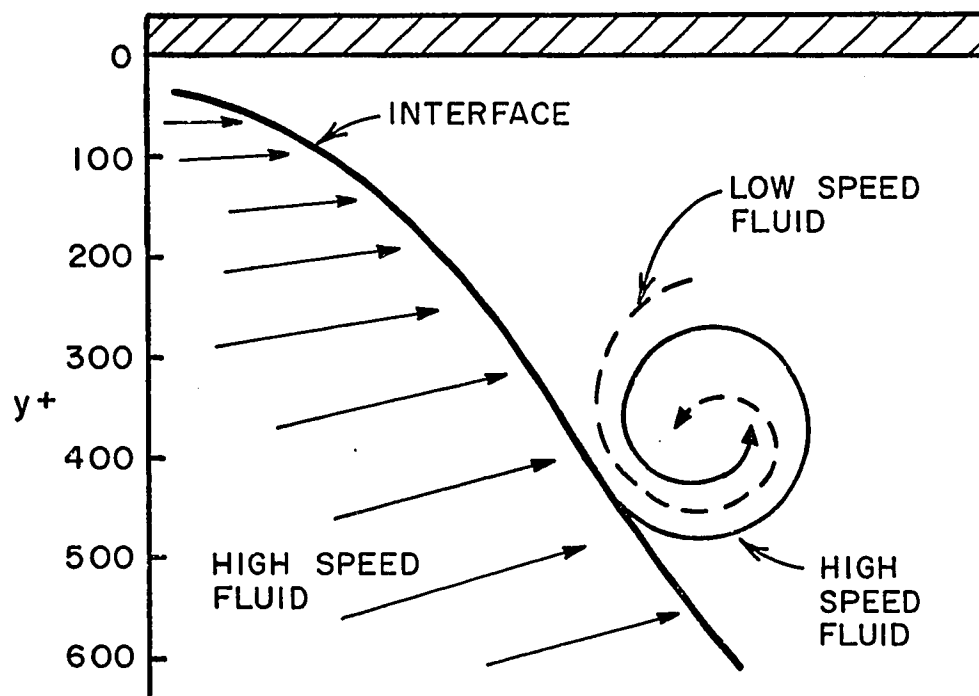


FIGURE 11. FORWARD TRANSVERSE VORTEX AND ITS RELATION TO LOW AND HIGH SPEED FLUID FLUIDS (CONVECTED VIEW)

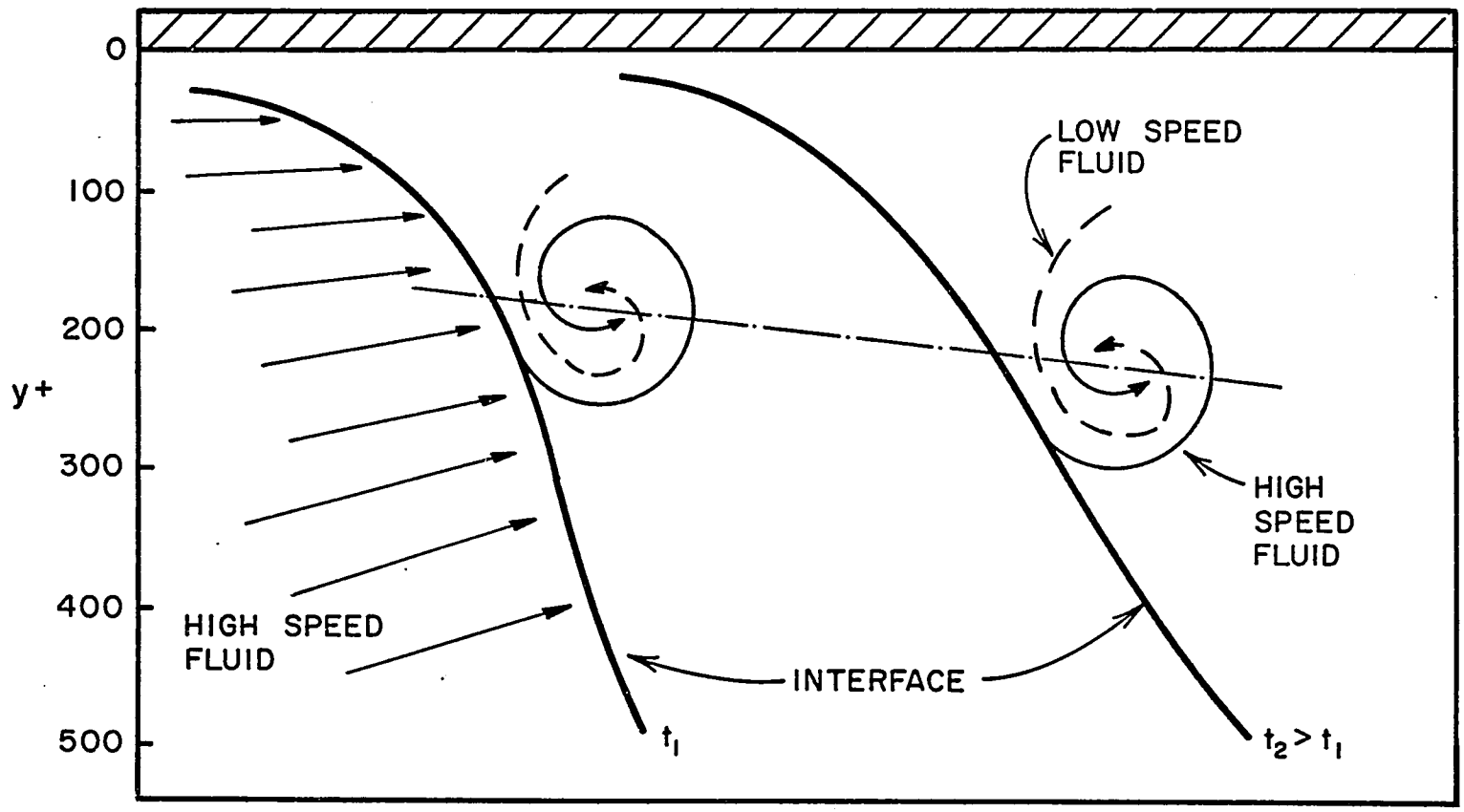


FIGURE 12. DOWNSTREAM MOTION OF A FORWARD TRANSVERSE VORTEX (CONVECTED VIEW)

It is to be emphasized at this point that the transverse vortex is composed of both high and low speed fluids. The "diameter" of the transverse vortex was changed slightly during its downstream movement. The word "diameter" should not be taken too literally; again a sharp distinct interface between the rotating and non-rotating fluids could not be established. The approximate scale of the transverse vortices was the equivalent of 200 y^+ units. They were observed to occur in a range of y^+ from about 200 to 400. In many cases two consecutive rotations were formed by the same region of high and low speed fluids. In some runs as many as five transverse vortices were observed while in others none were observed.

In a few cases where the angle of the entering high speed fluid was relatively large, a transverse vortex was formed rotating in the opposite direction. This will be referred to as a Reverse Transverse Vortex (RTV). Usually the formation of a RTV was followed by the formation of a FTV. Figure 13(a) is a sketch of a high speed fluid region entering with a large angle to the wall. Figure 13(b) illustrates the formation of a reverse transverse vortex followed by a forward one. Their scales were of the same order. Many of the ejections originating in the wall area occurred during the formation and downstream movement of these vortices. More about their relation to

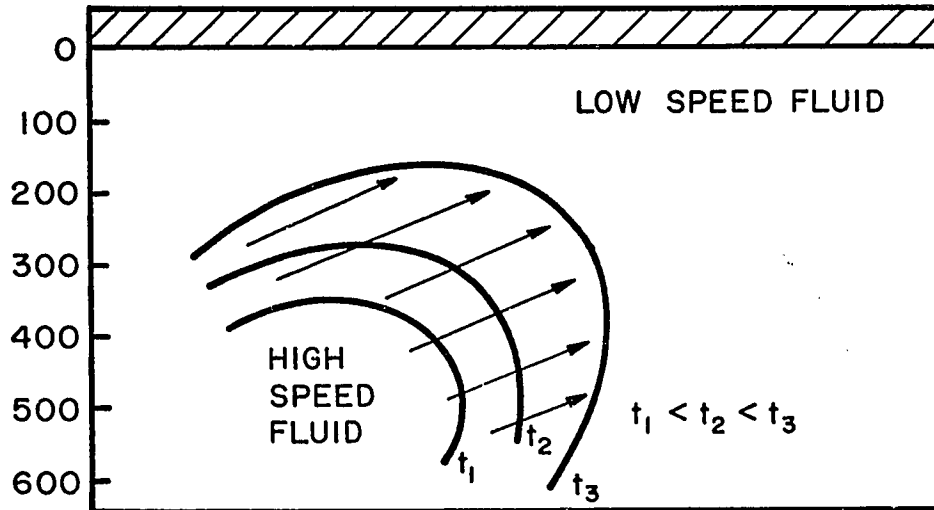


FIGURE 13(a). HIGH SPEED FLUID ENTERING AT A LARGE ANGLE TO THE WALL (CONVECTED VIEW)

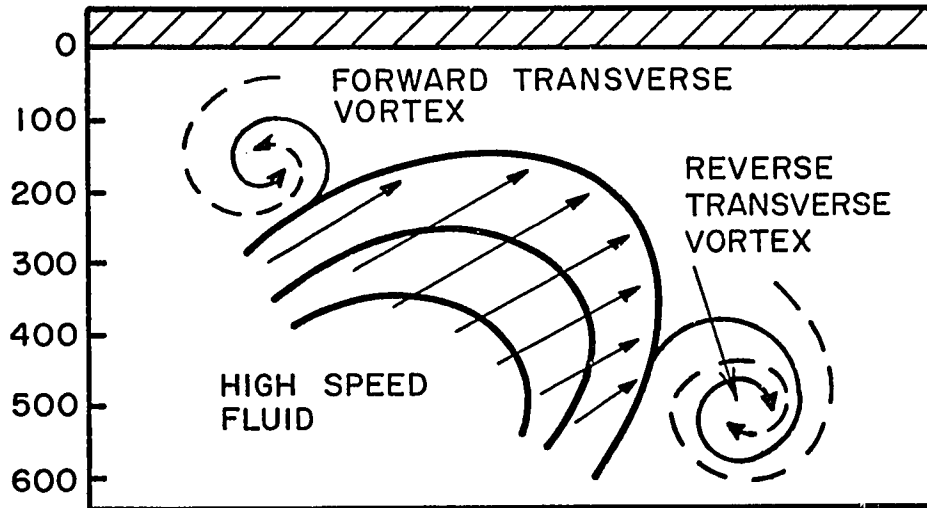


FIGURE 13(b). FORMATION OF A REVERSE TRANSVERSE VORTEX (CONVECTED VIEW)

the wall ejections will be said in the next section.

The flow field in the neighborhood of the transverse vortices was disturbed. In the convected view, the flow in the far outer region of the boundary layer looked like a flow around a cylinder with an axis parallel to the spanwise z -direction. After the transverse vortex has travelled some distance downstream its identity disappeared. A transverse vortex was always formed after the high speed fluid entered. For some time the two events occurred simultaneously, and then the transverse vortex persisted a little longer after the disappearance of the high speed fluid region.

The next major events were two very large scale motions, one directed toward the wall area (inflow) and the other away from it (outflow). The inflows were large masses of fluid usually moving downstream with a velocity approximately close to local mean \bar{U}_x and on an angle to the wall. In most cases they covered a range of y^+ from about 500 to 100, although a few fluid elements arrived as close as the wall area and sometimes even penetrated it (y^+ of about 40). Single fluid elements were observed to travel as much as 300 y^+ units. The flow inside the inflows was laminar-like; the marker particles moved towards the wall in almost parallel trajectories. Sometimes their trajectories were intermingling but no violent

motions were observed, see e.g., Figure 14(a) and 14(b). The nature and scales of the outflows were similar to those for the inflows. They usually occurred around a range of y^+ from about 200 to 500; they moved with a downstream velocity slightly smaller than the local mean \bar{U}_x . No violent motions or interactions inside them were observed. Most of the inflows observed occurred after a transverse vortex. Sometimes an inflow was followed by an outflow. There were motion picture runs where no outflows or inflows were observed.

Detailed Description of Events

In the previous section, a general overall picture was presented of the various events observed in the wall and the outer regions of the turbulent boundary layer. In this section the details of the flow phenomena mentioned before will be given. Each event will be described as it occurred in the observation of the motion picture runs. Actual fluid particle trajectories, geometry and scale of events, numerical values of instantaneous velocities and angles measured will be given for a number of runs. The mass of information contained in all the motion pictures obtained is too voluminous to be reported here. As every flow event will be described in detail, sufficient experimental information will be provided to support the argument. For reasons of preserving the continuity of this

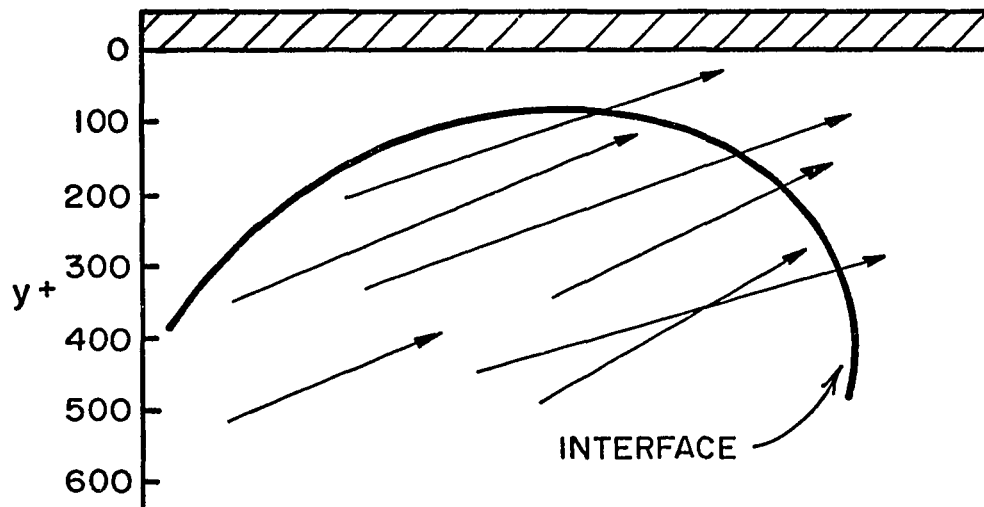


FIGURE 14(a). PARTICLE PATHS DURING A
LARGE SCALE INFLOW (CON-
VECTED VIEW)

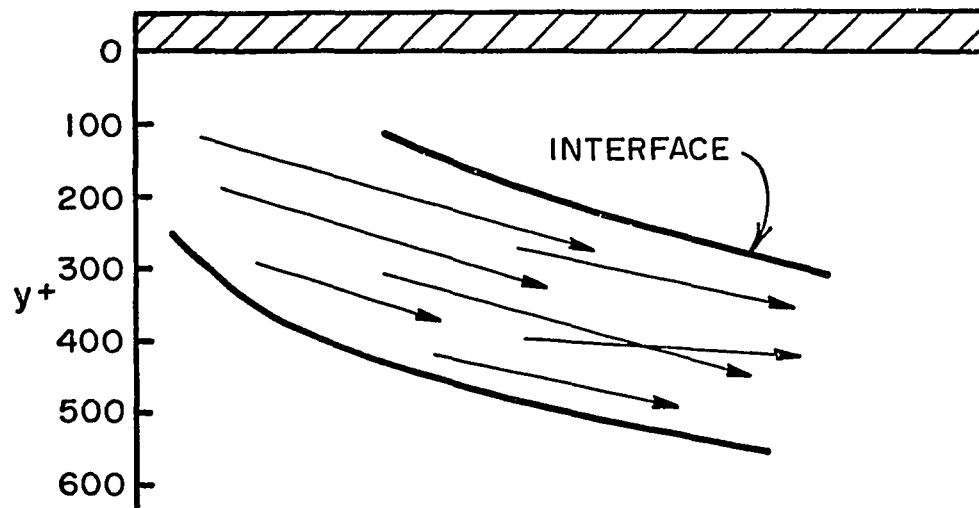


FIGURE 14(b). PARTICLE PATHS DURING A
LARGE SCALE OUTFLOW (CON-
VECTED VIEW)

text, additional information will be given in Appendix II.

The purpose of this investigation was to visually study the outer region of a turbulent boundary layer and to attempt to establish any connection between this region and the phenomena already known to occur in the wall area. The experimental technique used was directed mainly to the outer region, but it also permitted qualitative observation of those pertinent events of the wall region necessary to characterize the area. The study of the wall area by a similar experimental technique was the subject matter of the work of Corino (9). Reference to that work will frequently be made in a later section where the experimental results will be discussed and compared with other works.

Deceleration (Low Speed Fluid)

In the deterministic sequence of events, the first event involved a region of low speed fluid. In the motion picture runs studied, this was observed as a slow-down of the flow in the downstream direction. The convected camera view greatly facilitated its detection and discrimination from the subsequent events. Even at camera carriage velocities considerably lower than the local mean, several fluid particles appeared as stationary. In many cases the decelerated flow covered an area from the wall to about a y^+ of 500. It usually appeared in the field of view

following a region where the flow was moving with a velocity equal or higher than the mean \bar{U}_x . The lower speed fluid gradually replaced the higher. This decelerating effect was more pronounced in the outer region, where it appeared as moving as a plug flow. In Figures 15 and 16 the mean velocity profiles of two such decelerated regions are given; the averaging time was about 1 second, i.e., equal to the time the event lasted. The plug-like character of the flow can be clearly observed in these profiles ($70 \leq y^+ \leq 400$). The over-all measured and logarithmic mean velocity profiles are also given for comparison.

Although the present experimental technique did not allow reliable measurements of the velocity profile very close to the wall, it was visually observed that the plug-like character of the flow extended inside the wall area ($0 \leq y^+ \leq 70$). The disappearance of an appreciable velocity gradient through such a wide y^+ -region was an important characteristic of the flow and was a striking thing to observe. Inside the decelerated region the flow appeared laminar-like. Some of the fluid particles moved almost parallel to the flat plate wall, while the rest of them moved away or towards it on small angles. No violent motions or interactions inside this region were observed.

Figures 17 and 18 represent selected particle

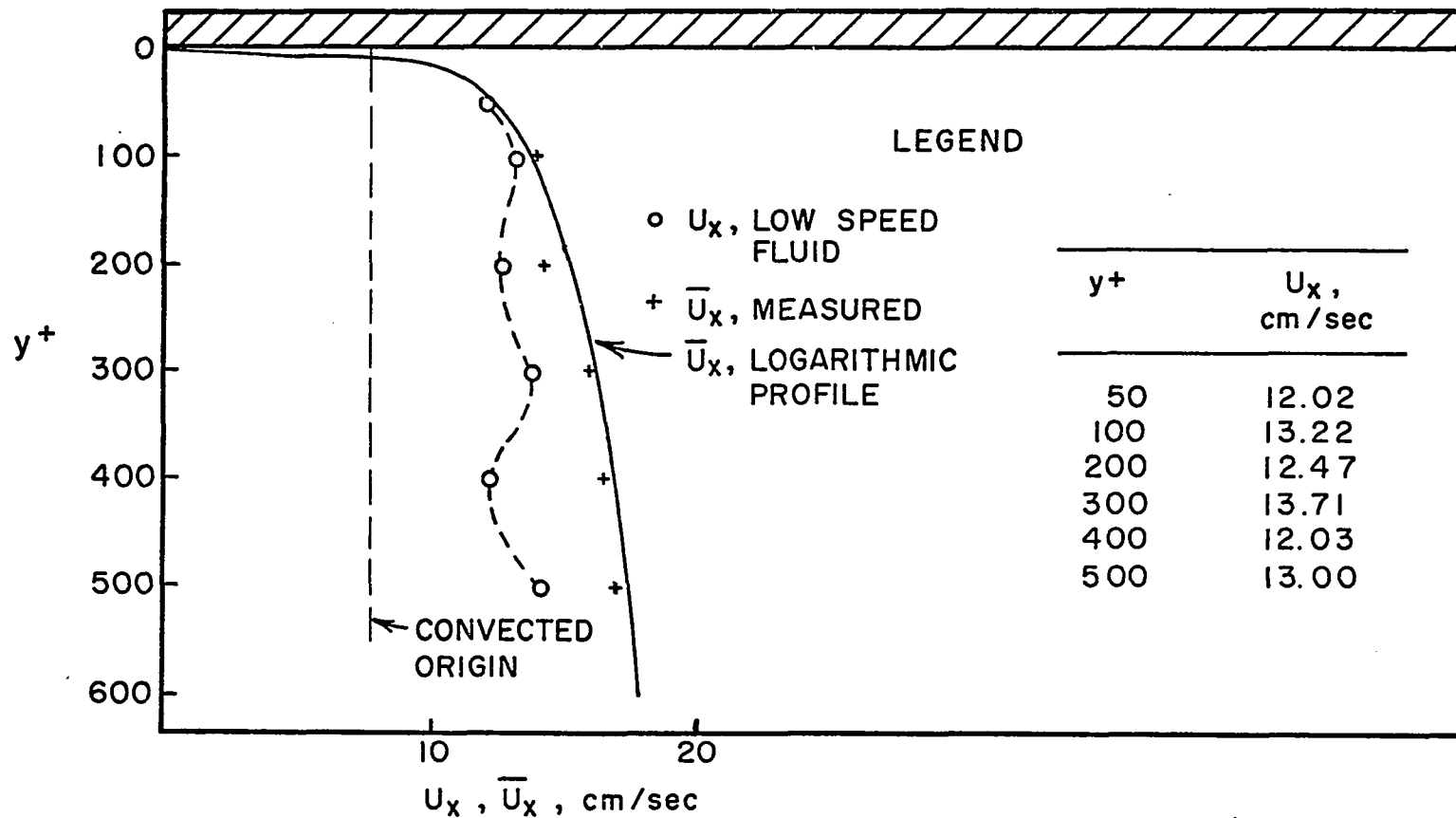


FIGURE 15. VELOCITY PROFILE OF A LOW SPEED FLUID REGION

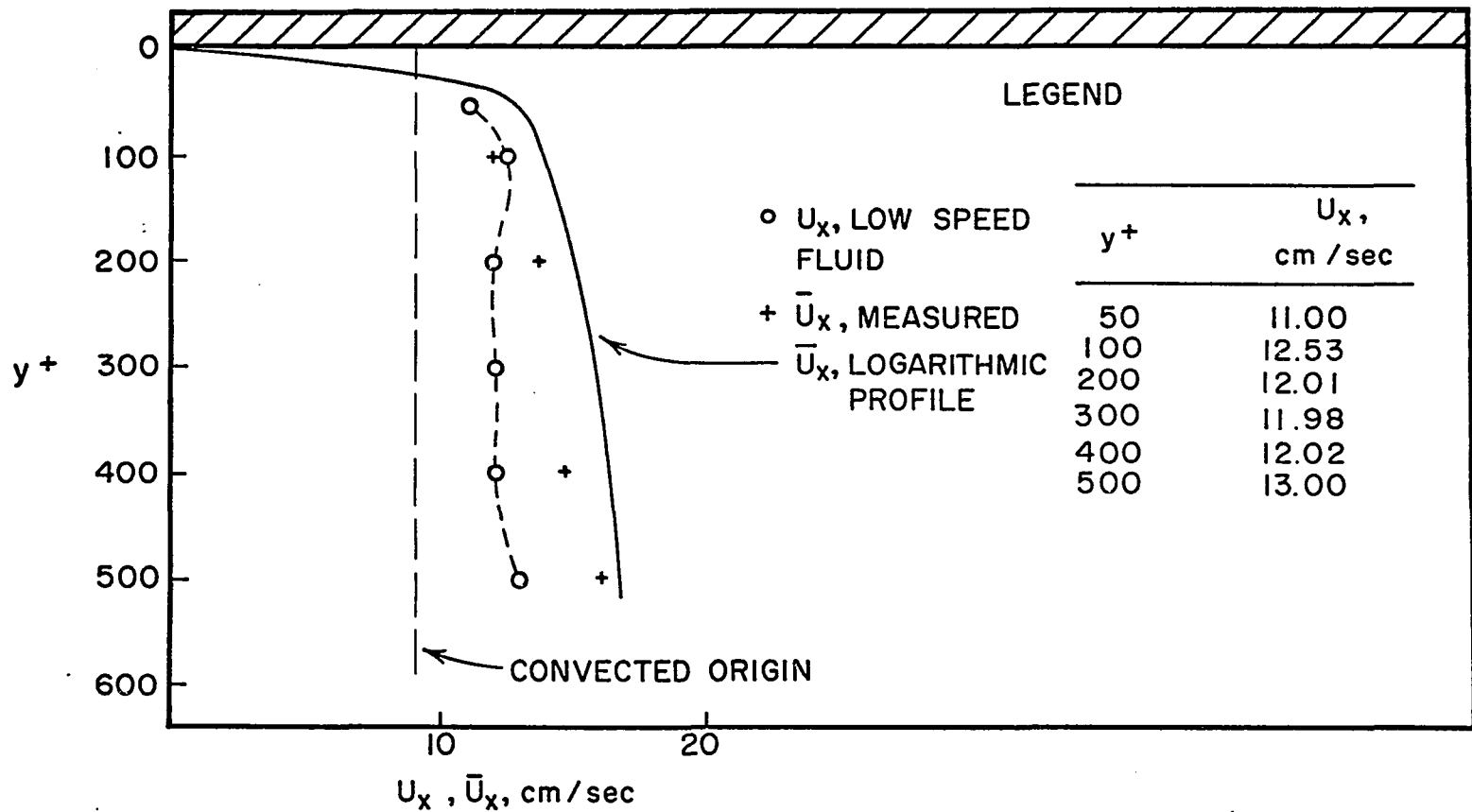


FIGURE 16. VELOCITY PROFILE OF A LOW SPEED FLUID REGION

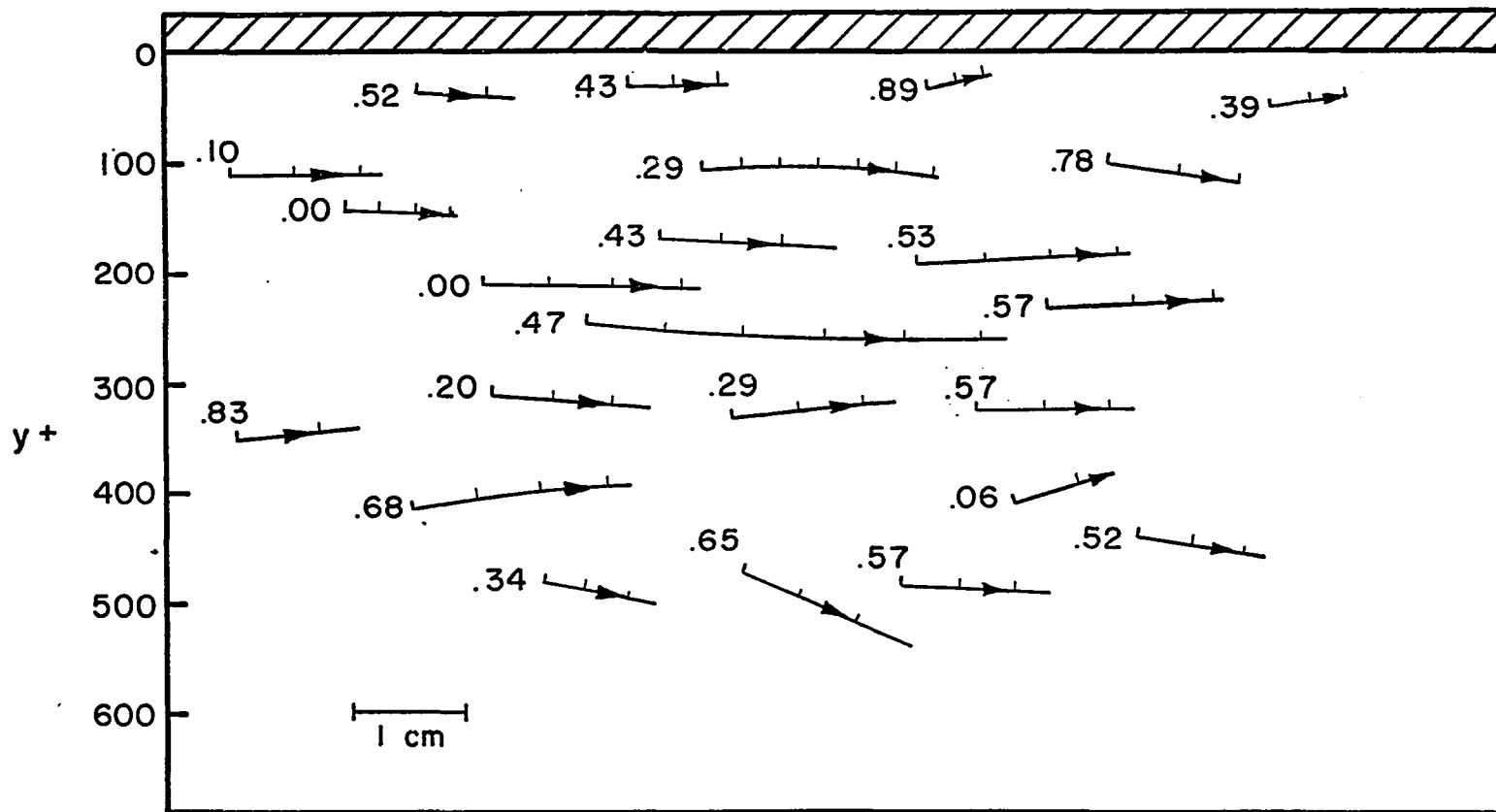


FIGURE 17. SELECTED PARTICLE PATHS DURING A DECELERATION EVENT (CONVECTED VIEW)

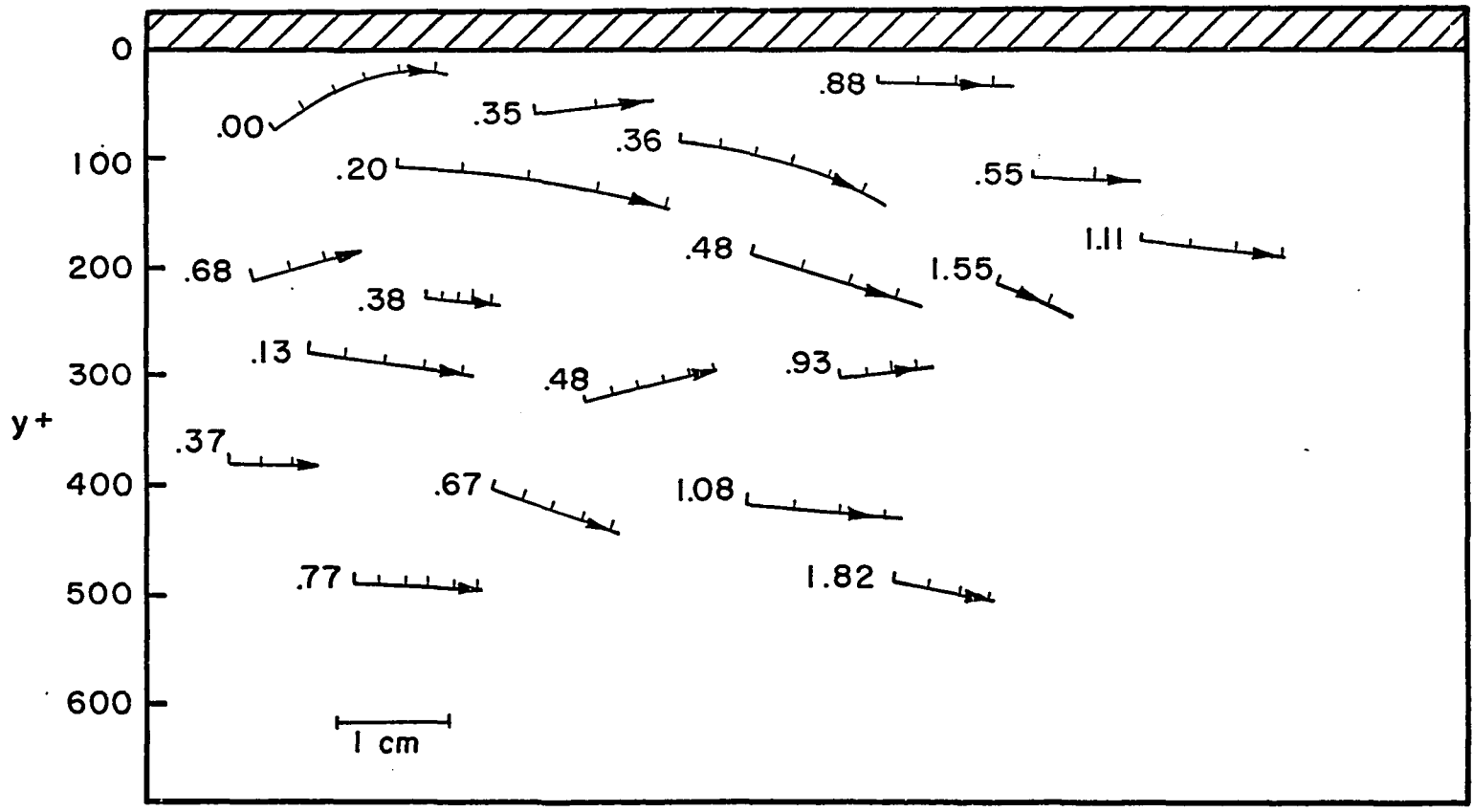


FIGURE 18. SELECTED PARTICLE PATHS DURING A DECELERATION EVENT (CONVECTED VIEW)

paths* of the deceleration events corresponding to Figures 15 and 16 respectively. When only the decelerated region was in view, in the convected observation, both the front (downstream) and back (upstream) parts of the region looked as if they were a plug flow. During the time the decelerated region was moving like a plug flow and before the entering high speed fluid had modified its character, one could observe a large y^+ -range of connected motions inside the decelerated region. Connected motions in the above sense manifested themselves as a large fluid region moving essentially as a unit. It was the global character between regions that was visually observed to be connected or disconnected and not the very localized one in the interface between regions.

The most important part of the low speed fluid region was the area close to the wall where the majority of ejections originated. As the high speed fluid entered the field of view, it modified asymmetrically the back part of the decelerated region [see e.g., Figure 10(b)]. It first accelerated the outer part of the low speed fluid more rapidly in comparison to the inner part of the low speed

*The numbers next to the particle paths represent times in seconds relative to a starting time in the process of observation, which was arbitrarily set equal to zero. The tic marks along the particle paths represent time intervals equal to 0.10 seconds.

fluid. Thus, as the high speed fluid moved toward the wall, it created a region of high shear. Near the wall the line of demarcation between the decelerated and accelerated regions was clearer. It was from this part of the low speed fluid, which was in a sense "trapped" between the solid wall and the high speed fluid region, that most of the ejections originated.

As the encroaching high speed fluid narrowed the y^+ -extent of the back part of the decelerated region continuously, one could clearly observe that the line of demarcation between decelerated and accelerated regions was at the same time a demarcation line between regions of connected motions. The onset of the ejection event marked the end of connected motions inside the low speed fluid region. At this point one could definitely observe the different character of the wall region from the outer flow. The ejections originated only in the wall area ($0 < y^+ \leq 70$) of the decelerated region and in only this area most of the interactions were observed. Since the ejections were basically small scale in nature, their penetration into the outer flow did not change significantly the line of demarcation between high and low speed fluid regions.

High Speed Fluid (Acceleration)

In most of the motion pictures studied a high speed fluid followed the deceleration. There were cases though

where an acceleration followed a large scale inflow or outflow. It usually entered at a y^+ of about 300 to 400 in the form of a bullet-like plug expanding as it moved downstream. This first part of the high speed fluid moved very fast in comparison to the decelerated fluid in front of it, and almost parallel to the wall. As soon as it entered, it interacted with the surrounding low speed fluid end, but a distinct sharp line of demarcation between the two did not exist. In Figures 19 and 20, two of the accelerations observed in the same motion picture run are presented; this is a convected view. The contour lines represent the approximate lines of demarcation between the high and low speed fluid areas. The traced arrows represent a number of selected particle trajectories (path lines). Additional figures for other runs are given in Appendix II.

The downstream expansion of the high speed fluid can be followed from the contour lines. The numbers next to them represent times in seconds relative to a starting time, in the process of observation, which it was arbitrarily set equal to zero. The numbers next to the particle paths represent times in seconds relative to the same zero starting time. The tic marks along the particle paths represent time intervals equal to 0.10 seconds. In the area of y^+ of about 300 to 400 the displacement of the

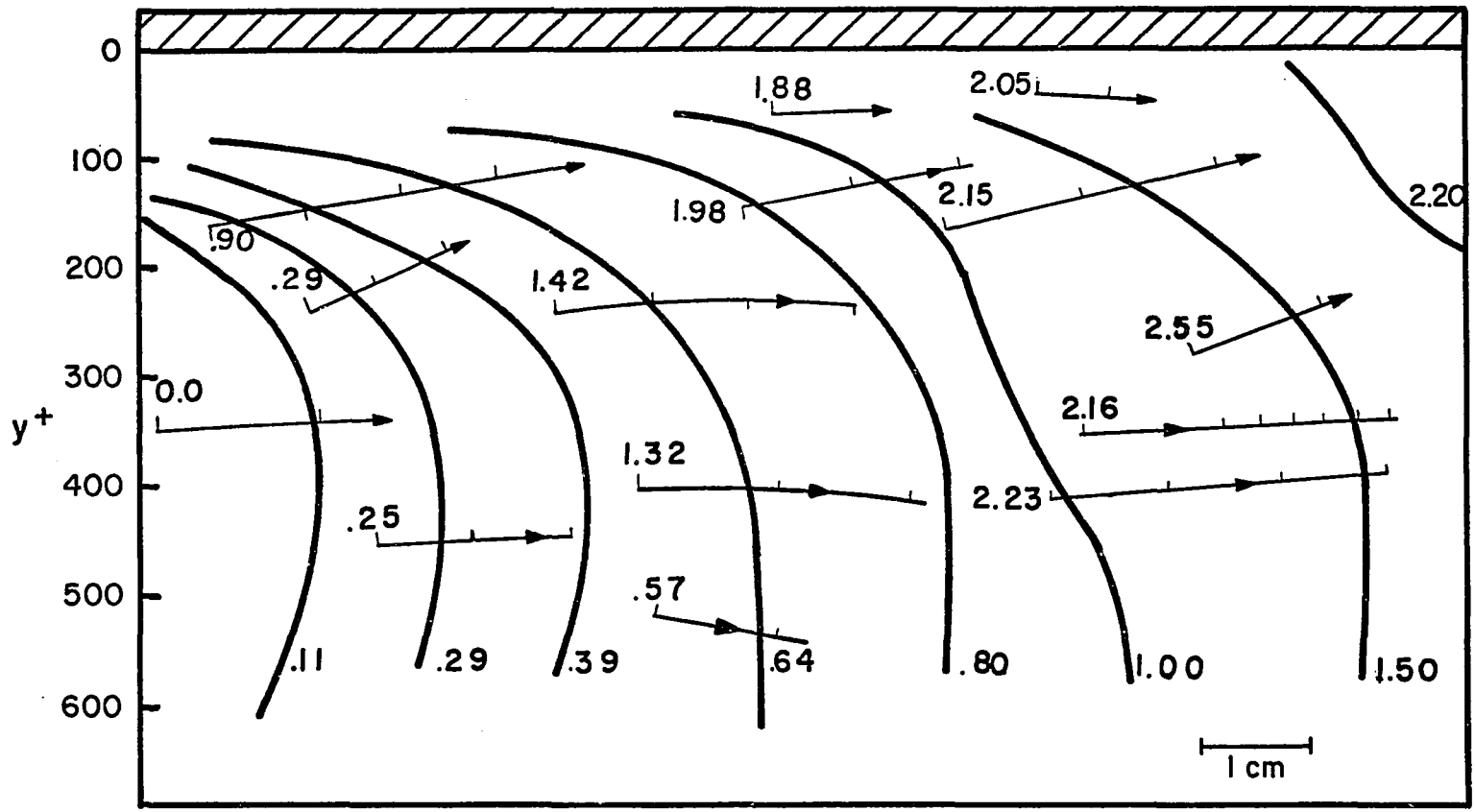


FIGURE 19. CONVICTED VIEW OF A DEVELOPING ACCELERATION EVENT

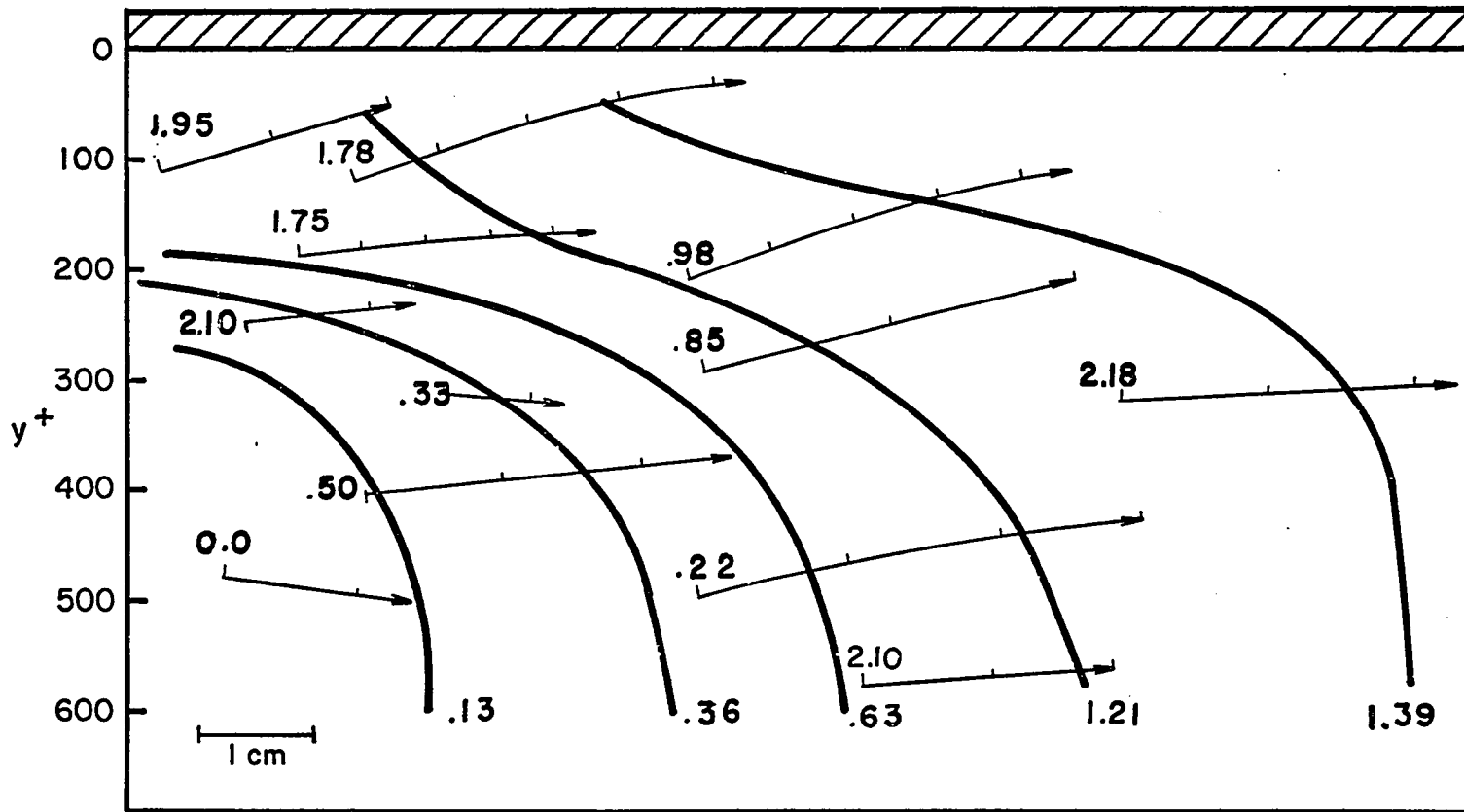


FIGURE 20. CONVICTED VIEW OF A DEVELOPING ACCELERATION EVENT

retarded fluid occurs faster. In the area closer to the wall the displacement takes place much slower, and it can be observed that for some time there is a region between the solid wall and the accelerated fluid of about $100 y^+$ units which contains only low velocity fluid. It is a region of high shear and the instantaneous velocity profile exhibits an inflection point. From the traced path lines the flow inside the accelerated region can be observed. The fluid particles move downstream and are directed wallward in a small angle (wallward flow); some few are directed outward (outward flow). The angles shown in this convected view have been intensified because of the downstream movement of the camera.

Tables 1 and 2 give numerical data on some of the particle paths; they correspond to Figures 19 and 20 respectively. The tabulated data refer to:

y_{or}^+, y_t^+ = y^+ distance at the starting and end points of the particle path line respectively.

\bar{y}^{\mp} = $1/2 (y_{or}^+ + y_t^+)$

$U_x(t)$ = instantaneous streamwise velocity of the particle while it moved from y_{or}^+ to y_t^+ .

$\bar{U}_x(\bar{y}^{\mp})$ = time average streamwise velocity at \bar{y}^{\mp} .

$u(t)$ = instantaneous streamwise velocity fluctuation obtained from $U_x(t) - \bar{U}_x(\bar{y}^{\mp})$.

$v(t)$ = instantaneous normal (y-direction) velocity fluctuation taken equal to the instantaneous normal velocity V .

TABLE 1

STUDY OF HIGH SPEED FLUID REGIONS (Run M-132)

| y_{or}^+ | y_t^+ | y^+ | $U_x(t)$, cm/sec | $\bar{U}_x(y^+)$, cm/sec | $u(t)$, cm/sec | $v(t)=V$ cm/sec | $-uv$, (cm/sec) ² | $-\frac{uv}{(U^*)^2}$ | U_t , cm/sec | ϕ_s or ϕ_e degrees |
|----------------------|---------|-------|----------------------|------------------------------|--------------------|--------------------|----------------------------------|-----------------------|-------------------|---------------------------------|
| <u>Wallward Flow</u> | | | | | | | | | | |
| 160 | 105 | 133 | 16.30 | 14.20 | 2.10 | -1.40 | 2.94 | 4.56 | 16.40 | 5.0 |
| 242 | 175 | 159 | 14.50 | 14.50 | 0.00 | -3.10 | 0.00 | 0.00 | 14.80 | 12.5 |
| 350 | 345 | 348 | 18.20 | 16.35 | 1.35 | -0.50 | 0.925 | 1.43 | 18.30 | 1.5 |
| 305 | 280 | 293 | 15.30 | 15.80 | -0.30 | -0.80 | -0.24 | -0.37 | 15.40 | 3.0 |
| 455 | 448 | 452 | 17.10 | 16.65 | 0.45 | -0.40 | 0.16 | 0.25 | 17.20 | 1.5 |
| 147 | 110 | 126 | 17.50 | 14.00 | 3.50 | -2.20 | 7.70 | 11.92 | 17.70 | 7.0 |
| 175 | 100 | 138 | 18.80 | 14.22 | 3.78 | -3.20 | 12.12 | 18.80 | 19.10 | 9.5 |
| 100 | 80 | 90 | 15.30 | 13.35 | 1.95 | -2.20 | 4.29 | 6.65 | 15.50 | 8.5 |
| 58 | 54 | 56 | 15.30 | 12.35 | 2.95 | -0.20 | 0.59 | 0.92 | 15.30 | 0.7 |
| 62 | 45 | 54 | 14.20 | | | -1.20 | | | 14.30 | 5.0 |
| <u>Outward Flow</u> | | | | | | | | | | |
| 42 | 45 | 43 | 14.35 | 11.75 | 2.60 | +0.50 | -1.30 | -2.01 | 14.40 | 2.0 |
| 400 | 416 | 408 | 19.45 | 16.63 | 2.82 | +0.70 | -1.97 | -3.06 | 19.50 | 2.5 |
| 514 | 540 | 527 | 15.00 | 17.15 | -2.15 | +1.70 | 2.66 | 4.12 | 15.20 | 6.5 |
| 514 | 544 | 529 | 23.40 | 17.20 | 6.20 | +2.60 | -16.11 | -25.00 | 23.50 | 6.5 |

TABLE 2

STUDY OF HIGH SPEED REGIONS (Run M-132)

| y_{or}^+ | y_t^+ | \bar{y}^+ | $U_x(t)$, cm/sec | $\bar{U}_x(\bar{y}^+)$, cm/sec | $u(t)$, cm/sec | $v(t)=V$ cm/sec | $-uv$, (cm/sec) ² | $-\frac{uv}{(U^*)^2}$ | U_t , cm/sec | ϕ_a or ϕ_e degrees |
|----------------------|---------|-------------|----------------------|------------------------------------|--------------------|--------------------|----------------------------------|-----------------------|-------------------|---------------------------------|
| <u>Wallward Flow</u> | | | | | | | | | | |
| *115 | 54 | 85 | 17.00 | 13.32 | 3.68 | -3.00 | 11.04 | 17.10 | 17.30 | 10.0 |
| *120 | 55 | 87 | 16.60 | 13.33 | 3.27 | -2.60 | 8.50 | 13.20 | 16.80 | 8.5 |
| * 55 | 53 | 44 | 15.70 | 11.75 | 3.25 | -1.20 | 3.90 | 6.05 | 15.80 | 4.2 |
| 188 | 168 | 178 | 18.90 | 14.85 | 4.05 | -1.00 | 4.05 | 6.28 | 19.00 | 3.3 |
| 300 | 266 | 283 | 18.95 | 15.75 | 4.20 | -1.20 | 5.04 | 7.82 | 19.10 | 4.0 |
| 325 | 305 | 315 | 21.80 | 16.00 | 5.80 | -1.00 | 5.80 | 9.00 | 22.00 | 2.5 |
| 495 | 428 | 462 | 19.40 | 16.85 | 2.55 | -2.00 | 5.10 | 7.91 | 19.50 | 6.2 |
| 450 | 433 | 442 | 20.00 | 16.65 | 3.35 | -0.60 | 2.01 | 3.12 | 20.10 | 1.7 |
| 580 | 566 | 573 | 19.50 | 17.50 | 2.00 | -0.90 | 1.80 | 2.79 | 19.60 | 2.8 |
| <u>Outward Flow</u> | | | | | | | | | | |
| 95 | 120 | 107 | 15.0 | 13.75 | 1.25 | +1.60 | -1.00 | -3.10 | 15.10 | 6.0 |
| 384 | 412 | 398 | 17.0 | 16.44 | 0.56 | +1.40 | -0.79 | -1.23 | 17.10 | 5.0 |
| 312 | 320 | 316 | 15.20 | 16.00 | -0.80 | +0.60 | 0.48 | 0.74 | 15.30 | 2.2 |
| 475 | 504 | 490 | 22.40 | 16.70 | 5.70 | +2.30 | -13.10 | -20.30 | 22.50 | 5.8 |

$uv, uv/(U^*)^2$ = instantaneous and normalized with the friction velocity U^* , products of the velocity fluctuations $u(t)$ and $v(t)$, respectively.

U_y = actual (non-convected) particle velocity; its direction is the tangent of the particle path line at the point \bar{y}^+ .

ϕ_s, ϕ_e = actual (non-convected) wallward and outward angles of the velocity vector U_y with respect to the wall, respectively.

These tables are not and were not meant to be complete; they show the general trend and provide sufficient supporting argument for the qualitative characterization of the event in question. For the purpose of this work, where complete quantitative measurements were not sought, numerical data like the above are considered to be sufficient. After the events have been detected and their general characteristics established, other more convenient methods, such as conditional sampling of hot-film data, can be applied for their complete quantitative determination.

As far as the characterization of a flow regime as a "High Speed Fluid" is concerned, it is emphasized that its velocity was observed to be higher than the velocity of the decelerated region upstream of it that characterized it as a High Speed Fluid region. The average velocity profile during the time period when the High Speed Fluid event was occurring was measured. There were cases where this conditional or "pseudo-instantaneous" velocity profile was higher than the local mean $\bar{U}_x(y^+)$ and other cases where it

was found to be lower than it. Figures 21 and 22 represent two such cases, where both the measured local mean $\bar{U}_x(y^+)$ for the whole length of the motion picture and the logarithmic profile are given for comparison. The conditional time average for the acceleration event was about 1.5 sec. From Figure 21 it can be seen that even at $y^+ = 100$, the local \bar{U}_x of the High Speed Fluid is about 26 percent higher than the local mean. In both these figures, the plug-like character of the high speed fluid region throughout a y^+ -area of about 400 can be observed.

In Figure 21 the velocity profile of the decelerated region from Figure 15 (it occurred just before the acceleration) is reproduced for comparison. It can be observed that at $y^+ = 400$ the streamwise velocity of the accelerated region is about 55 percent higher than that of the deceleration fluid. In the convected view of the travelling camera this difference in velocity is intensified; for the same $y^+ = 40$ the velocity of the acceleration appeared 2.5 times higher than the one of the deceleration. This was the reason the entering accelerated motion could be very clearly observed in the motion pictures. In Tables 3 through 5, data of High Speed fluid regions are given from a number of runs. Additional data and qualitative information obtained from other runs can be found in Appendix II.

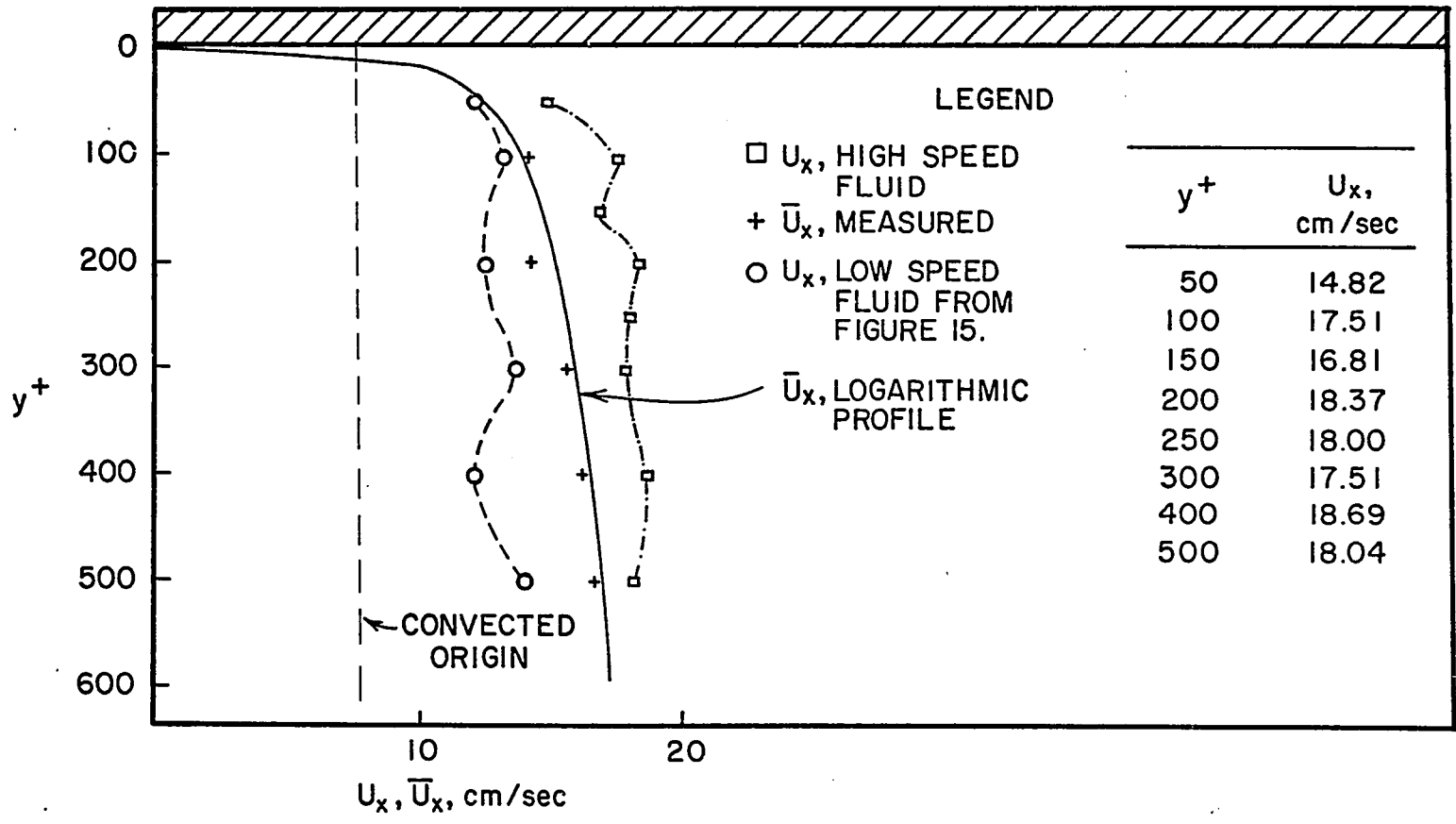


FIGURE 21. VELOCITY PROFILE OF A HIGH SPEED FLUID MOVING FASTER THAN THE MEAN \bar{U}_x

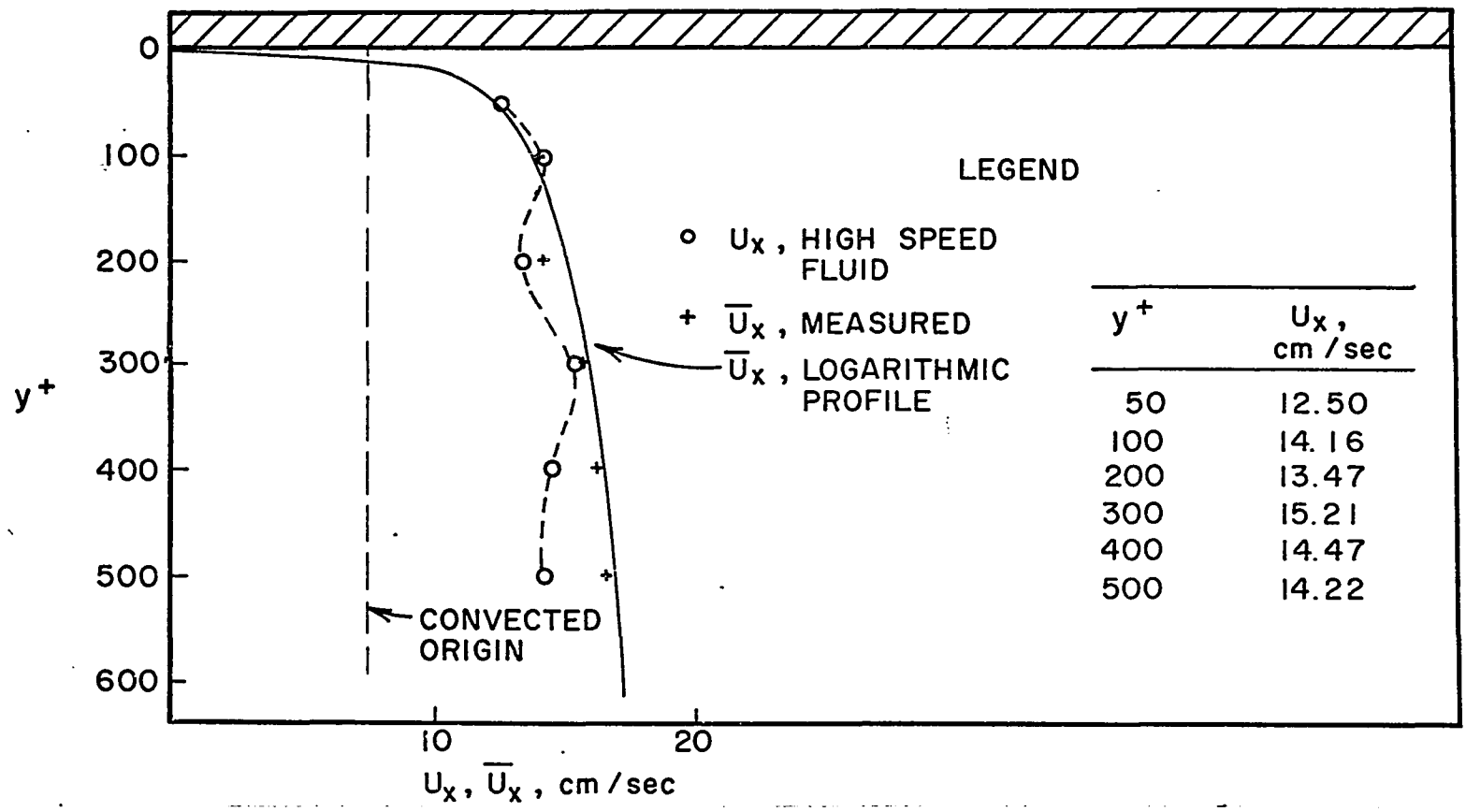


FIGURE 22. VELOCITY PROFILE OF A HIGH SPEED FLUID MOVING SLOWER THAN THE MEAN

TABLE 3

STUDY OF HIGH SPEED FLUID REGIONS (Run M-104)

| y_{or}^+ | y_t^+ | \bar{y}^+ | $U_x(t),$ cm/sec | $\bar{U}_x(\bar{y}^+),$ cm/sec | $u(t),$ cm/sec | $v(t)=V$ cm/sec | $-uv,$ (cm/sec) ² | $-\frac{uv}{(U^*)^2}$ | $U_t,$ cm/sec | ϕ_s or ϕ_e Degrees |
|----------------------|---------|-------------|---------------------|-----------------------------------|-------------------|--------------------|---------------------------------|-----------------------|------------------|---------------------------------|
| <u>Wallward Flow</u> | | | | | | | | | | |
| 330 | 250 | 290 | 16.00 | 15.35 | 0.65 | -0.60 | 0.39 | 0.604 | 16.10 | 2.3 |
| * 60 | 48 | 54 | 14.60 | 12.00 | 2.60 | -0.80 | 2.08 | 3.18 | 14.70 | 3.0 |
| *112 | 94 | 103 | 14.30 | 13.35 | 0.95 | -0.30 | 0.29 | 0.44 | 14.35 | 1.5 |
| 358 | 290 | 324 | 13.90 | 15.70 | -1.80 | -1.30 | -2.34 | -3.57 | 14.00 | 5.5 |
| 385 | 292 | 338 | 15.10 | 15.80 | -0.70 | -1.50 | -1.05 | -1.61 | 15.20 | 6.0 |
| 404 | 344 | 374 | 15.95 | 15.95 | 0.00 | -1.30 | 0.00 | 0.00 | 16.10 | 5.0 |
| <u>Outward Flow</u> | | | | | | | | | | |
| 224 | 258 | 242 | 17.40 | 15.05 | 2.35 | 0.60 | -1.38 | -2.11 | 17.50 | 2.0 |

TABLE 4

STUDY OF HIGH SPEED FLUID REGIONS (Run M-132)

| y_{or}^+ | y_t^+ | \bar{y}^+ | $U_x(t)$, cm/sec | $\bar{U}_x(\bar{y}^+)$, cm/sec | $u(t)$, cm/sec | $v(t)=V$ cm/sec | $-uv$ (cm/sec) ² | $-\frac{uv}{(U^*)^2}$ | U_t , cm/sec | ϕ_s or ϕ_e degrees |
|----------------------|---------|-------------|----------------------|------------------------------------|--------------------|--------------------|--------------------------------|-----------------------|-------------------|---------------------------------|
| <u>Wallward Flow</u> | | | | | | | | | | |
| *92 | 70 | 81 | 13.60 | 13.00 | 0.60 | -0.60 | 0.36 | 0.55 | 13.70 | 2.7 |
| 120 | 104 | 112 | 13.80 | 13.30 | 0.50 | -0.70 | 0.35 | 0.54 | 13.90 | 3.0 |
| <u>Outward Flow</u> | | | | | | | | | | |
| 200 | 280 | 240 | 12.10 | 14.70 | -2.60 | +1.80 | 4.18 | 6.42 | 12.20 | 8.2 |
| 280 | 342 | 311 | 14.40 | 15.35 | -0.95 | +1.20 | 1.14 | 1.75 | 14.50 | 5.0 |
| 312 | 346 | 329 | 14.45 | 15.50 | -1.05 | +1.30 | 1.36 | 2.09 | 14.50 | 5.5 |
| 396 | 400 | 398 | 22.70 | 16.20 | 6.50 | +0.40 | -2.60 | -3.99 | 22.80 | 1.0 |
| 228 | 236 | 232 | 14.40 | 14.65 | -0.25 | +0.35 | 0.87 | 1.34 | 14.50 | 1.5 |

TABLE 5

STUDY OF HIGH SPEED FLUID REGIONS (Run M-134)

| y_{or}^+ | y_t^+ | \bar{y}^+ | $U_x(t)$, cm/sec | $\bar{U}_x(\bar{y}^+)$ cm/sec | $u(t)$ cm/sec | $v(t)=V$ cm/sec | $-uv$, (cm/sec) ² | $-\frac{uv}{(U^*)^2}$ | U_t , cm/sec | ϕ_s degrees |
|----------------------|---------|-------------|----------------------|----------------------------------|------------------|--------------------|----------------------------------|-----------------------|-------------------|---------------------|
| <u>Wallward Flow</u> | | | | | | | | | | |
| * 80 | 50 | 65 | 13.60 | 12.50 | 1.10 | -2.40 | 2.64 | 4.13 | 13.80 | 10.0 |
| 300 | 326 | 168 | 15.10 | 13.70 | 2.40 | -1.80 | 4.32 | 6.76 | 15.20 | 6.7 |
| 300 | 250 | 275 | 16.43 | 14.70 | 1.73 | -2.20 | 3.81 | 5.96 | 16.60 | 7.5 |
| 250 | 200 | 225 | 16.20 | 14.35 | 1.85 | -1.40 | 2.59 | 4.06 | 16.30 | 5.0 |
| 495 | 380 | 438 | 16.60 | 16.00 | 0.60 | -3.35 | 2.01 | 3.15 | 17.00 | 11.5 |
| 230 | 104 | 167 | 15.10 | 13.70 | 1.40 | -1.00 | 1.40 | 2.19 | 15.30 | 7.5 |
| * 70 | 62 | 66 | 14.80 | 12.50 | 2.30 | -0.45 | 1.04 | 1.60 | 14.85 | 1.7 |
| *138 | 88 | 113 | 16.70 | 12.80 | 3.90 | -2.30 | 8.95 | 14.00 | 16.90 | 7.0 |
| * 88 | 50 | 69 | 13.60 | 12.60 | 1.00 | -2.60 | 2.60 | 4.07 | 13.90 | 10.5 |
| * 50 | 40 | 45 | 13.90 | 11.50 | 2.40 | -0.60 | 1.44 | 0.23 | 14.00 | 2.3 |
| * 50 | 50 | 50 | 14.76 | 11.60 | 3.16 | 0.00 | 0.00 | 0.00 | 14.76 | 0.0 |
| * 65 | 65 | 65 | 15.01 | 12.50 | 2.51 | 0.00 | 0.00 | 0.00 | 15.01 | 0.0 |
| 188 | 100 | 144 | 14.40 | 13.35 | 1.05 | -2.40 | 2.52 | 3.94 | 14.60 | 9.2 |
| *100 | 50 | 75 | 14.80 | 12.60 | 2.20 | -2.60 | 5.72 | 8.95 | 15.10 | 9.7 |
| 240 | 224 | 232 | 13.30 | 14.45 | -1.15 | -0.90 | -1.04 | -1.60 | 13.40 | 3.7 |
| 288 | 284 | 286 | 14.40 | 15.00 | -0.60 | -0.30 | -0.18 | -0.28 | 14.45 | 1.3 |
| 250 | 230 | 240 | 13.40 | 14.55 | -1.15 | -0.80 | -0.92 | -1.44 | 13.50 | 3.5 |
| 325 | 305 | 315 | 15.70 | 15.30 | 0.40 | -0.60 | 0.24 | 0.36 | 15.80 | 2.5 |
| 516 | 462 | 489 | 15.50 | 15.80 | 0.30 | -2.00 | 0.60 | 0.94 | 15.70 | 7.5 |
| 462 | 428 | 445 | 14.80 | 15.60 | 0.80 | -1.80 | 1.44 | 2.25 | 14.90 | 7.0 |

TABLE 5--(continued)

| y_{or}^+ | y_t^+ | \bar{y}^+ | $U_x(t)$, cm/sec | $\bar{U}_x(\bar{y}^+)$ cm/sec | $u(t)$, cm/sec | $v(t)=V$ cm/sec | $-uv$, (cm/sec) ² | $-\frac{uv}{(U^*)^2}$ | U_t , cm/sec | ϕ degrees |
|---------------------|---------|-------------|----------------------|----------------------------------|--------------------|--------------------|----------------------------------|-----------------------|-------------------|-------------------|
| <u>Outward Flow</u> | | | | | | | | | | |
| 75 | 84 | 80 | 16.00 | 12.65 | 3.35 | +0.50 | -1.67 | -2.62 | 16.10 | 1.5 |
| 134 | 176 | 150 | 16.30 | 13.40 | 2.90 | +1.60 | -4.64 | -7.27 | 16.40 | 5.7 |
| 120 | 134 | 137 | 11.80 | 13.30 | -1.50 | +1.20 | 1.80 | 2.82 | 11.90 | 5.7 |
| 320 | 350 | 335 | 13.20 | 15.40 | -2.20 | +1.90 | 4.18 | 6.56 | 13.30 | 8.0 |

Sweep Event

The part of the accelerated fluid approaching the wall region and penetrating inside this region is of particular importance for the phenomena of this area. As was mentioned before, the demarcation line between high and low speed fluids close to the wall appeared sharper than for the outer flow. In Figure 23 a sketch is given illustrating the convected view of the sweep event. In Tables 2, 3, 4, and 5, the wallward flows approaching and penetrating the wall region are marked with an asterisk. Their wallward angles are generally smaller than those for the high speed fluid of the outer region. When a wall ejection occurred, it was the part of the accelerated region close to the wall which interacted with the ejected fluid particles and swept them downstream. The largest wallward angle observed for the sweeps was 10 degrees and the smallest 0 degrees (flow parallel to the wall). Although the sweep event was an integral part of the accelerated region, it was its distinct role in the wall area mechanism that distinguished it from the rest of the High Speed fluid.

Ejection Event

Associated with the accelerations was the ejection event. As the high speed fluid entered from upstream, it interacted and accelerated the fluid in the decelerated region in front of it. The accelerating action of the high

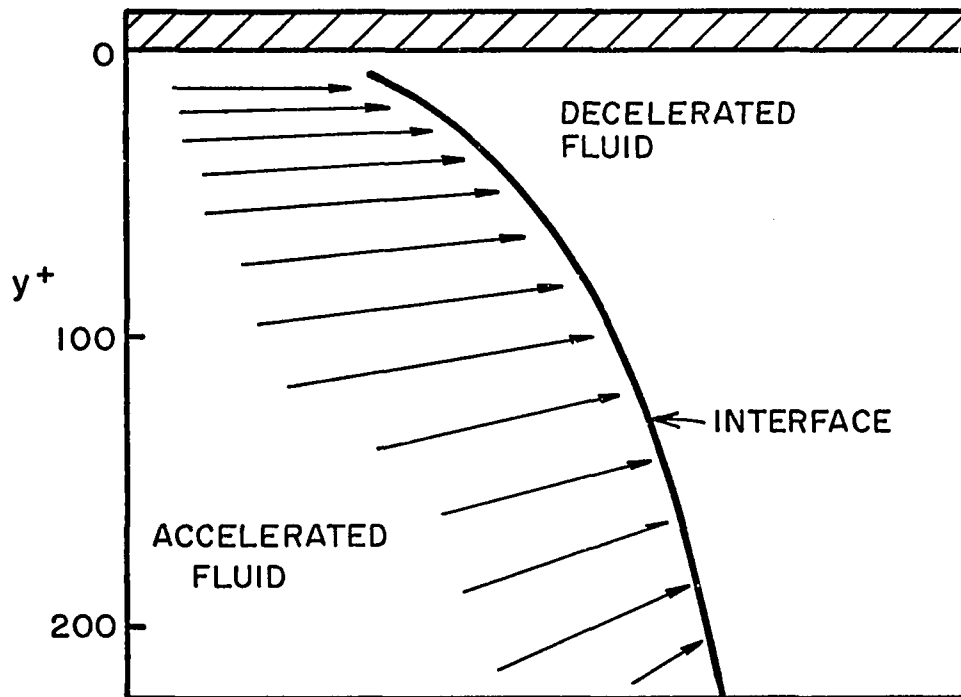


FIGURE 23. ILLUSTRATION OF SWEEP EVENT
(CONVECTED VIEW)

speed fluid was more pronounced in the outer region. Moving towards the wall, where the retarded fluid has a lower velocity and the high speed fluid displaces it more slowly, the accelerating effect was less effective. In this region the line of demarcation between low and high speed fluids was clearer. The ejection event occurred when a high shear layer was established between the two regions. The ejected fluid originated in the decelerated region. Many times the ejected fluid did not interact with the surrounding low speed fluid, and it continued moving outward, even penetrating the region of the high speed fluid.

In several instances during the time of ejection, fluid particles originating in the accelerated region moved on a slight angle towards the wall, passing very close to the ejected ones and not interacting with them. Apparently they were on different xy-planes separated in the transverse z-direction (two-layer velocity effect). In a few occasions, the ejected fluid element after travelling some y^+ -distance of about 30-40 units, turned back towards the wall, completed a loop and finally was swept downstream by the advancing high speed fluid.

In Figure 24 such a fluid element loop and a two-layer velocity effect are illustrated. In Table 6 a summary of the data of wall area ejections is presented. From the sign of the streamwise velocity fluctuation $u(t)$,

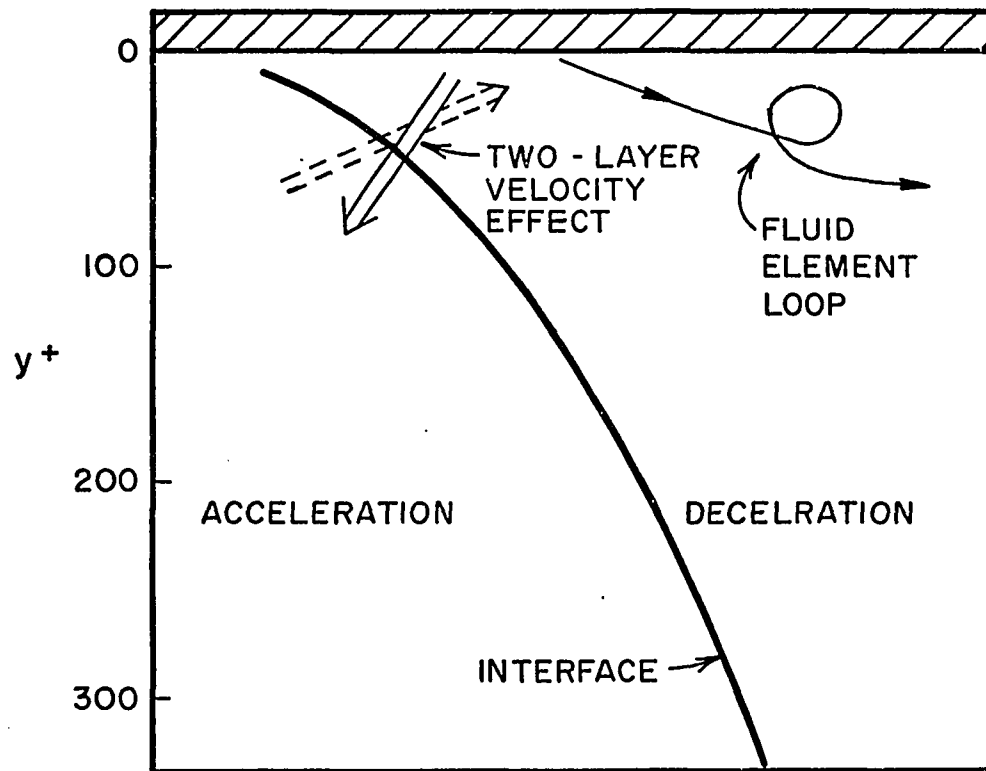


FIGURE 24. ILLUSTRATION OF A COMPLETE FLUID ELEMENT LOOP (CONVECTED VIEW)

TABLE 6

WALL AREA EJECTIONS

| Run No. | y_{or}^+ | y_t^+ | \bar{y}^+ | $U_x(t)$, cm/sec | $\bar{U}_x(\bar{y}^+)$ cm/sec | $u(t)$, cm/sec | $v(t)=V$ cm/sec | $-uv$ (cm/sec) ² | $-\frac{uv}{(U^*)^2}$ | U_t , cm/sec | ϕ_e degrees |
|---|------------|---------|-------------|----------------------|----------------------------------|--------------------|--------------------|--------------------------------|-----------------------|-------------------|---------------------|
| M-132 | 38 | 66 | 52 | 9.70 | 12.25 | -2.55 | 3.60 | 9.17 | 14.25 | 10.30 | 20 |
| | 38 | 100 | 69 | 9.40 | 12.82 | -3.42 | 2.00 | 6.84 | 11.78 | 9.60 | 12 |
| | 70 | 100 | 85 | 10.00 | 13.35 | -3.35 | 1.45 | 4.86 | 7.55 | 10.15 | 8.2 |
| | 42 | 45 | 43 | 14.33 | 11.75 | 2.60 | 0.50 | -1.30 | -2.01 | 14.40 | 2.0 |
| M-133 | 28 | 46 | 37 | 1.60 | 11.00 | -9.40 | 0.80 | 7.52 | 11.80 | 1.65 | 26.0 |
| | 38 | 50 | 44 | 2.10 | 11.22 | -9.12 | 0.50 | 4.56 | 7.00 | 2.20 | 6.5 |
| | 50 | 94 | 72 | 5.80 | 11.81 | -6.01 | 1.60 | 9.62 | 15.05 | 6.00 | 15.5 |
| M-134 | 30 | 85 | 54 | 8.50 | 11.15 | -2.65 | 2.20 | 5.84 | 9.14 | 8.80 | 14.5 |
| | 40 | 65 | 53 | 10.90 | 11.15 | -1.25 | 2.60 | 3.25 | 5.08 | 11.20 | 13.0 |
| | 67 | 142 | 105 | 9.50 | 12.00 | -2.50 | 5.70 | 14.28 | 22.58 | 11.10 | 31.0 |
| M-104 | 5 | 58 | | | | | | | | | |
| | 31 | 66 | | | | | | | | | |
| | 31 | 170 | | | | | | | | | |
| | 23 | 54 | | | | | | | | | |
| | 31 | 62 | | | | | | | | | |
| Five wall ejections, not analyzed in detail; data available in Appendix II. | | | | | | | | | | | |
| M-137 | 46 | 96 | | | | | | | | | |
| | 27 | 81 | | | | | | | | | |
| | 28 | 74 | | | | | | | | | |
| | 27 | 120 | | | | | | | | | |
| | 38 | 227 | | | | | | | | | |
| Five wall ejections, not analyzed in detail; data available in Appendix II. | | | | | | | | | | | |
| M-138 | 20 | 60 | | | | | | | | | |
| | 30 | 166 | | | | | | | | | |
| | 12 | 25 | | | | | | | | | |
| | 36 | 80 | | | | | | | | | |
| Four wall ejections, not analyzed in detail; data available in Appendix II. | | | | | | | | | | | |

it is clear that the ejections originated in a decelerated region. The largest outward angle observed was 31 degrees and the smallest 6.5 degrees. The ejection velocities U_t , were smaller than the local \bar{U}_x . An important point is that the magnitude of the normalized instantaneous Reynolds stress $(uv)/(U^*)^2$ is many times larger than the corresponding mean local value. This point will be further discussed in the next section.

Transverse Vortices

The single most important event observed in the outer region of the turbulent boundary layer was the transverse vortex. Previously, in the overall description of the events, the general characteristics and the relation of these vortices to the high speed fluid regions were mentioned. Sketches were used to point out their salient features. In this section actual experimental measurements and fluid particles paths will be presented for a number of motion picture runs. Additional measurements will be given in Appendix II. For the sake of continuity, some key observations mentioned before will be repeated.

All the transverse vortices observed in the various motion picture runs were the result of a large scale interaction between the high and low speed fluid in the outer region. The stages and flow conditions under which

the vortices were formed pointed to a Helmholtz instability as the causative factor. In the description of the high speed fluid region, the experimental data presented showed that the accelerated fluid areas in several instances had velocities as much as 55 percent higher than the decelerated ones. An interface between those two regions with such velocity gradients is unstable and gives rise to vortex formation known as Helmholtz instability vortices.

In Figure 25 the downstream motion of high speed fluid is presented for one of the runs; at the same time the gradual replacement of the decelerated region is shown. After the accelerated fluid had travelled some distance downstream, the formation of the transverse vortex started. This was a forward transverse vortex. It started approximately 1 second after the high speed fluid appeared in the field of view, and its center of rotation was at $y^+ = 370$. It had an approximate diameter of $150y^+$ units which remained almost unchanged during the downstream movement of the vortex. Here again no sharp demarcation line between the rotating and non-rotating fluid existed. Even so, in the convected view, the identity of the vortex could be easily established. As the vortex was transported downstream its center gradually moved to $y^+ = 400$; it lasted for about 0.8 seconds. The average downstream

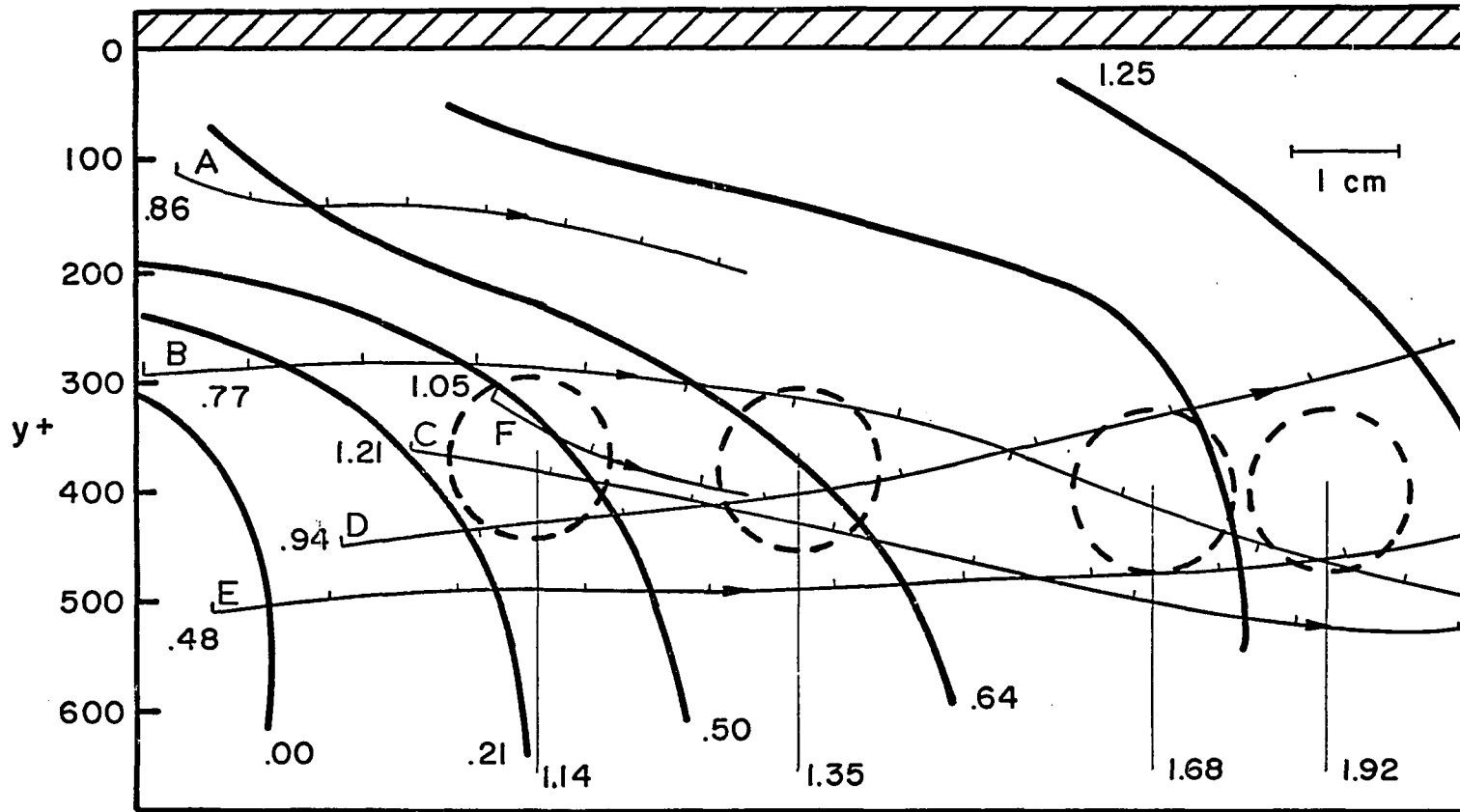


FIGURE 25. HIGH SPEED FLUID AND ASSOCIATED FORWARD TRANSVERSE VORTEX (CONVECTED VIEW)

velocity of the vortex during that time was 16.1 cm/sec compared with 16.7 cm/sec of the local mean at $y^+ = 385$; it travelled a downstream distance of $x^+ = 1,170$ before its identity disappeared.

A considerable effort was devoted to finding a way of presenting these transverse vortices directly from the motion picture runs, instead of using drawings. In the case of Figure 25, where the camera filming speed was 254 frames/second, the vortex corresponds to 211 frames. It is obvious that an arrangement of 211 frames side by side to represent the motion is not satisfactory. A time exposure method was tried by taking a single photograph of the movie of the particle paths during the time the event lasted. This method was faced with the difficulty of accounting for the differences in the downstream transport velocity of the vortex and the camera carriage velocity; i.e., the vortex did not stay in one spot. There was no way before the experiment to set the camera at a carriage speed equal to the velocity of the downstream transport of the vortex. The reason was, simply, that there was no way of knowing beforehand if a vortex would appear and what its downstream velocity would be. This problem was partially solved by placing the motion picture projector on a rotating table and trying to keep the vortex center at the same point during the projection time of the event and when

the time exposure photograph was taken. This method was extremely tedious and time-consuming. One or two worth presenting time exposure photographs were obtained, but hardly worth the effort. The information contained in these was much less than that in the motion pictures. Nevertheless, one will be presented for the sake of illumination.

Since the downstream transport velocity of the vortices was found to be almost constant, a linear relation exists between time and distance travelled. In Figure 25 selected particles paths are presented during the time the transverse vortex occurred. These paths can be transposed in the x-direction according to this linear relation with respect to the vortex center position. This process is equivalent to having the camera carriage speed almost perfectly matched with the downstream transport velocity of the vortices. This convected point of view is very useful for presentation purposes, as illustrated in Figure 26 for the same event as in Figure 25. It again should be emphasized that after the events have been established and one knows what to look for, they are clearer to see in the motion pictures than in any other way of presentation.

In Figure 27 fluid particle paths are presented for a forward transverse vortex observed in another motion

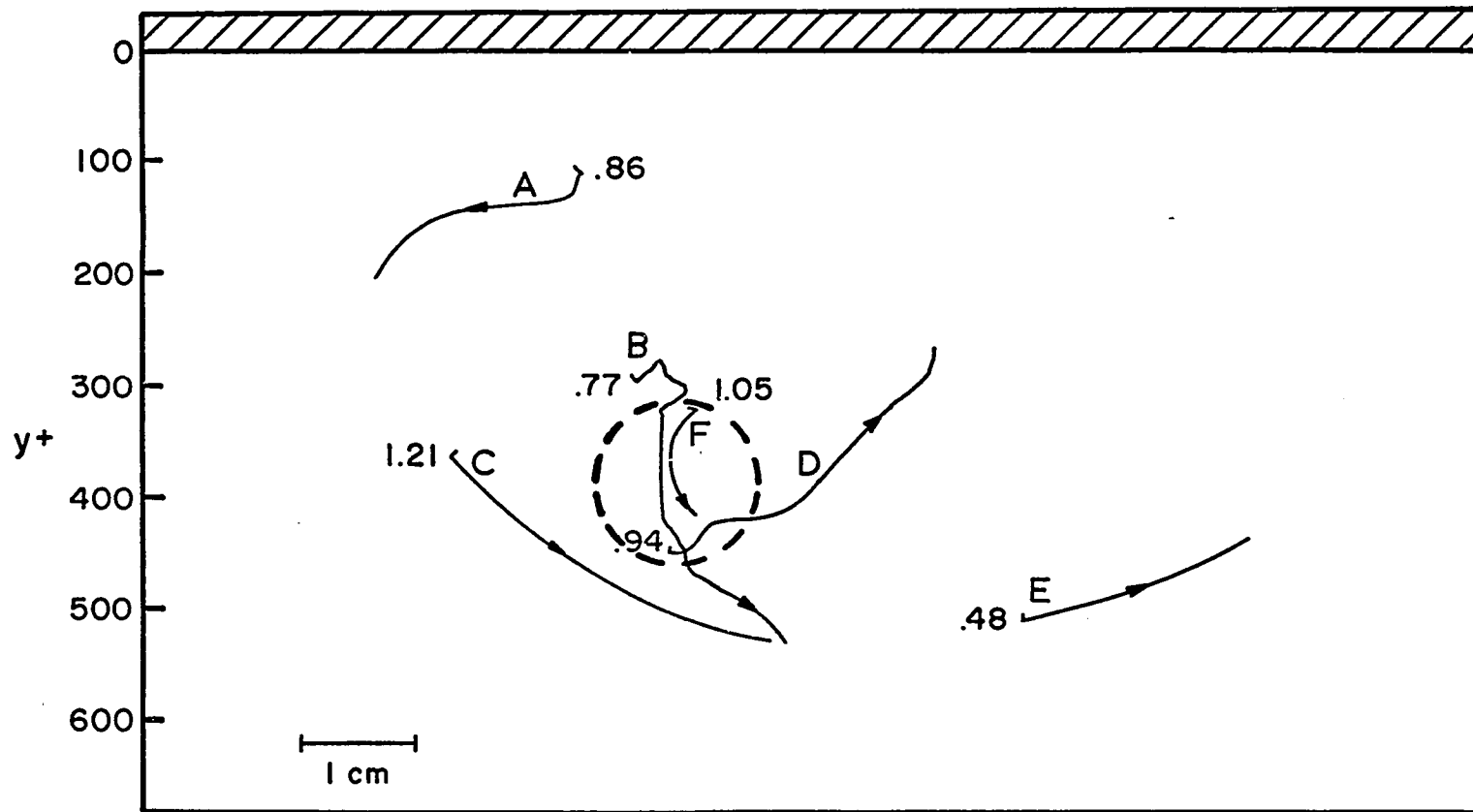


FIGURE 26. CONVICTED (STATIONARY VORTEX) VIEW OF A FORWARD TRANSVERSE VORTEX

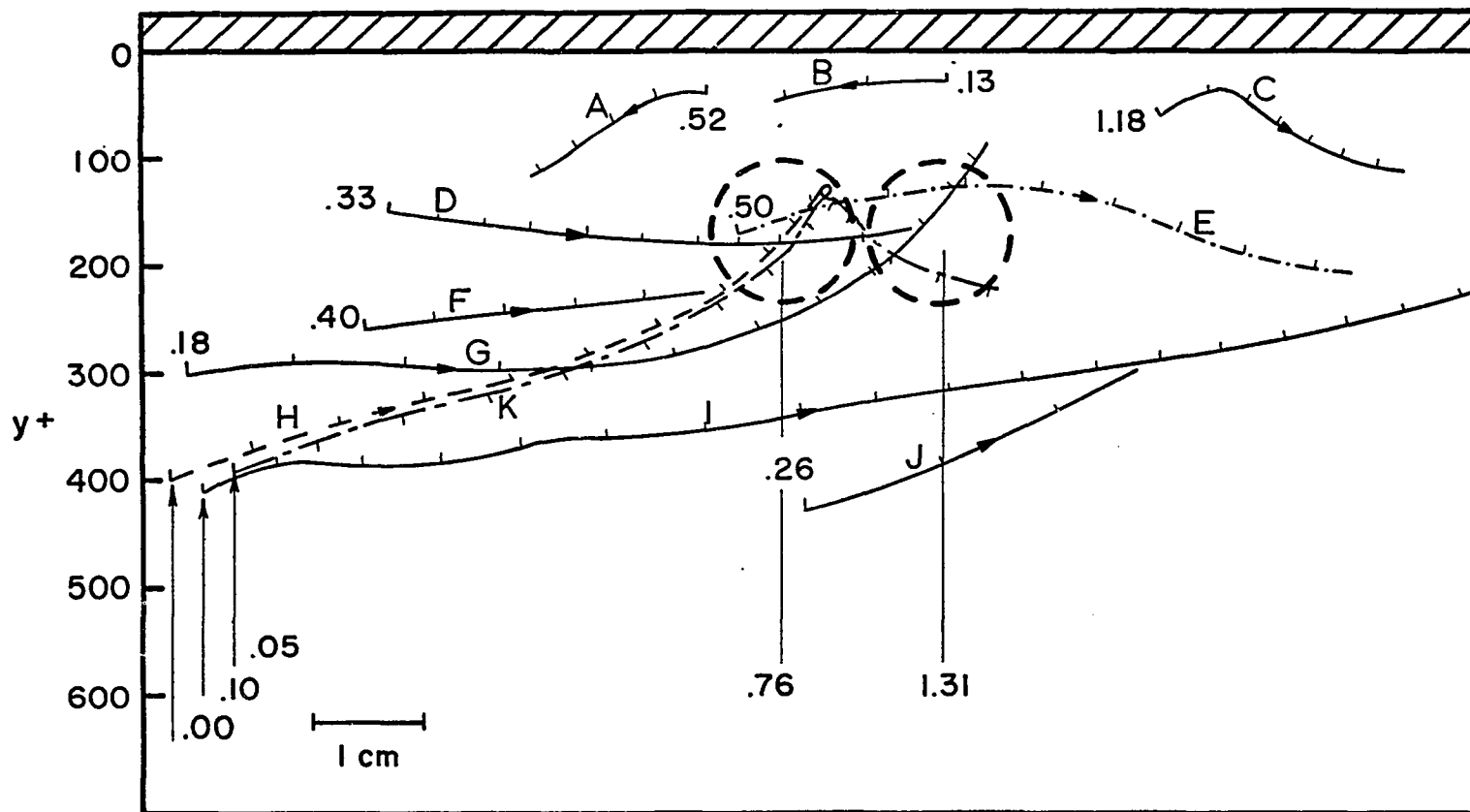


FIGURE 27. INDIVIDUAL PARTICLE PATHS DURING A FORWARD TRANSVERSE VORTEX (CONVECTED VIEW)

picture run. The convected view by transposing the particle paths to make the vortex stationary at a point is presented in Figure 28. The vortex lasted for about 0.7 seconds and travelled a streamwise distance of $x^+ = xU^*/\nu = 512$ before disappearing; its average velocity during that time was 11.9 cm/sec compared with 13.7 cm/sec of the local mean \bar{U}_x . It first appeared at about $y^+ = 170$ and moved downstream parallel to the wall; its approximate diameter was 120 y^+ units. In Figure 28 the mechanism of Helmholtz instability is dramatically illustrated. Individual fluid particles starting from a y^+ of about 400 move all the way to a y^+ of about 125 inside the vortex; one of them is seen to loop around the stationary vortex center and to be again directed downstream. Other fluid particles not participating in the vortex formation, but flowing around it, are shown; they give the picture of a flow past a cylinder with its axis in the spanwise z -direction.

The flow of the low speed fluid and its participation in the vortex formation is also shown in Figure 28. One very important observation was the close association of the wall area fluid ejections with the transverse vortices. Three wall ejections are shown in Figure 28; they occurred at the same time with the vortex. This point will be further discussed in a later section.

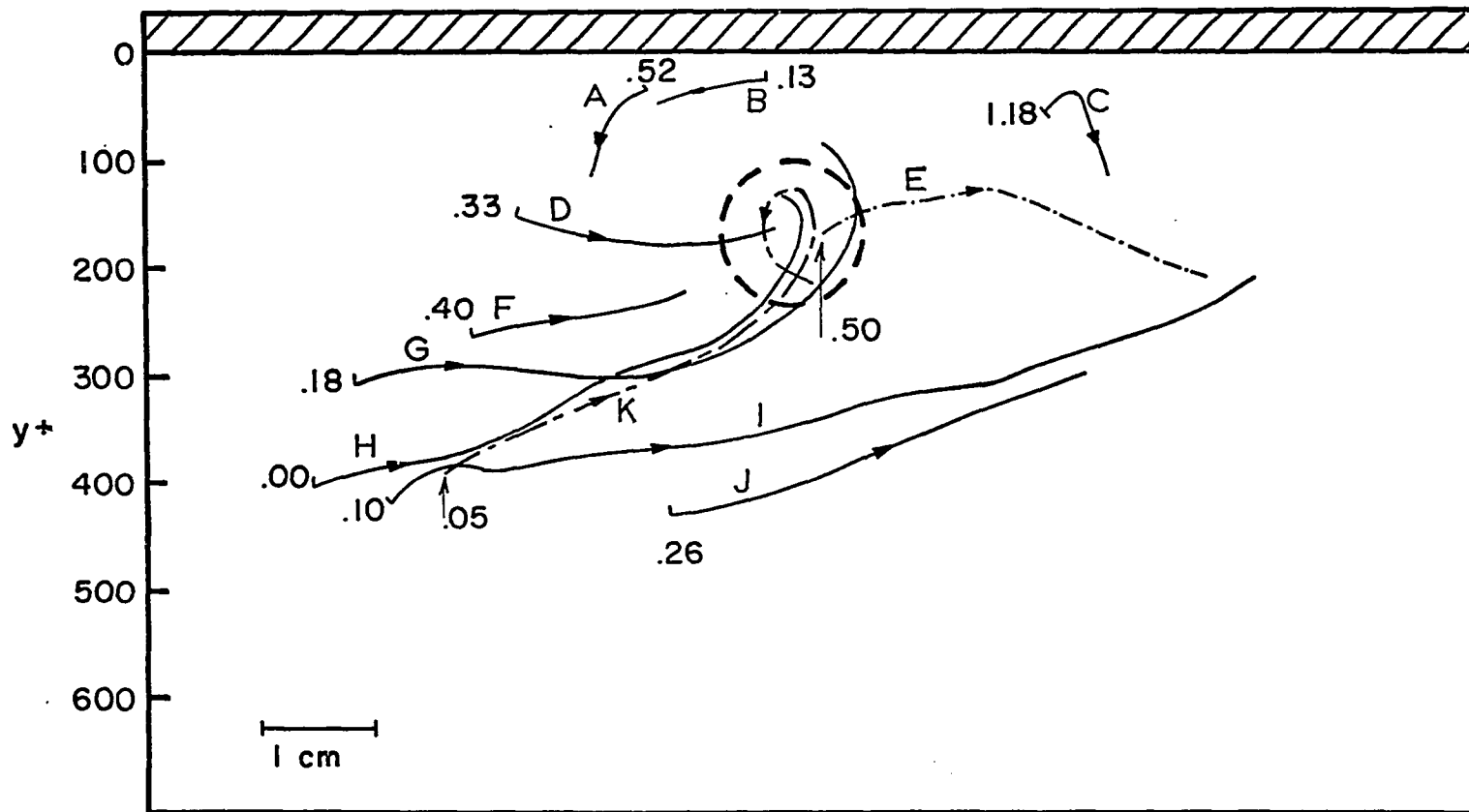


FIGURE 28. CONVICTED (STATIONARY VORTEX) VIEW OF A FORWARD TRANSVERSE VORTEX

The following visual facts supported by the limited measurements permitted in this investigation should be stressed. The first is that it was the high speed fluid region responsible for the starting of the vortex formation. In all the motion picture runs observed, the transverse vortex always was associated with the high speed fluid region. The low speed fluid region appeared to be passive just before the onset of the transverse vortex. The only active region of the decelerated flow was the wall area where the ejections originated. The very small scale of the wall ejections and the extent of their penetration into the outer flow, for most of the cases, did not suggest that they were the causative factor for the onset of the vortex motion. The accelerated fluid was the most active agent for the onset of the Helmholtz instability and the subsequent creation of the transverse vortices.

Figures 29 and 30 provide individual fluid paths and their transposition to a stationary vortex convected point of view, respectively. These are for another forward transverse vortex from another motion picture run. The event lasted for about 0.8 seconds; it had an approximate diameter of $200 y^+$ units and it moved a downstream distance of $x^+ = 850$, with an average velocity of 16.5 cm/sec and a slight outward angle to the wall of $\theta_e = 2.5$ degrees. Its center moved from $y^+ = 320$ to $y^+ = 400$. In the beginning

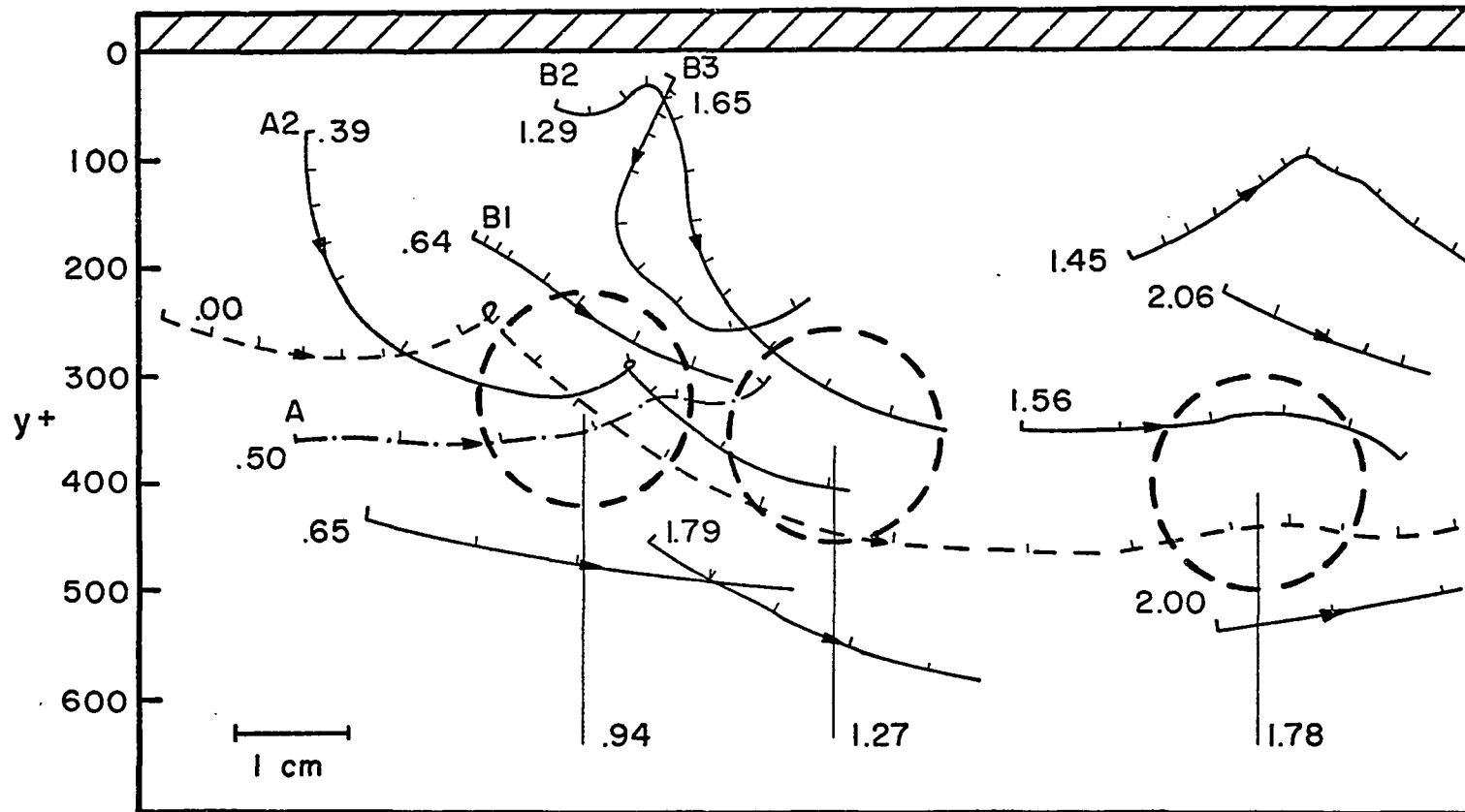


FIGURE 29. INDIVIDUAL PARTICLE PATHS DURING A FORWARD TRANSVERSE VORTEX (CONVECTED VIEW)

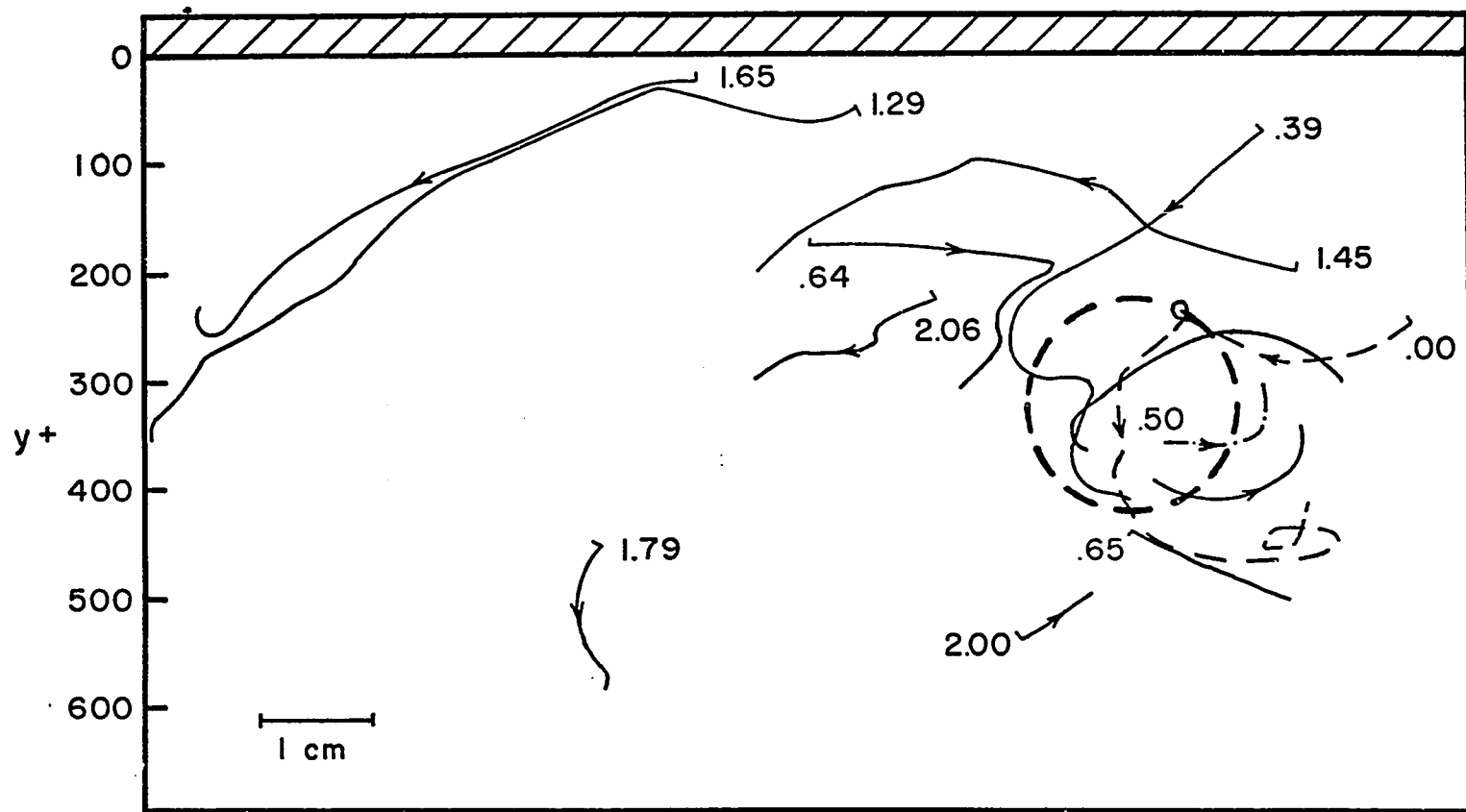


FIGURE 30. CONVICTED (STATIONARY VORTEX) VIEW OF A FORWARD TRANSVERSE VORTEX

it accelerated downstream from 16.3 cm/sec to 17.7 cm/sec and then decelerated to 16.7 cm/sec. The local mean velocity was $\bar{U}_x(y^+ = 320) = 15.3$ cm/sec and $\bar{U}_x(y^+ = 400) = 15.8$ cm/sec. Hence this transverse vortex was transported downstream faster than the local mean.

Individual fluid particle paths were traced as before, during and after the event; they are shown in Figure 30. One particle (A2) started in an ejected fluid element from the wall area ($y^+ = 67$) before the formation of the transverse vortex. It had an ejection angle of 31 degrees at $y^+ = 67$ and moved downstream with an ejection velocity of 11.1 cm/sec and a streamwise component of 9.5 cm/sec. The local mean velocity was $\bar{U}_x(y^+ = 67) = 12.3$ cm/sec; i.e., the particle was in a decelerated region. When the vortex started it was sort of "trapped" in it and arrived at a y^+ of about 350. Two other fluid particles B2 and B3, were also ejected from the wall area ($y^+ = 40$, $y^+ = 30$, respectively) after the onset of the vortex. Their ejection angles were 13 degrees, 14.5 degrees and ejection velocities of 11.2 cm/sec and 8.8 cm/sec, respectively. They were moving with a downstream velocity lower than the local mean and originated by a decelerated region. The extent of penetration of these two fluid particles inside the outer flow should be noted; they arrived at $y^+ = 350$ and $y^+ = 235$, respectively. The relation between these

small ejections and the vortices will be discussed in the next section.

A time exposure photograph (obtained from the motion picture run with the projector on a rotating table as explained before) is given in Figure 31. It corresponds to the transverse vortex of Figure 30. The extent of the vortex and the flow around it in this convected view can be observed. Another forward transverse vortex from the same motion picture run, corresponding to Figure 25, is presented in Figures 32 and 33. This vortex, while transported downstream, moved first towards the wall from $y^+ = 250$ to $y^+ = 167$, and then away from the wall, from $y^+ = 167$ to $y^+ = 300$. In the stationary vortex convected view of Figure 33, when a wall ejection (A) occurred before the onset of the vortex, it penetrated to $y^+ = 200$. Another fluid particle belonging to the low speed fluid (B) initially moved parallel to the wall; then the vortex started and directed it outward. Still another fluid particle (C) started from a $y^+ = 170$, moved towards the wall area to $y^+ = 68$ and then became "trapped" in the vortex motion arriving at $y^+ = 315$.

In a number of cases two consecutive forward transverse vortices were formed by the interaction of the same high and low speed fluid regions. The mechanism involved was the same, i.e., a Helmholtz instability. After the

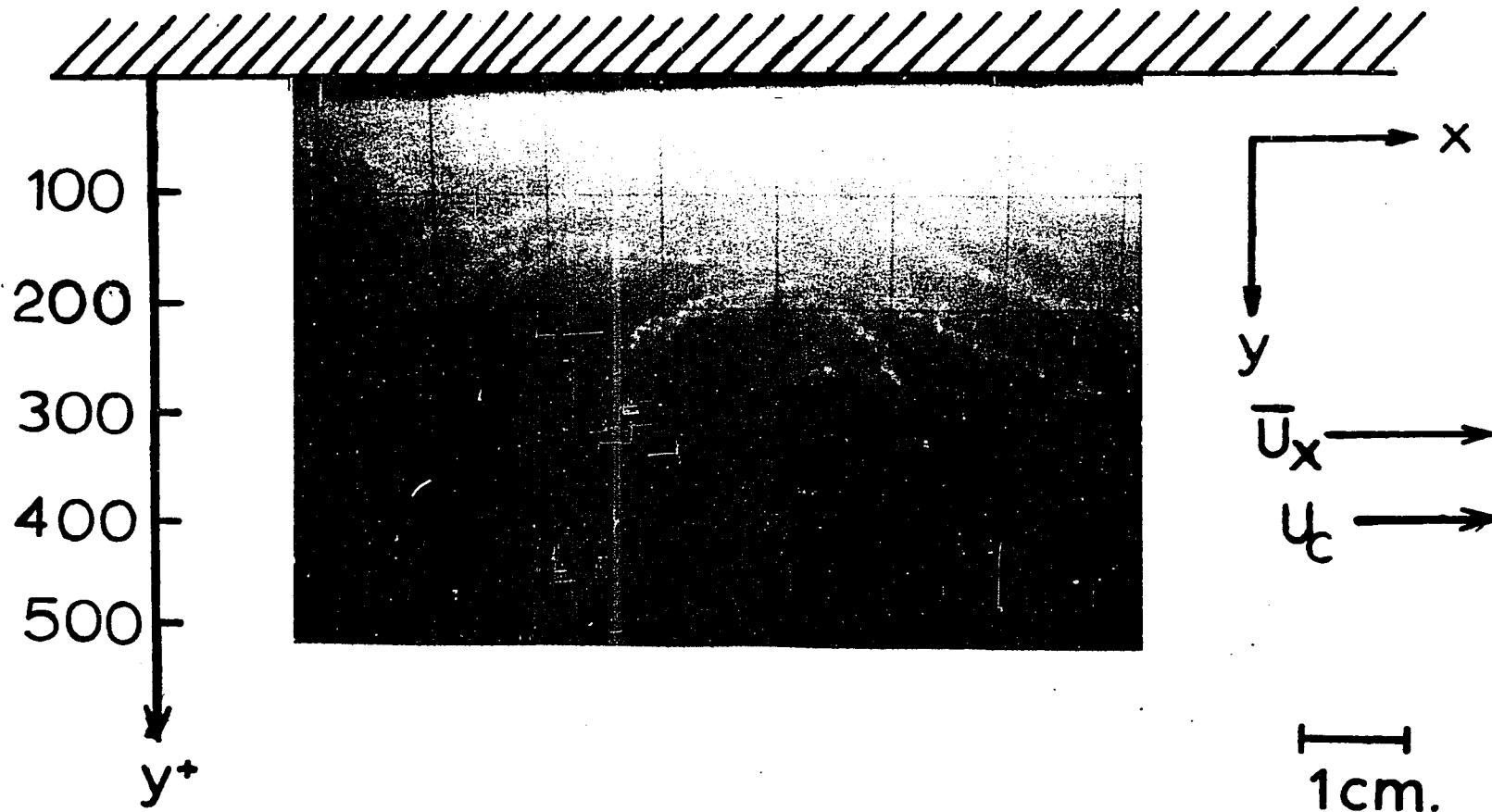


FIGURE 31. TIME EXPOSURE PHOTOGRAPH CORRESPONDING TO THE
 TRANSVERSE VORTEX OF FIGURE 30

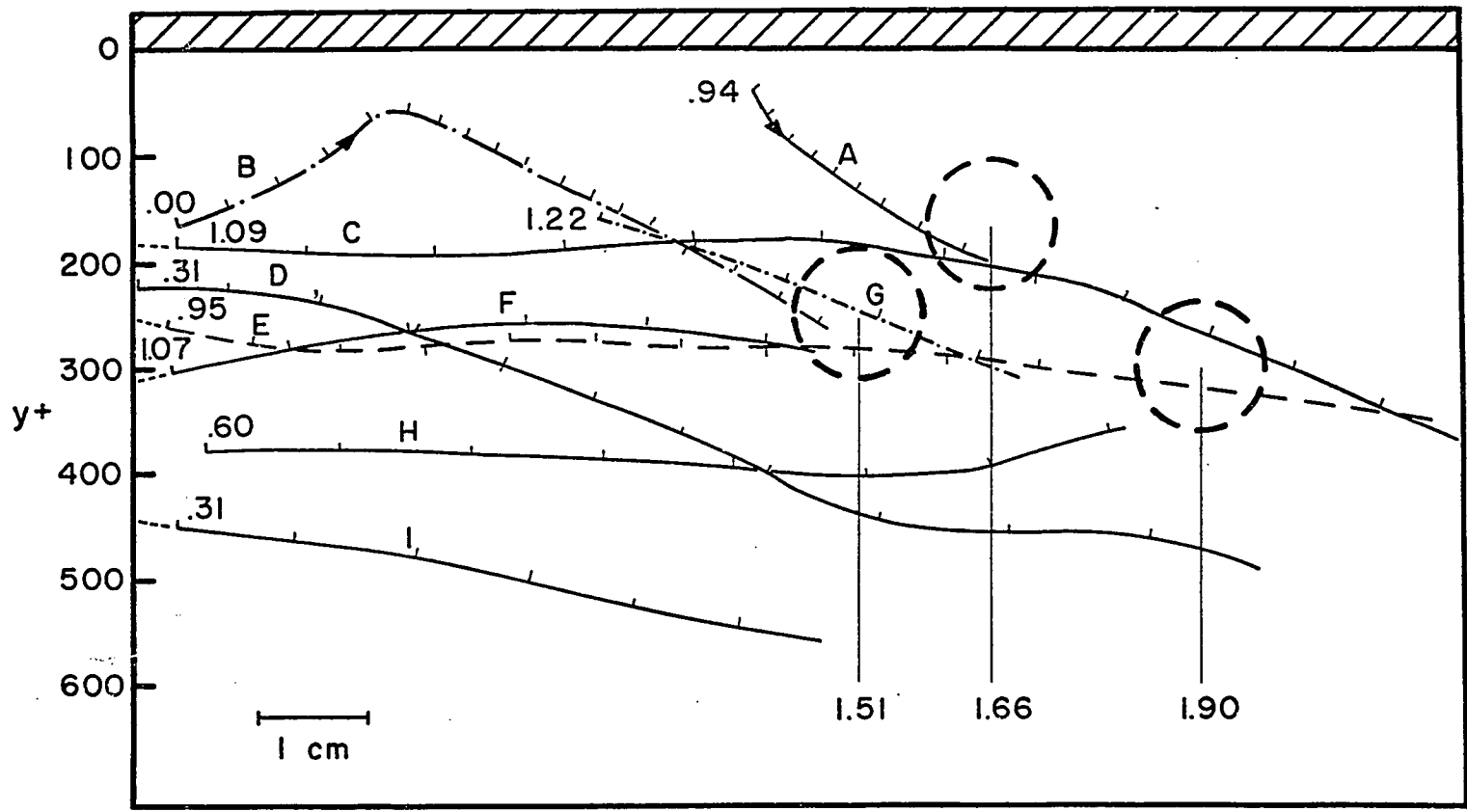


FIGURE 32. INDIVIDUAL PARTICLE PATHS DURING A FORWARD TRANSVERSE VORTEX (CONVECTED VIEW)

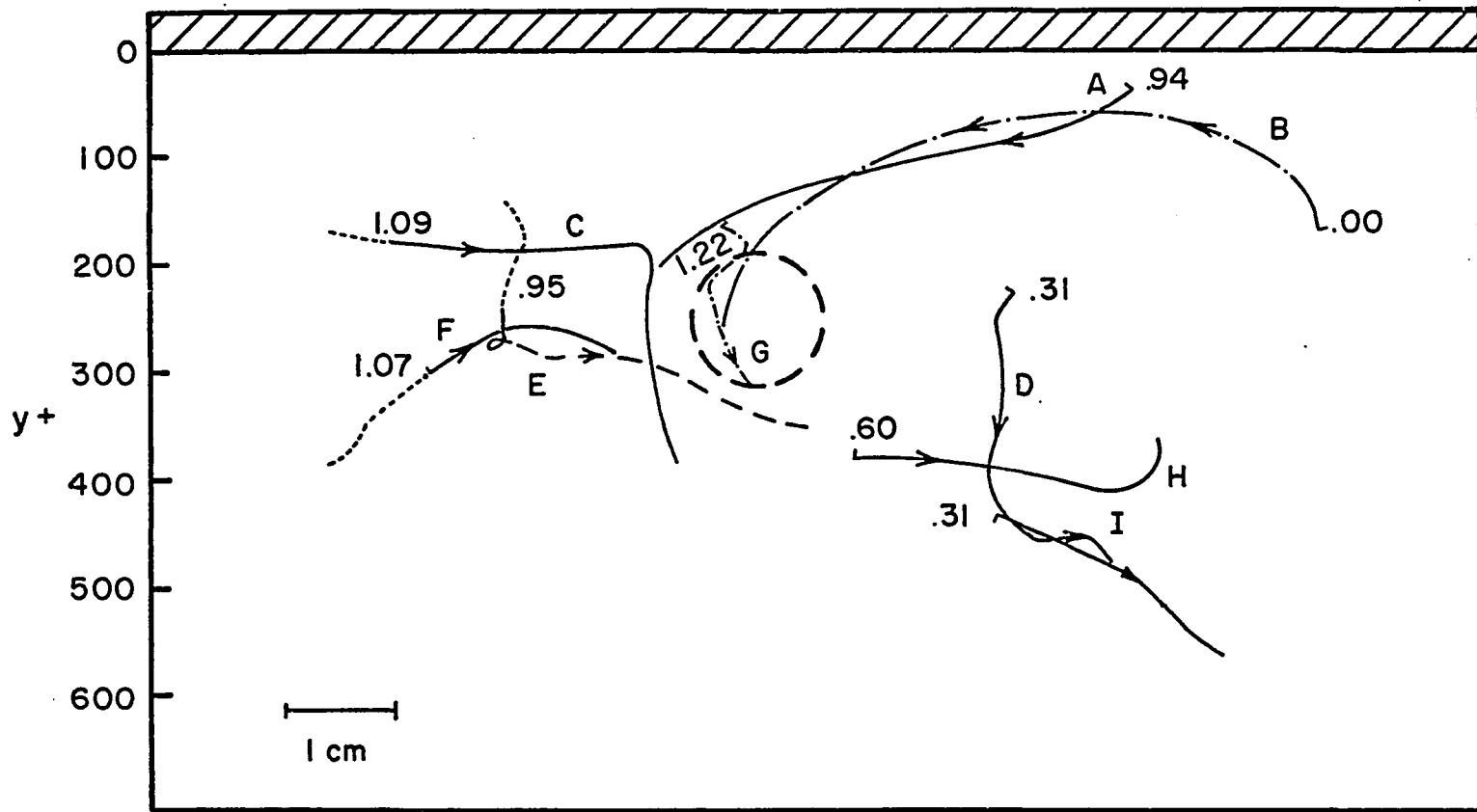


FIGURE 33. CONVICTED (STATIONARY VORTEX) VIEW OF A FORWARD TRANSVERSE VORTEX

first vortex was formed and travelled some distance downstream a second vortex appeared at the same high and low speed interface. No difference in the nature and characteristics of the second vortex were observed except that it was formed in a position closer to the wall than the first. In one movie as many as three consecutive vortices were observed; the third one was considerably smaller and lasted for a very short period of time in comparison to the first.

In Figures 34 and 35 are shown a forward transverse vortex that followed the one in Figures 25 and 26. It started about 0.05 seconds after the disappearance of the first. It lasted for 0.58 seconds and its center travelled a streamwise distance of $x^+ = 700$ moving from $y^+ = 270$ to $y^+ = 300$. Its average streamwise velocity was 14.9 cm/sec compared with 15.8 cm/sec of the local mean at $y^+ = 285$. The approximate diameter of this vortex was 150 y^+ units, i.e., the same magnitude as the first one.

As was mentioned in the general description of the events, there were a few cases where a reverse transverse vortex was observed. The basic mechanism responsible for its formation was the same as for the forward transverse vortex, i.e., a Helmholtz type of instability. In the cases observed the accelerated fluid approached the wall at a large angle while penetrating the decelerated region. In Figures 36 and 37 a reverse transverse vortex is pre-

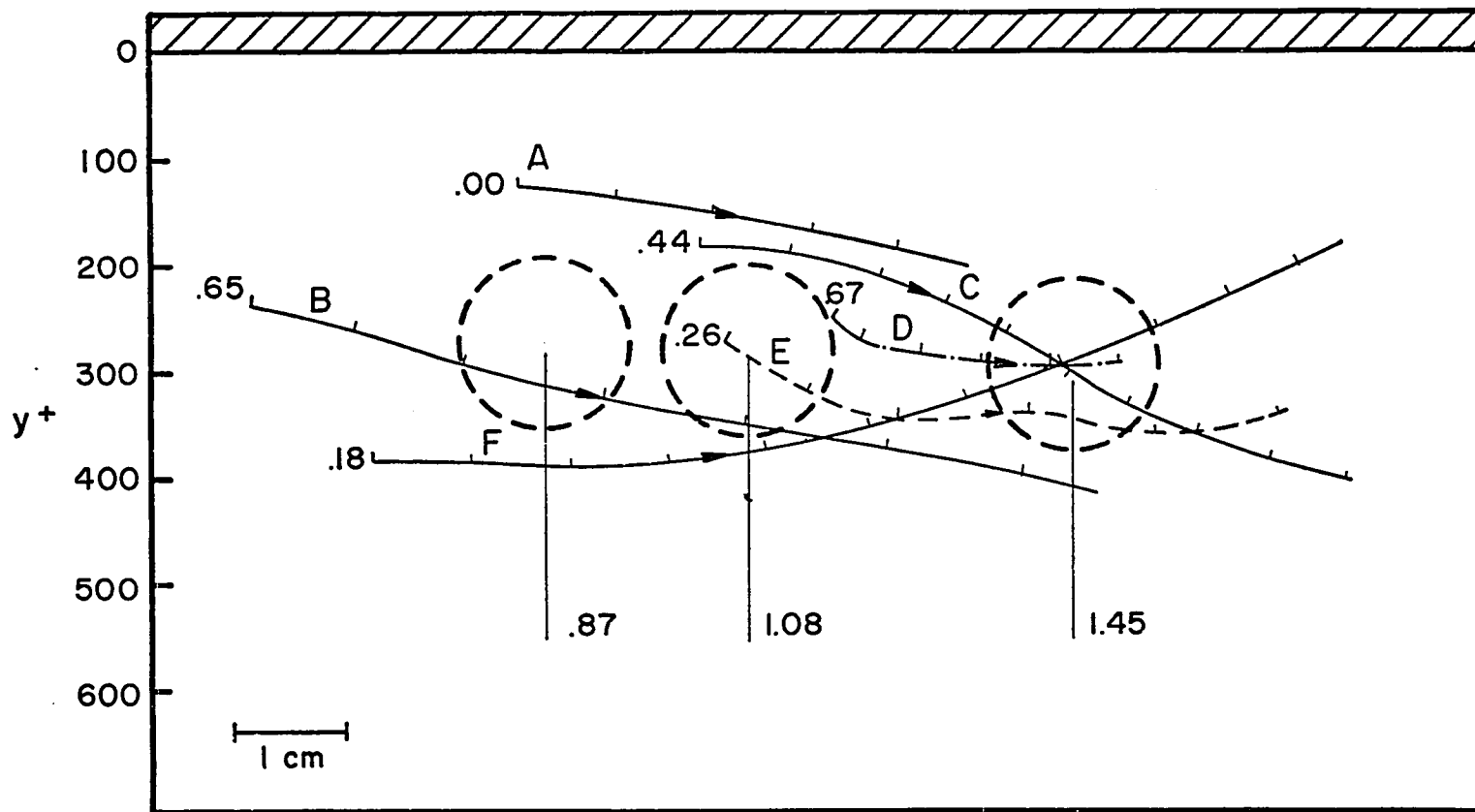


FIGURE 34. FORWARD TRANSVERSE VORTEX FOLLOWING THE VORTEX IN FIGURE 26 (CONVECTED VIEW)

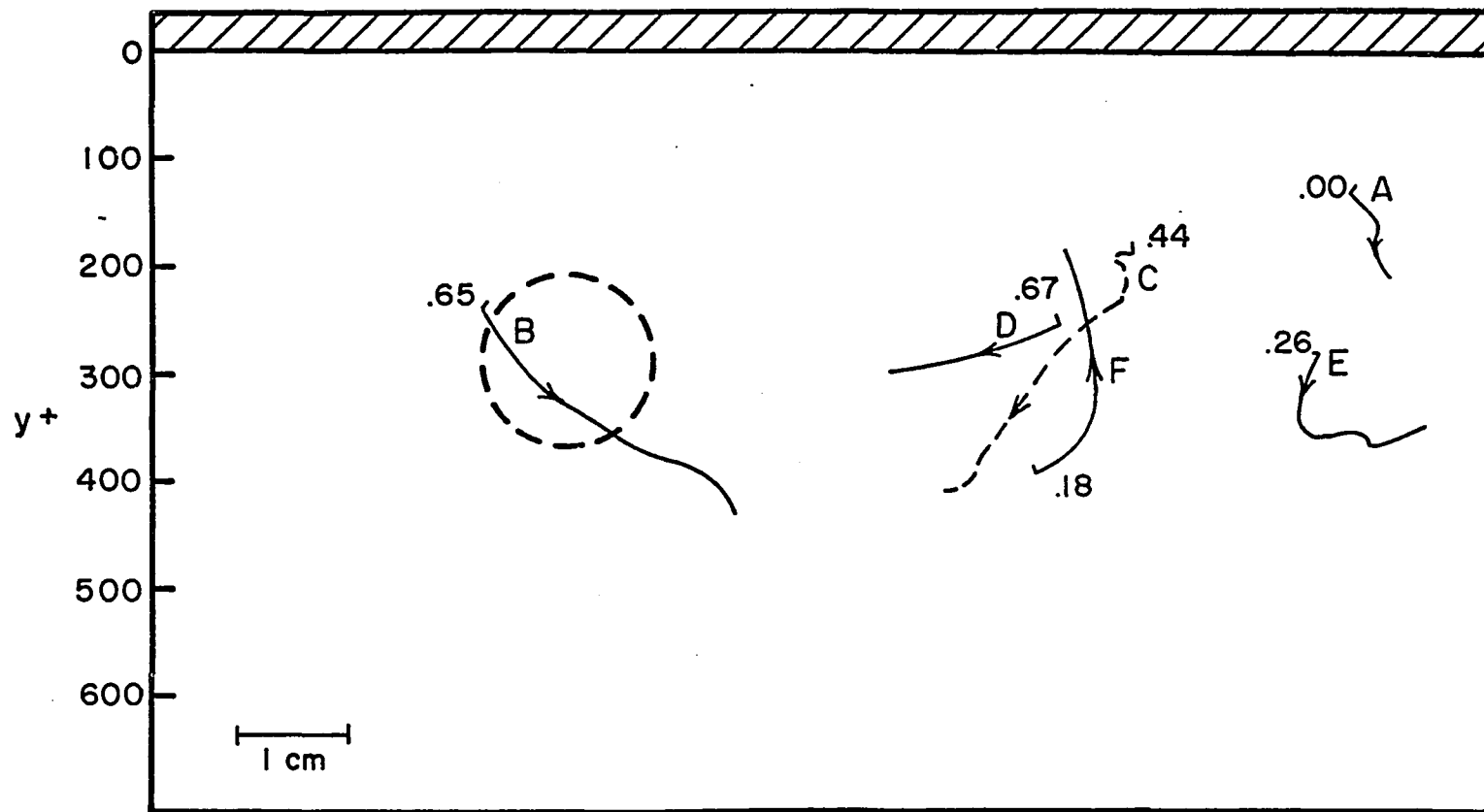


FIGURE 35. CONVICTED (STATIONARY VORTEX) VIEW OF THE VORTEX CORRESPONDING TO FIGURE 34

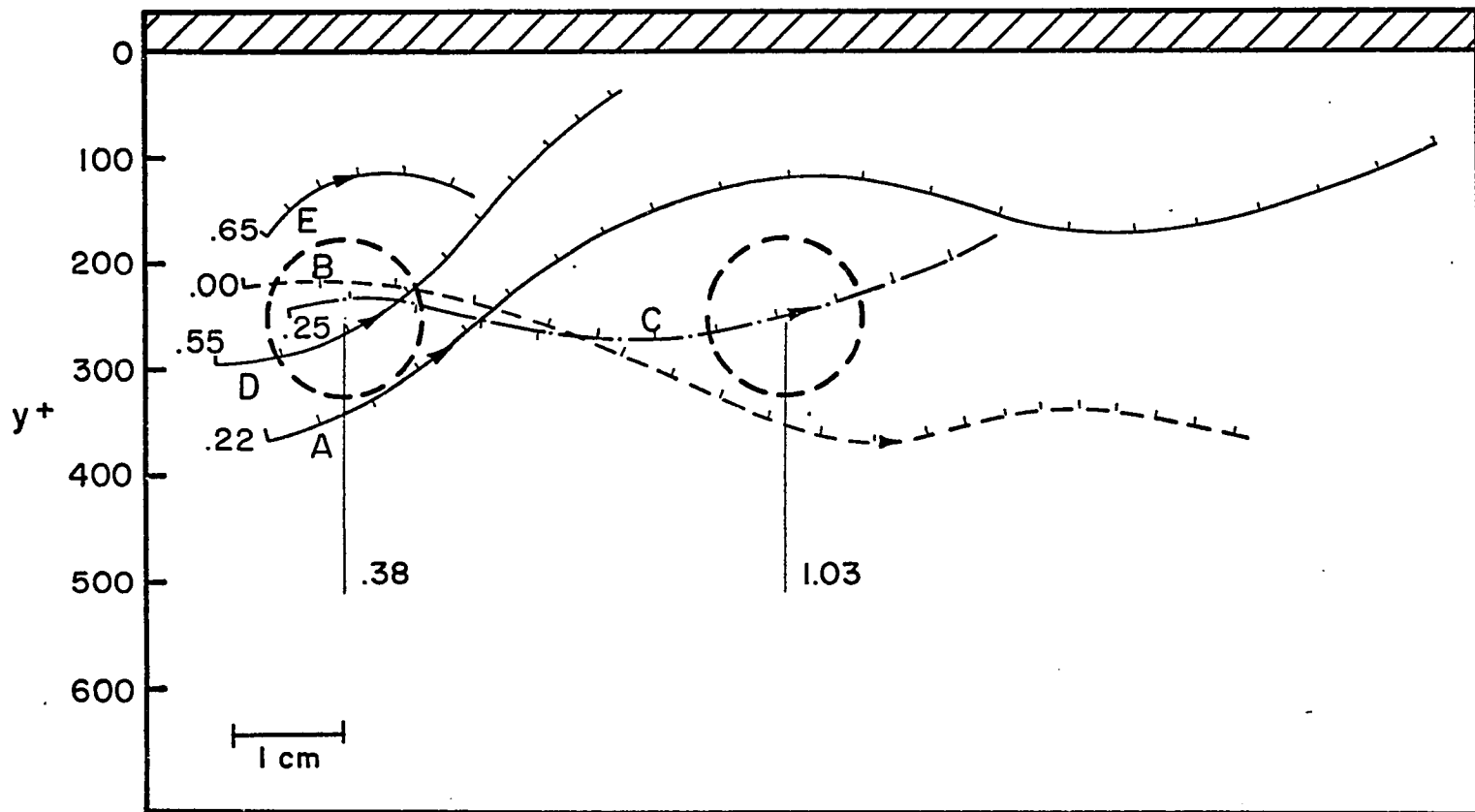


FIGURE 36. INDIVIDUAL PARTICLE PATHS OF A REVERSE TRANSVERSE VORTEX (CONVECTED VIEW)

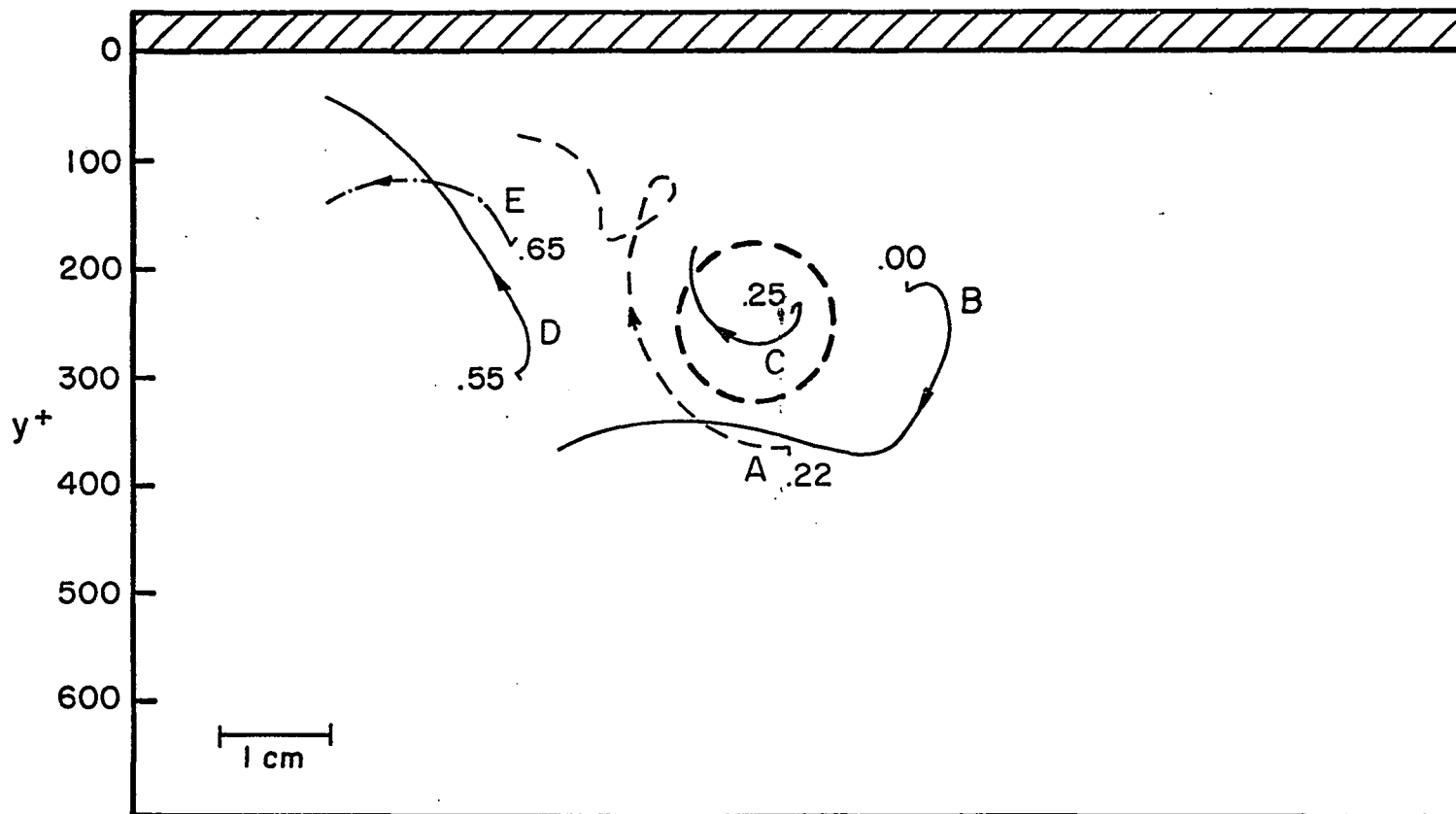


FIGURE 37. CONVICTED (STATIONARY VORTEX) VIEW OF A REVERSE TRANSVERSE VORTEX

sented. The stationary vortex convected view in Figure 37 clearly shows the reverse flow character of fluid particles belonging to high and low speed fluids. The contrast between this figure and any of the preceding ones is obvious. This particular reverse vortex lasted for 0.68 seconds and its center travelled a downstream distance of $x^+ = 740$ moving parallel to the wall at $y^+ = 250$. Its average streamwise velocity was 13.3 cm/sec compared with 15.6 cm/sec for the local mean at $y^+ = 250$; its approximate diameter was $140 y^+$ units.

A number of measurements were made of the fluid particle paths during the time the transverse vortices occurred. The paths were selected in such a way as to cover the y^+ -range where the event occurred. These particle paths were separated in two groups: inflow or wallward and outward flow or away from the wall. These measurements are summarized in Tables 7, 8, 9, 10, and 11, and correspond to transverse vortices given in Figures 25, 27, 29, 32, and 36, respectively. The tabulated quantities are the same as in Table 1 and they were previously explained.

Large Scale Inflow

This event was a large scale motion usually dominating all of the outer region and sometimes even penetrating to some degree the wall area. In the motion picture runs

TABLE 7

STUDY OF A FORWARD TRANSVERSE VORTEX (Run M-132)

| y^+ or y_t^+ | y_t^+ | \bar{y}^+ | $U_x(t)$, cm/sec | $\bar{U}_x \bar{y}^+$, cm/sec | $u(t)$, cm/sec | $v(t)=V$ cm/sec | $-uv$, (cm/sec) ² | $-\frac{uv}{(U^*)^2}$ | U_t , cm/sec | ϕ_s or ϕ_e degrees |
|------------------------|---------|-------------|----------------------|-----------------------------------|--------------------|--------------------|----------------------------------|-----------------------|-------------------|---------------------------------|
| <u>Wallward Flow</u> | | | | | | | | | | |
| 212 | 200 | 206 | 18.70 | 14.70 | 4.00 | -1.90 | 7.60 | 11.80 | 18.80 | 6.5 |
| 200 | 232 | 216 | 18.10 | 14.72 | 3.38 | -2.60 | 8.80 | 13.66 | 18.30 | 9.5 |
| 296 | 264 | 280 | 22.80 | 15.73 | 7.07 | -4.60 | 32.50 | 50.40 | 23.20 | 11.5 |
| 396 | 320 | 358 | 19.80 | 16.35 | 3.45 | -2.75 | 9.48 | 14.70 | 20.00 | 12.7 |
| 480 | 460 | 470 | 19.10 | 16.72 | 2.38 | -0.65 | 1.58 | 2.45 | 19.20 | 2.5 |
| 460 | 434 | 447 | 19.90 | 16.70 | 2.20 | -2.00 | 4.40 | 6.82 | 20.00 | 5.8 |
| 508 | 492 | 500 | 19.20 | 16.73 | 2.47 | -0.65 | 1.59 | 2.46 | 19.30 | 2.5 |
| <u>Outward Flow</u> | | | | | | | | | | |
| 112 | 136 | 124 | 15.50 | 13.98 | 1.52 | 2.40 | -3.65 | -5.65 | 15.70 | 9.0 |
| 180 | 200 | 190 | 15.50 | 14.65 | 0.85 | 2.00 | -1.70 | -2.64 | 15.70 | 7.5 |
| 234 | 316 | 300 | 17.90 | 16.01 | 1.89 | 0.80 | -1.51 | -2.34 | 18.00 | 2.5 |
| 320 | 344 | 332 | 14.70 | 16.18 | -1.48 | 3.20 | +4.74 | 7.35 | 14.90 | 15.5 |
| 400 | 434 | 417 | 19.50 | 16.60 | 2.90 | 2.50 | -8.40 | -13.02 | 20.10 | 7.3 |
| 470 | 430 | 450 | 22.30 | 16.70 | 6.60 | 2.60 | -17.20 | -26.70 | 22.40 | 6.7 |

TABLE 8

STUDY OF A FORWARD TRANSVERSE VORTEX (Run M-133)

| y_{or}^+ | y_t^+ | y^+ | $U_x(t)$, cm/sec | $\bar{U}_x(y^+)$, cm/sec | $u(t)$, cm/sec | $v(t)=V$ cm/sec | $-uv$, (cm/sec) ² | $-\frac{uv}{(U^*)^2}$ | U_t , cm/sec | ϕ_s or ϕ_e degrees |
|----------------------|---------|-------|----------------------|------------------------------|--------------------|--------------------|----------------------------------|-----------------------|-------------------|---------------------------------|
| <u>Wallward Flow</u> | | | | | | | | | | |
| 50 | 42 | 46 | 10.35 | 11.23 | -0.88 | -0.75 | -0.66 | <u>-1.01</u> | 10.40 | 4.0 |
| 156 | 116 | 136 | 11.80 | 13.42 | -1.62 | -1.70 | -2.75 | <u>-3.84</u> | 12.10 | 13.0 |
| 192 | 156 | 174 | 11.65 | 13.85 | -2.20 | -3.20 | -7.04 | <u>-11.02</u> | 12.10 | 15.5 |
| 246 | 216 | 231 | 14.20 | 14.28 | -0.08 | -3.20 | -0.25 | <u>-0.33</u> | 14.60 | 13.0 |
| 350 | 304 | 327 | 15.90 | 14.90 | 1.00 | -1.10 | 1.10 | <u>1.69</u> | 16.00 | 4.2 |
| 466 | 432 | 449 | 15.90 | 15.68 | 0.22 | -0.70 | 0.15 | <u>0.23</u> | 16.00 | 5.5 |
| 520 | 512 | 516 | 17.00 | 16.22 | 0.78 | -0.40 | 0.36 | <u>0.55</u> | 17.10 | 1.5 |
| <u>Outward Flow</u> | | | | | | | | | | |
| *28 | 46 | 37 | 1.60 | 11.00 | -9.40 | 0.80 | 7.52 | <u>11.80</u> | 1.65 | 26.0 |
| *38 | 50 | 44 | 2.10 | 11.22 | -9.12 | 0.50 | 4.56 | <u>7.00</u> | 2.20 | 6.5 |
| *50 | 94 | 72 | 5.80 | 11.81 | -6.01 | 1.60 | 9.62 | <u>15.05</u> | 6.00 | 15.5 |
| 136 | 140 | 88 | 16.20 | 12.67 | 3.53 | 0.65 | -2.29 | <u>-3.52</u> | 16.25 | 2.3 |
| 170 | 208 | 189 | 15.60 | 13.92 | 1.68 | 1.70 | -2.85 | <u>-4.38</u> | 15.70 | 6.0 |
| 550 | 568 | 559 | 2.25 | 16.70 | 5.55 | 3.30 | -18.32 | <u>-23.17</u> | 22.50 | 8.3 |

TABLE 9

STUDY OF A FORWARD TRANSVERSE VORTEX (Run M-134)

| y_{or}^+ | y_t^+ | \bar{y}^+ | $U_x(t)$, cm/sec | $\bar{U}_x(\bar{y}^+)$, cm/sec | $u(t)$, cm/sec | $v(t)=V$ cm/sec | $-uv$, (cm/sec) ² | $-\frac{uv}{(U^*)^2}$ | U_t , cm/sec | ϕ_s or ϕ_e degrees |
|----------------------|---------|-------------|----------------------|------------------------------------|--------------------|--------------------|----------------------------------|-----------------------|-------------------|---------------------------------|
| <u>Wallward Flow</u> | | | | | | | | | | |
| 196 | 160 | 178 | 10.20 | 13.33 | -3.15 | -1.50 | -4.72 | -7.37 | 10.80 | 8.5 |
| 296 | 274 | 285 | 14.20 | 14.42 | -0.22 | -2.40 | -0.53 | -8.28 | 14.40 | 10.0 |
| 52 | 40 | 46 | 9.70 | 11.00 | -1.30 | -1.20 | -1.56 | -2.46 | 9.80 | 7.0 |
| <u>Outward Flow</u> | | | | | | | | | | |
| *30 | 85 | 54 | 8.50 | 11.15 | -2.65 | 2.20 | +5.84 | 9.14 | 8.80 | 14.5 |
| *40 | 65 | 53 | 10.90 | 11.15 | -1.25 | 2.60 | +3.25 | 5.08 | 11.20 | 13.0 |
| *67 | 142 | 105 | 9.50 | 12.00 | -2.50 | 5.70 | +14.28 | 22.58 | 11.10 | 31.0 |
| 120 | 182 | 151 | 7.60 | 12.60 | -5.00 | 3.20 | +16.00 | 25.00 | 8.10 | 22.5 |
| 194 | 240 | 217 | 10.40 | 13.70 | -3.30 | 1.60 | +5.28 | 8.22 | 10.45 | 8.2 |
| 294 | 366 | 330 | 13.50 | 14.80 | -1.30 | 4.90 | +6.36 | 9.95 | 14.30 | 19.7 |
| 388 | 440 | 414 | 18.50 | 15.30 | 3.20 | 4.80 | -15.33 | -24.10 | 19.20 | 14.3 |
| 476 | 500 | 488 | 19.00 | 15.50 | 4.50 | 1.50 | -6.75 | -10.58 | 19.10 | 4.5 |
| 544 | 570 | 557 | 14.90 | 15.80 | -0.90 | 0.80 | +0.72 | 1.13 | 15.00 | 3.0 |

TABLE 10

STUDY OF A FORWARD TRANSVERSE VORTEX (Run M-132)

| y^+ or y_t^+ | y_t^+ | \bar{y}^+ | $U_x(t)$, cm/sec | $\bar{U}_x(\bar{y}^+)$, cm/sec | $u(t)$, cm/sec | $v(t)=V$, cm/sec | $-uv$ (cm/sec) ² | $-\frac{uv}{(U^*)^2}$ | U_t , cm/sec | ϕ_s or ϕ_e degrees |
|------------------------|---------|-------------|----------------------|------------------------------------|--------------------|----------------------|--------------------------------|-----------------------|-------------------|---------------------------------|
| <u>Wallward Flow</u> | | | | | | | | | | |
| 286 | 266 | 276 | 18.10 | 15.74 | 2.36 | -1.70 | 4.02 | 6.25 | 18.50 | 5.5 |
| 400 | 358 | 379 | 15.86 | 16.20 | -0.40 | -2.40 | -0.96 | -1.49 | 15.90 | 8.5 |
| 192 | 180 | 186 | 18.80 | 14.92 | 3.88 | -0.40 | 1.50 | 2.33 | 18.85 | 1.5 |
| <u>Outward Flow</u> | | | | | | | | | | |
| 38 | 66 | 52 | 9.70 | 12.25 | -2.55 | 3.60 | 9.17 | <u>14.25</u> | 10.30 | 20. |
| 38 | 100 | 69 | 9.40 | 12.82 | -3.42 | 2.00 | 6.84 | <u>11.78</u> | 9.60 | 12. |
| 104 | 175 | 140 | 12.00 | 14.20 | -2.20 | 2.30 | 5.06 | <u>7.87</u> | 12.20 | 10.7 |
| 70 | 100 | 85 | 10.00 | 13.35 | -3.35 | 1.45 | 4.86 | <u>7.55</u> | 10.15 | 8.2 |
| 137 | 200 | 169 | 8.60 | 14.50 | -5.90 | 2.15 | 12.70 | <u>19.75</u> | 8.90 | 13.7 |
| 212 | 280 | 246 | 17.20 | 15.51 | +1.68 | 4.10 | -6.90 | -10.72 | 17.70 | 13.5 |
| 220 | 266 | 243 | 13.60 | 15.50 | +1.90 | 4.30 | 8.16 | 12.70 | 14.30 | 17.0 |
| 270 | 292 | 281 | 18.40 | 15.75 | +1.75 | 0.50 | -8.75 | -13.60 | 18.45 | 1.5 |
| 292 | 330 | 311 | 19.50 | 16.00 | +3.50 | 2.00 | -7.00 | -10.89 | 19.60 | 5.7 |
| 460 | 492 | 476 | 17.00 | 16.60 | +0.40 | 3.90 | -1.56 | -2.43 | 17.20 | 10.0 |

TABLE 11

STUDY OF A REVERSE TRANSVERSE VORTEX (Run M-132)

| y_{or}^+ | y_t^+ | \bar{y}^+ | $U_x(t)$, cm/sec | $\bar{U}_x(\bar{y}^+)$, cm/sec | $u(t)$, cm/sec | $v(t)=V$ cm/sec | $-uv$ (cm/sec) ² | $-\frac{uv}{(U^*)^2}$ | U_t , cm/sec | ϕ_s or ϕ_e degrees |
|----------------------|---------|-------------|----------------------|------------------------------------|--------------------|--------------------|--------------------------------|-----------------------|-------------------|---------------------------------|
| <u>Wallward Flow</u> | | | | | | | | | | |
| 296 | 284 | 290 | 14.20 | 15.74 | -1.54 | -1.30 | -2.00 | -3.15 | 14.30 | 11.0 |
| 284 | 258 | 271 | 12.60 | 15.73 | -3.13 | -2.60 | -7.87 | -12.23 | 12.90 | 11.7 |
| 188 | 126 | 157 | 10.50 | 14.60 | -4.10 | -3.85 | -15.80 | -20.55 | 11.00 | 19.2 |
| 70 | 36 | 53 | 10.30 | 12.25 | -1.95 | -2.50 | -4.38 | -6.77 | 10.60 | 13.5 |
| 176 | 134 | 155 | 11.30 | 14.59 | -3.29 | -3.90 | -12.82 | -19.80 | 12.00 | 19.0 |
| 270 | 216 | 243 | 14.00 | 15.50 | -1.50 | -1.10 | -1.65 | -2.56 | 14.10 | 4.5 |
| 366 | 356 | 361 | 10.50 | 15.70 | -5.20 | -0.95 | -4.94 | -7.67 | 10.50 | 5.0 |
| 172 | 134 | 153 | 14.60 | 14.59 | -0.01 | -2.70 | -0.02 | -0.03 | 14.90 | 10.5 |
| 258 | 210 | 234 | 13.00 | 15.35 | -2.35 | -1.60 | -2.76 | -4.27 | 13.20 | 7.0 |
| <u>Outward Flow</u> | | | | | | | | | | |
| 116 | 138 | 122 | 11.20 | 13.98 | -2.78 | 1.00 | 2.78 | 4.28 | 11.30 | 4.7 |
| 216 | 246 | 131 | 14.70 | 14.08 | +0.62 | 1.65 | -1.02 | -1.58 | 14.90 | 6.5 |
| 260 | 316 | 288 | 15.60 | 15.74 | -0.14 | 3.20 | 0.45 | 0.70 | 15.90 | 11.5 |
| 316 | 366 | 341 | 12.00 | 16.20 | -4.20 | 1.90 | 7.98 | 12.39 | 12.10 | 8.5 |

they appeared as large masses of fluid moving toward the wall with a small wallward angle. They were usually moving with a streamwise velocity component close to the local \bar{U}_x . In Figure 38 the fluid particle paths for such an inflow are presented. In Table 12 numerical data calculated on some of these paths are listed. The continuity of motions from a y^+ of about 500 to a y^+ of about 100 is dramatically illustrated in Figure 38. This particular inflow covered a streamwise area of at least $x^+ = 1500$. Usually an inflow followed an outflow or vice versa or it occurred after a transverse vortex. It was easily distinguished from the accelerated or decelerated flow regions and was rarely observed to follow them.

There were motion picture runs where no large scale inflows were observed whereas in some runs as many as two and seldom three occurred. In Figures 39 and 40 two inflows are presented which occurred in the same run. The second one was of considerably smaller scale from the first. The penetration of some fluid particles originating in the far outer region of the turbulent boundary layer into the wall area is worth noting. Table 13 summarizes numerical data obtained from the last two inflows. The alternating positive and negative signs of the streamwise velocity fluctuations $u(t)$ suggests that these inflows tend to move downstream with the mean average velocity.

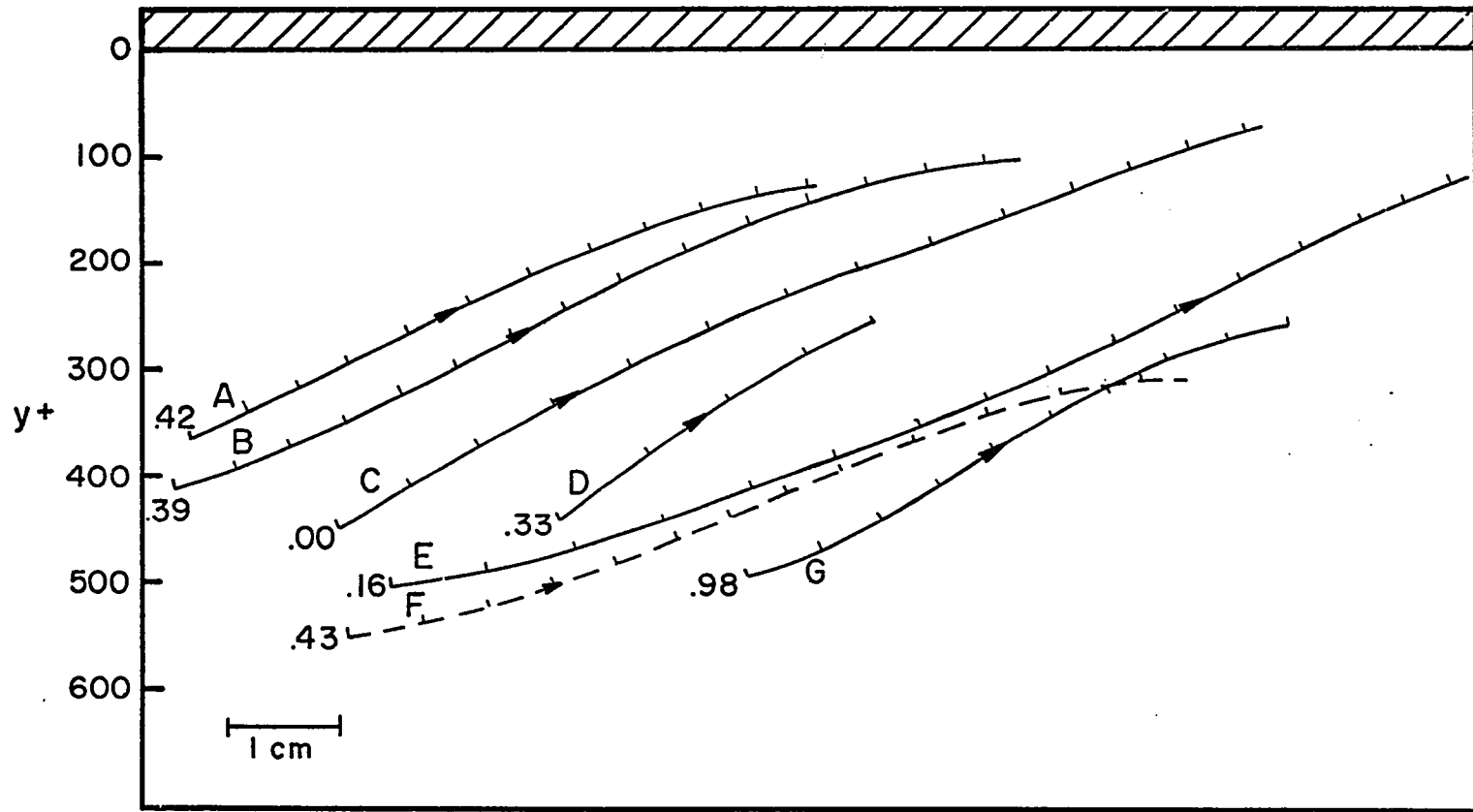


FIGURE 38. PARTICLE PATHS DURING A LARGE SCALE INFLOW (CONVECTED VIEW)

TABLE 12

STUDY OF A LARGE SCALE INFLOW (Run M-134)

| y_{or}^+ | y_t^+ | \bar{y}^+ | $U_x(t),$ cm/sec | $\bar{U}_x(\bar{y}^+),$ cm/sec | $u(t)$ cm/sec | $v(t)=V$ cm/sec | $-uv$ (cm/sec) ² | $-\frac{uv}{(U^*)^2}$ | $U_t,$ cm/sec | ϕ_s degrees |
|------------|---------|-------------|---------------------|-----------------------------------|------------------|--------------------|--------------------------------|-----------------------|------------------|---------------------|
| 135 | 108 | 122 | 13.40 | 12.35 | 1.05 | -1.00 | 1.05 | 1.65 | 13.50 | 4.5 |
| 117 | 104 | 110 | 14.50 | 12.01 | 2.49 | -0.60 | 1.49 | 2.34 | 14.50 | 2.5 |
| 160 | 125 | 142 | 13.90 | 12.67 | 1.23 | -1.00 | 1.23 | 1.93 | 14.00 | 4.2 |
| 550 | 486 | 518 | 15.50 | 15.82 | -0.32 | -1.80 | -5.76 | -9.04 | 17.70 | 6.5 |
| 292 | 246 | 268 | 14.20 | 14.28 | -0.08 | -2.85 | -0.29 | -0.45 | 14.50 | 8.5 |
| 350 | 125 | 243 | 15.07 | 14.02 | 1.05 | -2.00 | 2.10 | 3.29 | 15.20 | 7.0 |
| 450 | 70 | 260 | 15.80 | 14.32 | 1.48 | -2.40 | 3.55 | 5.56 | 15.90 | 8.7 |
| 440 | 250 | 345 | 16.20 | 14.92 | 1.28 | -3.60 | 4.61 | 7.22 | 16.40 | 12.0 |
| 135 | 70 | 103 | 14.20 | 11.90 | 2.30 | -1.80 | 4.14 | 6.49 | 14.40 | 7.0 |
| 485 | 330 | 407 | 16.20 | 15.25 | 0.95 | -2.50 | 2.47 | 3.87 | 16.50 | 8.5 |
| 500 | 260 | 380 | 14.50 | 15.08 | -0.58 | -1.75 | -1.03 | -1.61 | 14.70 | 6.9 |

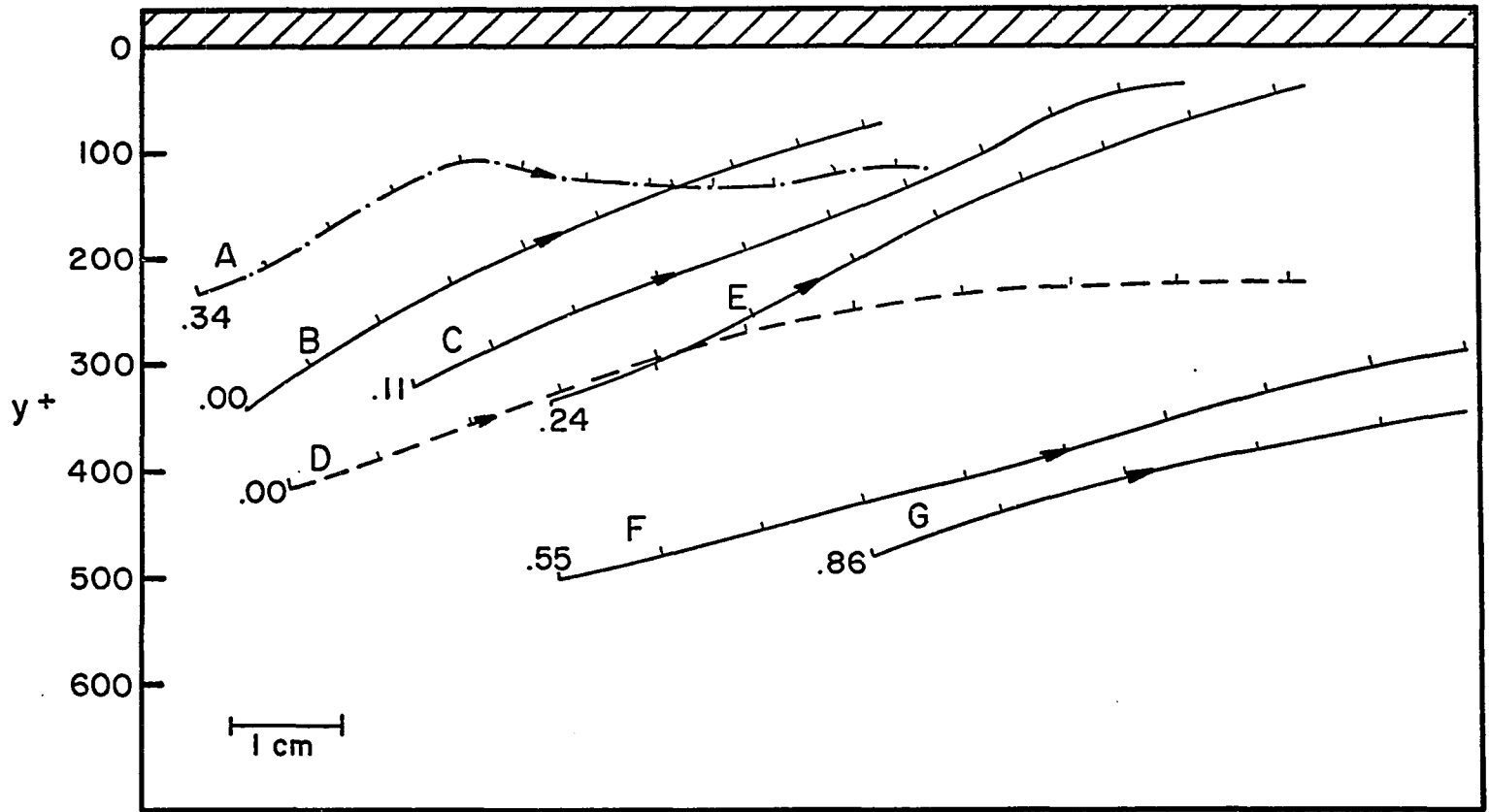


FIGURE 39. PARTICLE PATHS DURING A LARGE SCALE INFLOW (CONVECTED VIEW)

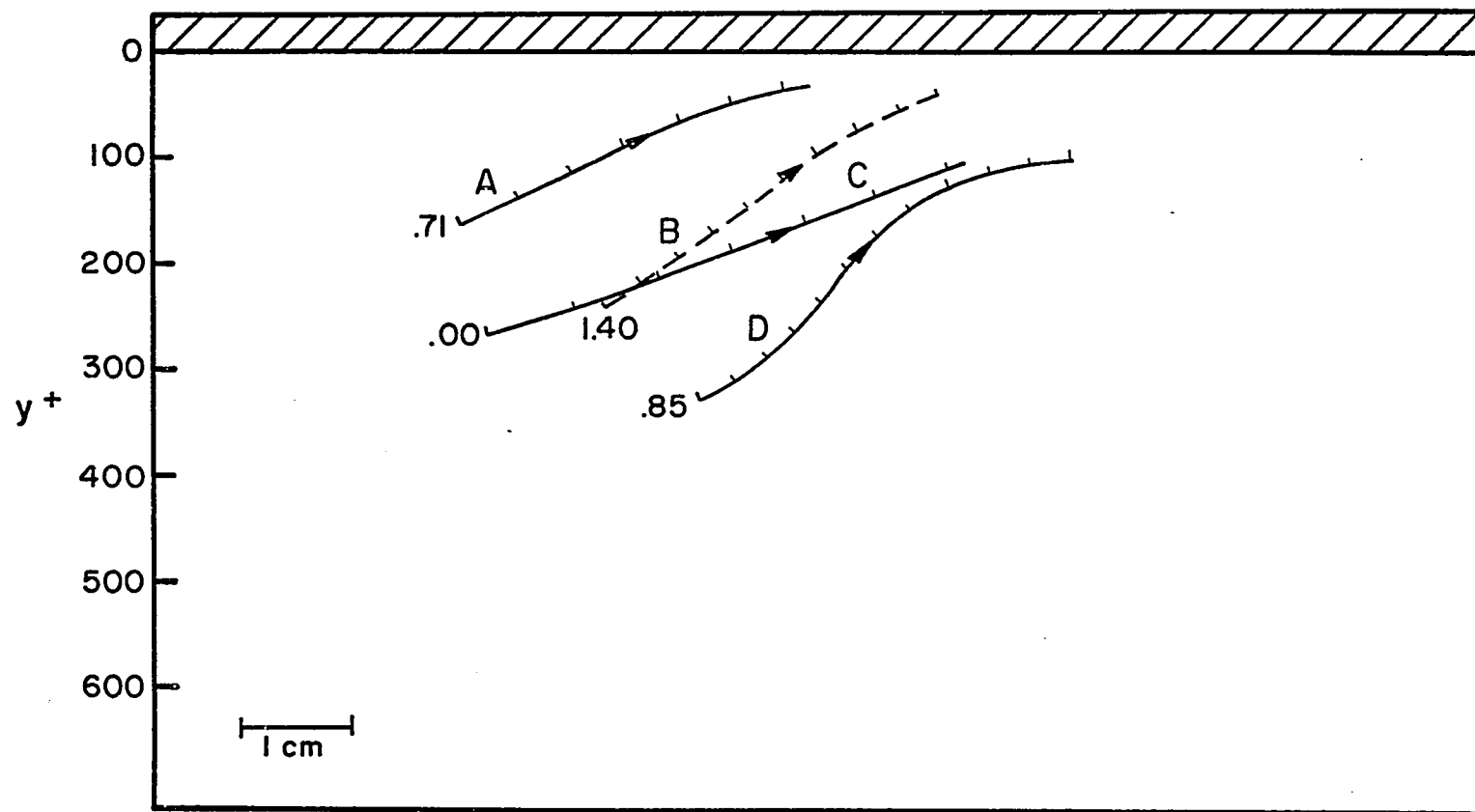


FIGURE 40. PARTICLE PATHS DURING A LARGE SCALE INFLOW (CONVECTED VIEW)

TABLE 13

STUDY OF LARGE SCALE INFLOWS (Run M-132)

| y_{or}^+ | y_t^+ | \bar{y}^+ | $U_x(t),$ cm/sec | $\bar{U}_x(\bar{y}^+),$ cm/sec | $u(t),$ cm/sec | $v(t),$ cm/sec | $-uv,$ (cm/sec) ² | $-\frac{uv}{(U^*)^2}$ | $U_t,$ cm/sec | $\phi_s,$ degrees |
|----------------------|---------|-------------|---------------------|-----------------------------------|-------------------|-------------------|---------------------------------|-----------------------|------------------|----------------------|
| <u>First Inflow</u> | | | | | | | | | | |
| 120 | 67 | 94 | 13.00 | 13.92 | -0.92 | -2.00 | -1.84 | -2.35 | 13.20 | 7.3 |
| 92 | 40 | 66 | 14.50 | 12.81 | 1.69 | -2.60 | 4.38 | 6.80 | 14.80 | 10.0 |
| 86 | 56 | 71 | 14.45 | 12.82 | 1.63 | -3.00 | 4.88 | 7.57 | 14.75 | 12.0 |
| 174 | 140 | 157 | 16.00 | 14.50 | 0.50 | -3.80 | 1.90 | 2.95 | 16.50 | 13.5 |
| 194 | 154 | 174 | 13.10 | 14.55 | -1.35 | -3.50 | -4.72 | -7.30 | 13.60 | 15.0 |
| 294 | 250 | 172 | 15.10 | 14.55 | 0.55 | -4.30 | 2.36 | 3.66 | 15.70 | 16.0 |
| 280 | 234 | 257 | 16.75 | 15.73 | 1.02 | -2.00 | 2.04 | 3.11 | 16.80 | 6.7 |
| 400 | 360 | 380 | 16.80 | 16.20 | 0.60 | -2.30 | 1.38 | 2.14 | 17.00 | 7.5 |
| 416 | 368 | 392 | 13.70 | 16.44 | -2.74 | -3.40 | -9.35 | -14.50 | 17.10 | 11.5 |
| 500 | 468 | 484 | 17.50 | 16.72 | 0.78 | -2.00 | 1.58 | 2.45 | 17.70 | 11.5 |
| 480 | 400 | 440 | 18.50 | 16.70 | 0.90 | -3.90 | 3.51 | 5.44 | 19.00 | 11.5 |
| 350 | 167 | 259 | 14.40 | 15.67 | -1.27 | -3.90 | -4.95 | -7.68 | 14.80 | 15.2 |
| 320 | 142 | 231 | 18.50 | 15.35 | 3.25 | -4.40 | 14.40 | 22.30 | 19.00 | 13.5 |
| 500 | 200 | 350 | 16.40 | 16.35 | 0.05 | -2.10 | 0.10 | 0.15 | 16.60 | 7.5 |
| 235 | 110 | 133 | 13.70 | 14.10 | -0.40 | -3.20 | -1.28 | -1.98 | 14.20 | 13.0 |
| <u>Second Inflow</u> | | | | | | | | | | |
| 165 | 50 | 108 | 12.60 | 13.80 | 0.80 | -2.35 | 1.88 | 2.92 | 12.90 | 10.5 |
| 220 | 100 | 110 | 11.20 | 13.80 | -2.60 | -2.50 | -6.50 | -10.10 | 11.40 | 12.4 |
| 267 | 104 | 185 | 15.70 | 14.90 | 0.80 | -2.75 | 2.40 | 3.72 | 16.00 | 10.0 |
| 54 | 34 | 44 | 13.90 | 11.75 | 2.15 | -1.40 | 3.05 | 4.73 | 14.00 | 6.0 |
| 100 | 43 | 77 | 11.60 | 13.15 | -1.55 | -1.90 | -2.95 | -4.57 | 11.70 | 9.2 |
| 172 | 104 | 138 | 13.30 | 14.05 | -0.75 | -4.00 | -3.00 | -4.65 | 13.70 | 12.0 |
| 328 | 280 | 304 | 10.10 | 16.01 | -5.91 | -1.90 | -11.22 | -17.40 | 10.20 | 10.7 |
| 280 | 234 | 257 | 10.00 | 15.60 | -5.60 | -3.20 | -17.92 | -27.80 | 10.50 | 17.5 |

The part of the inflow motion which penetrates the wall area shows a similar character to the sweep events, as can be observed from the magnitude and sign of the instantaneous Reynolds stresses $-\rho(uv)$. Their wallward angles in the wall area are generally larger than the ones corresponding to the sweep events. Moreover, these wall inflows were rarely associated with wall area ejections. The smallest wallward angle observed was 2.5 degrees whereas the largest one was 17.5 degrees. The very large positive or negative contributions to the instantaneous $-\rho uv$ Reynolds stresses can be observed in Tables 12 and 13. These and other implications from these tables will be further discussed in the next section.

The flow field during the large scale inflow events appeared laminar-like and no violent interactions inside it were observed. Here again, no sharp demarcation line could be observed between the inflow region and the regions surrounding it. The inflow event appeared to be a stage during which the flow field reestablished the mean velocity profile.

Large Scale Outflow

This event constituted a large scale motion similar in scale with the inflow event. It appeared as a mass of fluid moving on a small angle away from the wall while transported downstream with a velocity slightly lower than

the local mean \bar{U}_x . Usually an outflow followed just after an inflow event or vice versa. There were cases where an outflow followed a transverse vortex. No cases were observed where a large scale outflow followed a deceleration or acceleration event. Very rarely it was observed that the fluid particles of a large scale inflow after approaching a y^+ of 150 to 200 then started moving outward giving rise to a large scale outflow event. Most of the outflows observed originated from a region of a y^+ of 150 to 200 and extended to a $y^+ = 500$ and sometimes to $y^+ = 600$.

In contrast to the inflows which penetrated as far as the wall area, the outflows were observed to occur in the outer region only. The fact that they did not extend up to the wall area (including it) and that the outflowing fluid particles did not include elements originating from this region, distinguished them easily from the decelerated regions. In Figures 41 and 42 two large scale outflows observed in two different motion picture runs are presented. In Table 14 measurements and numerical data for these two outflows are summarized. Both of them cover a range from a y^+ of about 150 to 200 up to a y^+ of about 500 to 550; their streamwise extent was about $x^+ = 900$. The smallest outward angle ϕ_e measured was 1.0 degree and the largest 13.2 degrees. There are two fluid particles

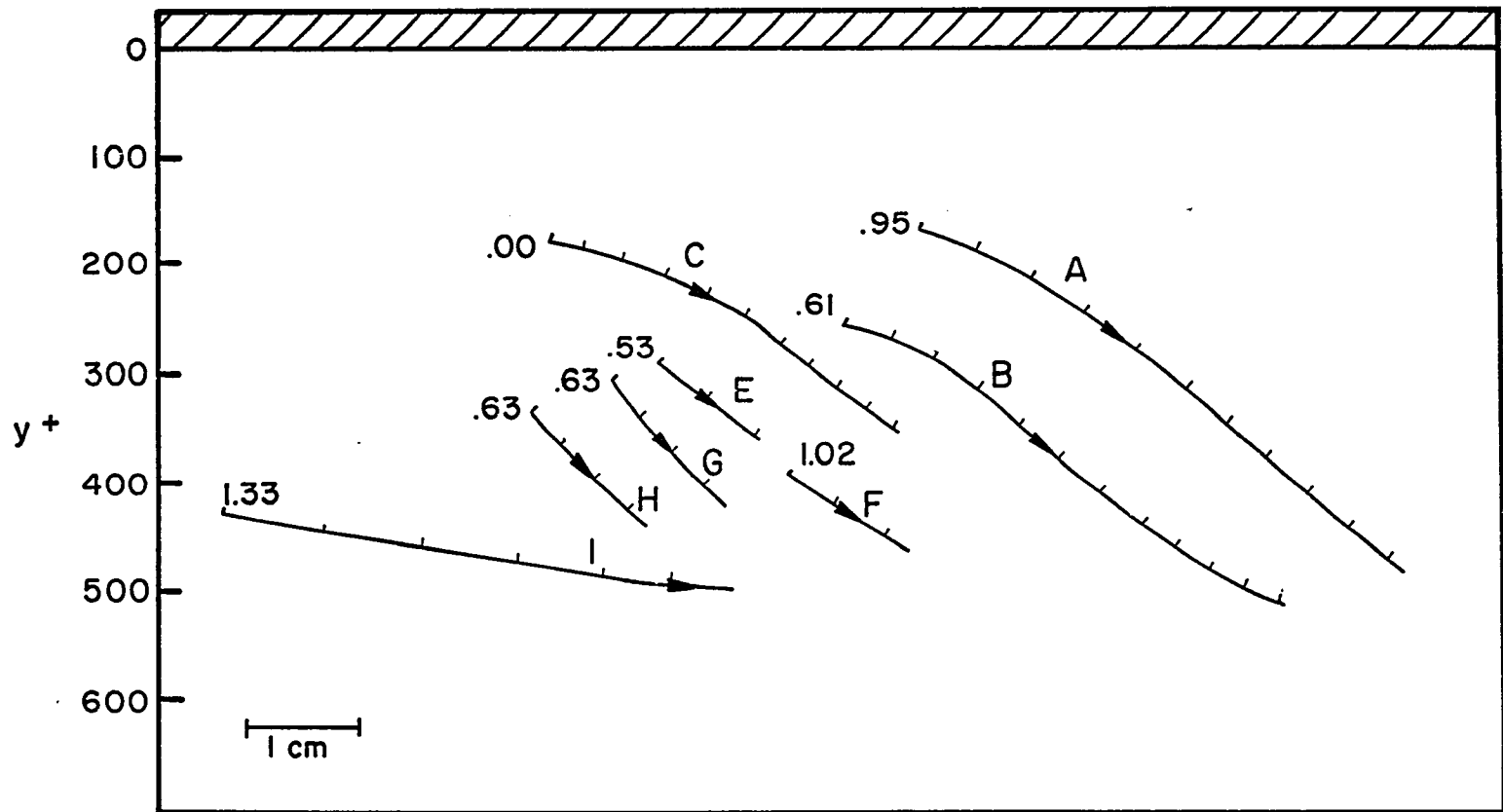


FIGURE 41. PARTICLE PATHS DURING A LARGE SCALE OUTFLOW (CONVECTED VIEW)

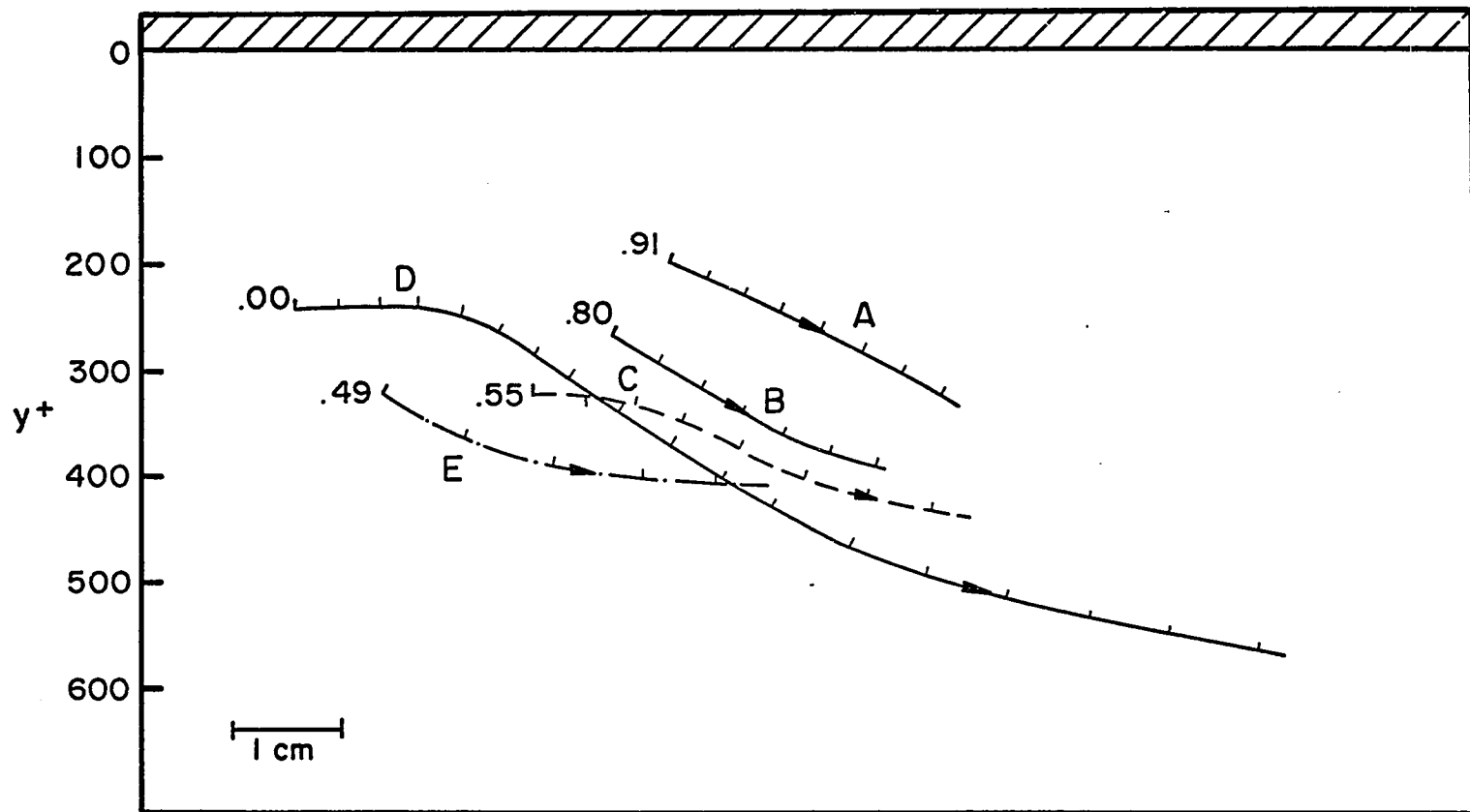


FIGURE 42. PARTICLE PATHS DURING A LARGE SCALE OUTFLOW (CONVECTED VIEW)

TABLE 14

STUDY OF LARGE SCALE OUTFLOWS

| y_{or}^+ | y_t^+ | \bar{y}^+ | $U_x(t)$, cm/sec | $\bar{U}_x(\bar{y}^+)$ cm/sec | $u(t)$, cm/sec | $v(t)=V$ cm/sec | $-uv$ (cm/sec) ² | $-\frac{uv}{(U^*)^2}$ | U_t , cm/sec | ϕ_e degrees |
|------------------|---------|-------------|----------------------|----------------------------------|--------------------|--------------------|--------------------------------|-----------------------|-------------------|---------------------|
| <u>Run M-133</u> | | | | | | | | | | |
| 200 | 246 | 223 | 11.80 | 14.27 | -2.47 | 1.60 | 2.93 | 4.50 | 11.90 | 7.5 |
| 278 | 312 | 295 | 13.30 | 14.79 | -1.49 | 3.00 | 4.46 | 6.85 | 13.60 | 12.5 |
| 350 | 400 | 375 | 13.40 | 15.25 | -1.85 | 2.40 | 4.44 | 6.82 | 13.60 | 10.0 |
| 416 | 464 | 440 | 12.30 | 15.64 | -3.34 | 2.20 | 5.15 | 7.90 | 12.50 | 10.0 |
| 500 | 568 | 534 | 16.30 | 16.30 | 0.00 | 1.65 | 0.00 | 0.00 | 16.50 | 6.0 |
| 265 | 368 | 337 | 13.70 | 15.10 | -1.40 | 2.50 | 3.50 | 5.37 | 13.90 | 10.0 |
| <u>Run M-134</u> | | | | | | | | | | |
| 340 | 440 | 390 | 12.10 | 15.18 | -3.08 | 2.90 | 8.95 | 14.00 | 12.50 | 13.2 |
| 255 | 518 | 387 | 12.80 | 15.12 | -2.32 | 2.30 | 5.34 | 8.37 | 13.05 | 10.3 |
| 167 | 485 | 326 | 13.60 | 14.85 | -1.25 | 3.00 | 3.75 | 5.86 | 13.80 | 12.3 |
| 44 | 70 | 67 | 14.70 | 11.50 | 3.20 | 2.20 | -7.04 | -11.02 | 14.80 | 8.2 |
| 70 | 110 | 90 | 13.50 | 11.75 | 1.75 | 1.80 | -3.15 | -4.93 | 13.60 | 7.5 |
| 170 | 200 | 185 | 14.30 | 13.35 | 0.95 | 2.00 | -1.90 | -2.97 | 14.40 | 8.0 |
| 244 | 284 | 264 | 12.46 | 14.25 | -1.79 | 2.70 | 4.84 | 7.57 | 12.60 | 12.5 |
| 284 | 320 | 302 | 12.85 | 14.58 | -1.73 | 2.70 | 4.66 | 7.29 | 13.15 | 10.5 |
| 430 | 476 | 453 | 17.80 | 15.30 | 2.50 | 1.30 | -3.25 | -5.08 | 17.90 | 4.5 |
| 570 | 584 | 577 | 16.60 | 16.00 | 0.60 | 0.30 | -0.18 | -0.28 | 16.62 | 1.0 |

listed in Table 14 that did originate from the wall area. It can be seen from the sign of the streamwise velocity fluctuation $u(t)$ that they belonged to high speed fluid, so that they can be definitely distinguished from wall ejections originating in a decelerated flow region. The large values of positive contribution to the instantaneous Reynolds stress $-\rho uv$ from these outflows in the outer region is to be noted. This point will be further discussed in the next section.

The flow field inside the outflows appeared laminar-like. Most of the fluid particle paths either were observed to move almost parallel to each other or in a small angle. In a few cases their paths crossed each other, at least as long as they remained in the field of view. No violent interactions were observed inside the region of the outflow events.

Connected Fluid Motions

Certain visual observations will now be presented in the light of the individual events already described. The extent of the common features of fluid motions characterizing an event constitute at the same time a region of connected fluid motions. To illustrate and further clarify the above, some sketches will be used based solely on the visual observations.

In Figure 43 the connected and non-connected fluid motions during the acceleration and deceleration events are illustrated. Along the line AA', fluid motions appear visually connected; they all belong to the same region of high speed fluid which extends from the wall to the far outer region. The same thing is observed along the line CC' belonging to the low speed fluid region; but here the nature of connected motions is different from the first one. From the above viewpoint fluid motions appear non-connected along BB' and DD' (all in the wall region), EE' (all in the outer region) and BB" (between wall and outer regions).

In Figure 44 connected and non-connected fluid motions are illustrated during inflow (a) and outflow (b) events. In both cases the wall region (AA') is observed to exhibit a different character of fluid motions than the other region (BB').

Summary of Observations

In the preceding sections the detailed description of the nature of turbulent motions in the outer region and wall region were presented. This presentation, for the sake of clarity, was somewhat fragmented. In this section a summary of these observations in the form of a composite picture will be given. The region extending approximately

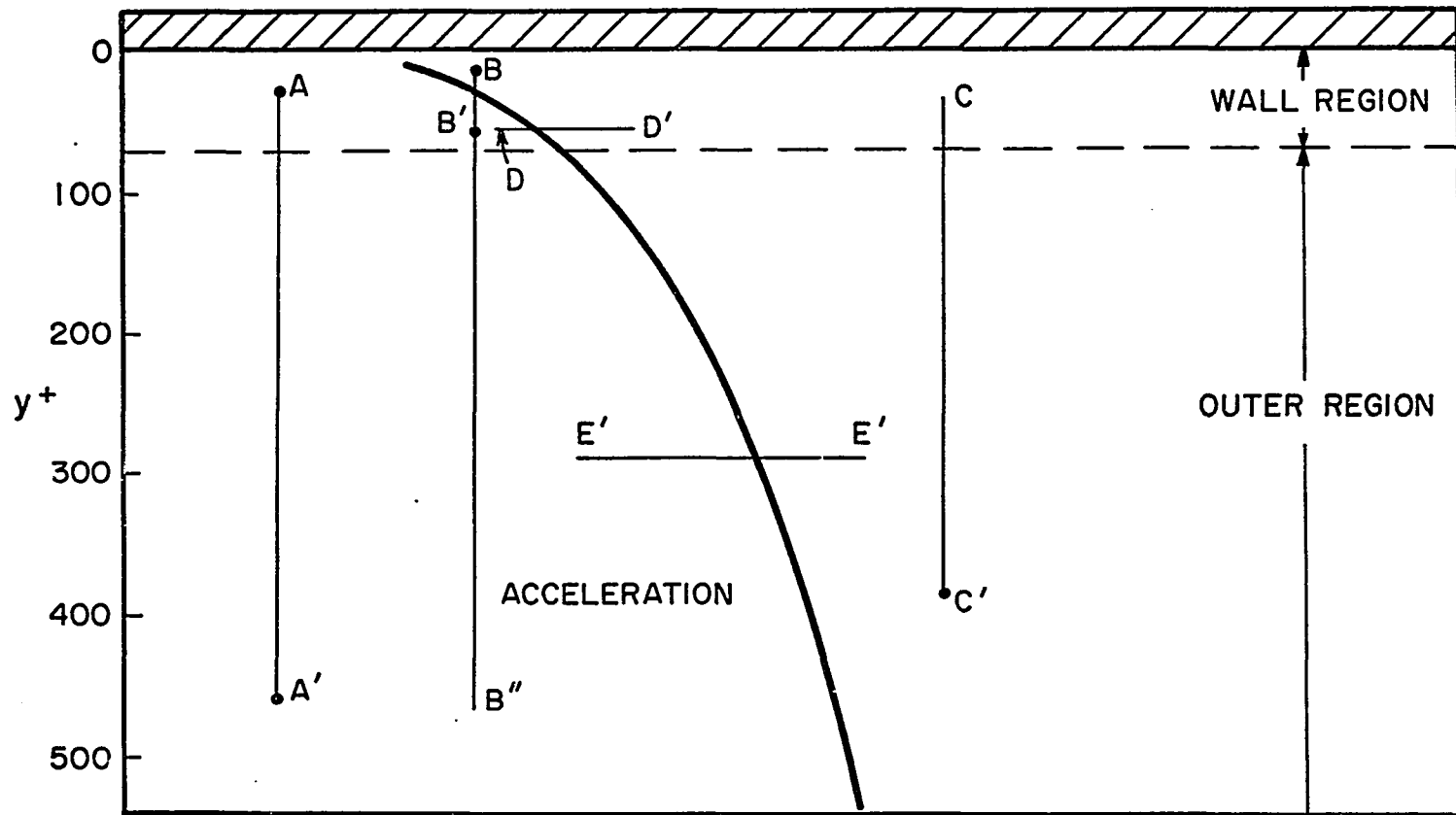
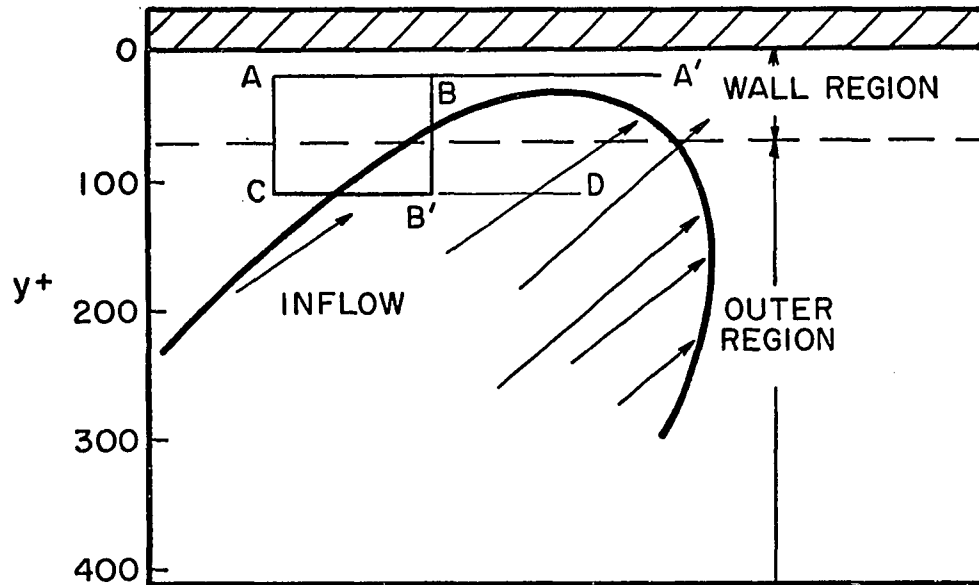
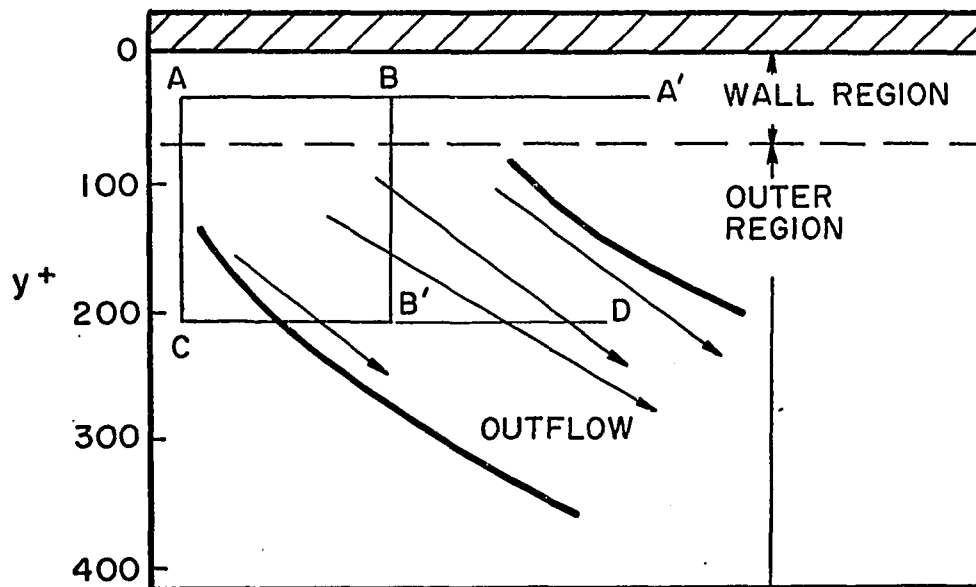


FIGURE 43. CONNECTED AND NON-CONNECTED FLUID MOTIONS DURING ACCELERATION AND DECELERATION EVENTS (CONVECTED VIEW)



(a) INFLOW



(b) OUTFLOW

FIGURE 44. CONNECTED AND NON-CONNECTED FLUID MOTIONS DURING INFLOW (a) AND OUTFLOW (b) EVENTS (CONVECTED VIEW)

from $0 \leq y^+ \leq 70$ is considered as the wall region, whereas the region extending from $y^+ > 70$ is considered as the outer region.

In both the wall and outer regions distinct and well identifiable events were observed. Each of these events was part of a deterministic sequence, although this sequence occurred randomly in space and time.

The first of these events was a deceleration of the streamwise velocity extending from the wall to the outer region. The degree of deceleration varied with deficiencies as great as 50 percent of the local mean streamwise velocity.

While the flow field was thus decelerated, the second event occurred. This event was an acceleration of the streamwise velocity. It appeared as a mass of fluid entering from upstream and extending from the wall up to the outer region. As the accelerated fluid moved downstream, it displaced and accelerated the decelerated fluid which was in front of it. This accelerating action occurred faster in the outer than in the wall region.

The most important event of the outer region was a fluid motion which, in the convected view of the travelling camera, appeared as a transverse vortex. This was a large scale motion (typical diameter of about $150 y^+$ units) transported downstream almost parallel to the wall with an

average velocity slightly smaller than the local mean \bar{U}_x . The formation of the transverse vortices was the result of an instability interaction (Helmholtz instability) between accelerated and decelerated fluid regions. One or more transverse vortices were formed by the interaction of the same accelerated and decelerated fluid regions. Although decelerated fluid participated in the formation of the transverse vortices, it was the accelerated fluid that was responsible for its participation.

The most important events of the wall region were the ejections and sweeps. These events occurred as follows: while the transverse vortex was transported downstream, small scale fluid elements, originating in the wall area of the decelerated flow, were ejected outwards (ejection event). After travelling some outward distance, the ejected elements interacted with the oncoming accelerated fluid in the wall region and were subsequently swept downstream (sweep event).

Two large scale fluid motions also were involved in the deterministic sequence of events. These were inflows (motions toward the wall) and outflows (motions away from the wall); they both extended from the far outer region up to an area adjacent to the wall region. Usually an inflow followed an outflow or vice versa and occurred some time after the transverse vortex.

In the deterministic sequence of events, not all the events appear all the time nor in exactly the same order; but for most of the cases they occurred as described.

Estimated positive and negative contributions to the instantaneous Reynolds stress $-\rho uv$, during the events were many times higher than the local mean averages. Values of $-\rho uv$ of 40 to 100 times higher than the local $-\overline{\rho uv}$ were measured.

DEDUCTIONS AND HYPOTHESIS FROM THE EXPERIMENTAL DATA

In the present section an attempt will be made to construct a hypothesis on the structure of a turbulent boundary layer and on some of the turbulence transport processes occurring in it. The visual observations and measurements presented in the previous section will be used as a basis for this hypothesis; whenever necessary they will be supplemented by measurements of others. As mentioned before, the emphasis of the present experimental work was on the outer region. The visual study of the wall region by a similar experimental technique was the subject of Corino's work (7). Since only limited visual observations and measurements of the wall area were permitted by the present experimental work, frequent reference to the work of Corino will be made to supplement the suggestions for this area. The discussion of this work and its comparison with other works will be presented in the next section.

It has been previously emphasized that sharp lines of demarcation between the various regions and events do not exist. In spite of a certain degree of overlapping between

adjacent zones, the distinct features and fluid motion behavior in each region permitted its characterization and differentiation from the others. It will be convenient to divide the y^+ -distance from the solid wall to the edge of the boundary layer into two zones. It should be kept in mind that such a division does not involve a sharp interface. It is to be thought of as a division in regions exhibiting a particular character of fluid motions.

Wall Region ($0 \leq y^+ \leq 70$)

This region can be divided (e.g., see Corino) into the sublayer ($0 \leq y^+ \leq 5$) and the generation region ($5 \leq y^+ \leq 70$). The present visual study did not permit such a division, therefore the whole region $0 \leq y^+ \leq 70$ will be treated as one. Very close to the wall the fluid motions were not laminar. Even in cases where fluid particle paths appear rectilinear for some time, they were usually directed at some small angle. During a deceleration or acceleration event and before an ejection had occurred, the fluid motions appeared laminar-like, but this did not last long. It was from the wall region that all the ejections originated. These were very energetic motions and their large positive contribution to the instantaneous Reynolds stress, $-\rho uv$, has already been cited. The sweep events occurring in the same region appeared equally energetic. The measurements on these also showed very large positive contribution to the instantaneous Reynolds stress. In

addition the wall area was the location where most of the interactions occurred. The whole region therefore appeared as the region where most of the turbulent energy was generated.

The interface between the accelerated and decelerated fluid exhibited a high velocity gradient. It will be recalled that this demarcation line appeared sharper in the wall area than in the outer region. Thus in the wall area, the velocity gradients were probably higher along this interface than further out. When an ejection occurred, the ejected fluid elements penetrated into the accelerated region. Since the ejected fluid was actually low speed fluid, the interface between it and the accelerated fluid also constituted a region of high velocity gradients. Hence locally, high shear rates are created by these high velocity gradients; these in turn, locally create regions of high turbulent dissipation into heat, since for a Newtonian fluid the rate of dissipation is equal to the square of the velocity gradient times the viscosity.

In Figure 45 are illustrated the interfaces between decelerated and accelerated fluid where those high velocity gradients occur. Thus the wall region is not only the area where most of the turbulent energy is generated, but also where it is dissipated. The events responsible for the production of turbulent energy (as expressed by $-\rho uv$)

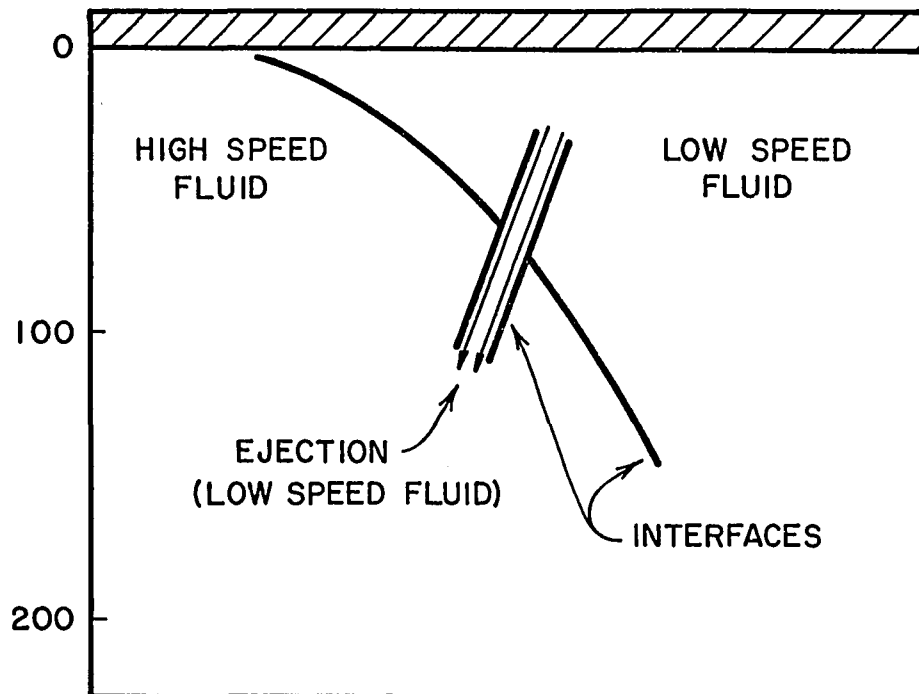


FIGURE 45. INTERFACES OF HIGH AND LOW SPEED FLUIDS EXHIBITING HIGH VELOCITY GRADIENTS (CONVECTED VIEW)

appear to be the ejections and sweeps, whereas the interactions at the interface between high and low speed fluid are mainly responsible for its dissipation. Since these events and their interactions are phenomena very localized in space and time, the processes of turbulent energy generation and dissipation in the wall region would appear to be highly intermittent. This is apparent from the data where the positive contributions to the instantaneous Reynolds stress $-\rho uv$ are shown to be as high as 40 times the local mean $-\rho \overline{uv}$. The turbulent energy which is not locally dissipated diffuses or is convected towards the wall or the outer region. The deep penetration of the ejected wall fluid elements into the outer region is closely associated with such an outward turbulent energy convection. The large values of the positive contributions to the instantaneous Reynolds stress from the sweep can be associated with a wallward turbulent energy transfer. Whether this energy transfer extends to the viscous sublayer region ($0 \leq y^+ \leq 5$) is not evident from the present data and visual observations.

Energy transfer of a similar nature was observed in Corino's work, the emphasis of which was placed in the wall region. Corino observed that the region $0 \leq y^+ \leq 5$ the character of fluid motions was definitely not laminar and that the velocity fluctuations in the sublayer were sustained by energy transferred from the generation region. This

energy was transferred both by viscous transport and turbulent diffusion. In addition, Corino observed that the turbulence level within the sublayer region was a function of that in the generation region and thus indirectly of the Reynolds number.

The character of the sweep event depended on the local conditions of the wall region as well as the outer region. The fluid participating in the sweep event was part of the accelerated region and thus one understands the dependency of the sweep event on the conditions of the outer flow. But by its definition the sweep event (in the Corino sense, i.e., following an ejection) did not manifest itself until an ejection had occurred. Since these events originated only in the wall region, one can understand the dependency of the sweep event on conditions of the wall region.

The visual observations of this work did not indicate that the ejection events were dependent on wall region conditions. The ejection event, with regard to its frequency of occurrence, was closely associated with the transverse vortices of the outer flow. This close association strongly suggests that the transverse vortices induce conditions in the wall region to cause an ejection to occur. The modification of the pressure field during the time of a transverse vortex is an obvious candidate. The study of the instantaneous pressure gradient ($\partial p / \partial y$) near

the wall and its correlation with the decelerated flow associated with the ejections, would give insight concerning the role of transverse vortices in the occurrence of ejections. Although the observations are strongly suggestive of this as being a causative factor for the wall ejections, they do not exclude other mechanisms as being equally important.

Outer Region $y^+ > 70$

The change in the character of fluid motions from the wall to the outer region is not abrupt. It occurs in a zone of approximately $70 < y^+ < 150$, which can be considered a sort of a transition area. Beyond y^+ of about 150 the distinct character of the outer region manifests itself.

A deterministic sequence of events occurs in this region although the events do occur randomly in space and time. The visual observations and data suggest the following idealized picture of the flow field. The picture is termed idealized because in some experimental runs neither all the events were observed nor in the same order. But for most of the cases, the sequence of events was as follows: the first event of the sequence was a decelerated region extending from the wall up to the far outer region. The origin of this event is not apparent from the visual character of the flow and its continuity implications. But no obvious causative factors for such a velocity defect and

for such a wide y^+ -region were apparent from the present observations. Moreover due to the nature of the experimental technique there was no way of observing its spanwise extent. This outer part of the decelerated region appeared to depend on upstream flow conditions, whereas the wall region zone of the low speed fluid appeared to depend on local conditions. This is supported by the fact that a sharper demarcation line was observed between the high and low speed fluids in the wall region rather than in the outer region. Apparently the action of the solid boundary (viscous effects) slows down the propagation of upstream influences within the wall zone of the decelerated fluid.

The deceleration event is immediately followed by the acceleration event. The origin of this high speed fluid is not apparent from the visual observations. The outer part of it definitely depends on the upstream history of the flow. As the high speed fluid moves towards the wall region, displacing the decelerated fluid, its character is more and more dependent on local or adjacent to it downstream conditions (i.e., the decelerated fluid in front of it). The decrease of wallward angles toward the wall region is a manifestation of this. Even after the interaction of low and high speed fluids in the wall region has progressed to some degree, the outer part of the accelerated fluid depends mainly on the upstream history of the flow.

This results from a convection of the history of flow events faster by the high velocities of the outer flow than the local influences can diffuse outward from the wall region.

It is proposed that the acceleration event is one of the mechanisms by which energy from the outer flow is transferred towards the wall region. This is apparent from the large positive contributions to the instantaneous Reynolds stress $-\rho uv$ during this event (wallward flow). The data also show that the accelerated fluid included some fluid elements moving away from the wall (outward flow). This outward flow of high speed fluid gives a negative contribution to the instantaneous Reynolds stress $-\rho uv$. From the limited measurements of instantaneous Reynolds stresses made here nothing can be said about a balance of these positive and negative contributions. The visual observations do show that most of the high speed fluid elements are directed wallwards, hence being a net positive contribution to the instantaneous Reynolds stress $-\rho uv$.

The single most important event of the outer region is the transverse vortex. This vortex is the result of an instability interaction between accelerated and decelerated flow events. As the high speed fluid moves downstream faster than the decelerated region, a highly inflexional instantaneous velocity profile is formed. This is exactly the situation observed in free stream shear layers (e.g., jets)

with the only difference being that in the outer region of the turbulent boundary layer, it is an unsteady developing situation. It occurs only when the acceleration event manifests itself. This acceleration event always originates in the outer region and, by encroaching inwards, transmits its influence towards the wall. This wallward encroachment of the acceleration event is nothing more than an entrainment of high speed fluid into the decelerated region. This entrainment process is more dramatically observed in the case where a reverse transverse vortex is formed (see Figure 13). When this entrainment has progressed to a degree where an inflexional instantaneous velocity profile is formed, it becomes unstable (Helmholtz instability) and one or more transverse vortices are formed. The visual observations do not suggest that the low speed fluid causes this instability. It does, however, participate in it; but it is the high speed fluid responsible for its participation in the formation of the transverse vortices. According to this picture, decelerated fluid moves outward and accelerated fluid inwards during the vortex formation. The vortex travels some distance downstream by the continuously existing instantaneous inflexional velocity profile which feeds the Helmholtz instability.

The very large values of the positive contributions to the instantaneous Reynolds stresses during a transverse vortex from Tables 7 through 11 should be noted. These come from either high speed fluid moving towards the wall or low speed fluid moving outwards, i.e., the two events participating in the formation of the transverse vortex. Some individual positive contributions to the instantaneous Reynolds stresses are 100 times higher than the local mean $-\overline{\rho uv}$. At the same time some very large negative contributions to the instantaneous $-\rho uv$ can be observed. Hence the transverse vortices appear as events where high rates of turbulent energy production (positive and negative) occur.

There is, of course, no doubt loss of turbulent energy to heat via viscous dissipation as a result of relatively high velocity gradients and thus high values of $\mu(\partial U_i/\partial x_j)^2$. This viscous dissipation should be distinguished from the negative $-\rho uv$ which is a negative contribution (loss) to the turbulent energy production if a time average of both positive and negative $-\rho uv$ would be taken. The loss of turbulent energy comes mainly from accelerated fluid moving outwards or decelerated fluid moving wallwards. Only for a few selected fluid particles were values of $-\rho uv$ estimated and no conclusion can be drawn as to a net balance for the turbulent energy production. However, it did appear

from the movies that the large majority of fluid particles were moving so as to positively contribute to the instantaneous Reynolds stress.

The turbulent energy not locally dissipated is convected or transferred by molecular means towards and away from the wall. In the outer region of the turbulent boundary layer, convective energy transfer is expected to be much higher than diffusive transport. No conjecture can be made about what part of the non-dissipated turbulent energy is convected wallwards or outwards. It is proposed that the transverse vortices are one of the mechanisms of turbulent energy exchange by convection between the outer and the wall regions.

It is most important to emphasize the close association of the transverse vortices with the wall region ejections. The very high instantaneous rate of turbulent energy production, both positive and negative, during a transverse vortex is liable to cause correspondingly high pressure fluctuations. Molo-Christensen (24) has similarly commented on this question. By a simple modification of the momentum equation, he arrived at a differential equation associating the pressure field with a turbulent production event. Grant (11) has attempted to explain similar type events, i.e., "outward eruptions" originating in the wall region, by introducing the effects of pressure fluctuations

and gradients, and local instabilities due to vortex stretching. Pertinent to the question of the origin of wall ejections are the measurements of Bakewell and Lumley (1). These measurements suggest a large eddy structure of elongated streamwise extent that gives rise to an region of strong updraft of the fluid between the eddies.

An analytic relation providing information about a functional dependence of these pressure fluctuations on the instantaneous $-p_{uv}$ and their propagation to the wall area is still lacking. However, some qualitative remarks on this matter are now in order. The wall zone of the decelerated fluid is at a higher pressure p_2 than the pressure p_1 of the outer region at a given x -location during a transverse vortex (see Figure 46). The justification can be obtained from a simple Bernoulli balance between points 1 (high velocities) and 2 (low velocities). If one adds to this already positive pressure gradient $(\partial p / \partial y)$, the instantaneous high pressure fluctuation, then a large $(\partial p / \partial y) > 0$ occurs in the wall region. It is thus proposed that the transverse vortices are one of the causative factors for the wall region ejections. This proposition is further enhanced by the visual facts that the majority of the ejections were observed to be closely associated with the occurrence of transverse vortices. The

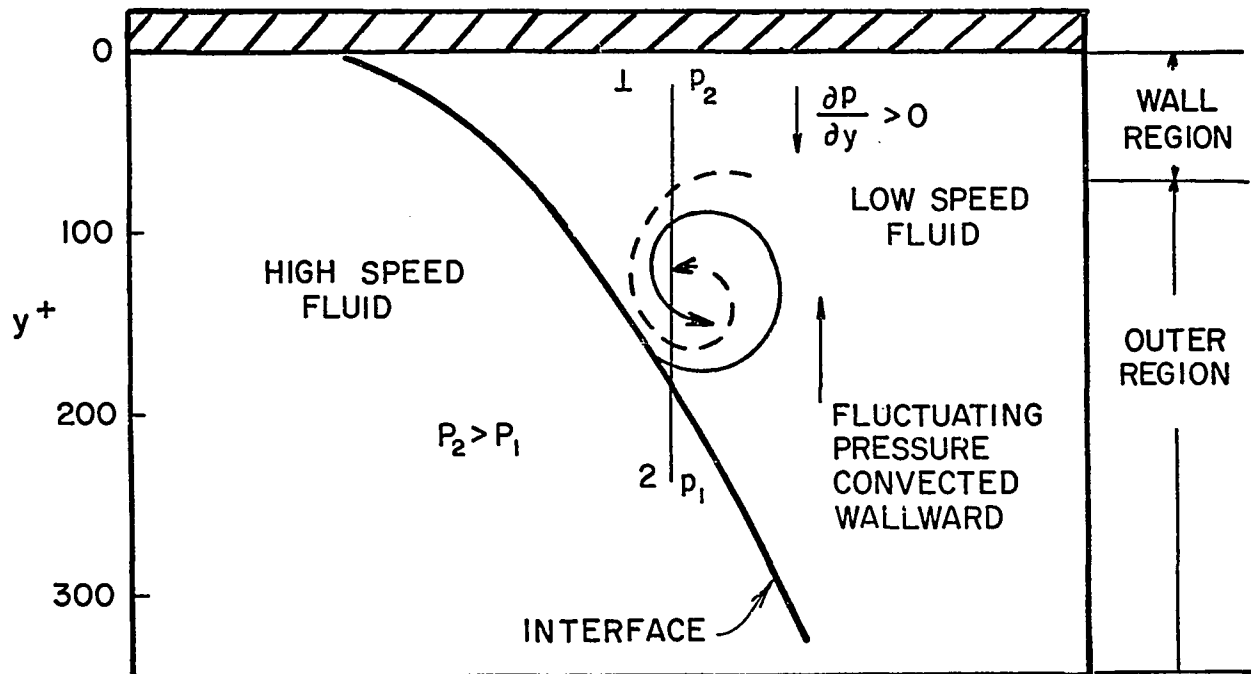


FIGURE 46. PRESSURE FIELD DURING A FORWARD TRANSVERSE VORTEX

present study does not exclude other possibilities creating favorable conditions for all ejections to occur. It simply suggests one of them. Obviously the whole question of the origin of wall ejections is still open.

The other important events observed in the outer region are the large scale inflows and outflows. Their role from a viewpoint of turbulent energy production, dissipation or exchange is not clear from the limited measurements of instantaneous Reynolds stresses presented in Tables 12, 13, and 14. This is in spite of the fact that some instantaneous positive and negative contributions to the $-\rho uv$ are many times higher than the local mean averages. Few inflows penetrated to the wall region; the majority of them seemed to extend up to an area adjacent to it. The outflows started further out (y^+ of about 150). Visually both the inflows and outflows were mainly confined to the outer region and covered its entire extent. It is suggested that they are part of the three-dimensional character of the flow.

In Figure 47, a diagram of the turbulent energy generation, dissipation and exchange between the wall and outer regions based on the visual observations and measurements is presented. According to this diagram, turbulent energy is mainly generated in the wall region. The events responsible for this generation are the ejections, sweeps

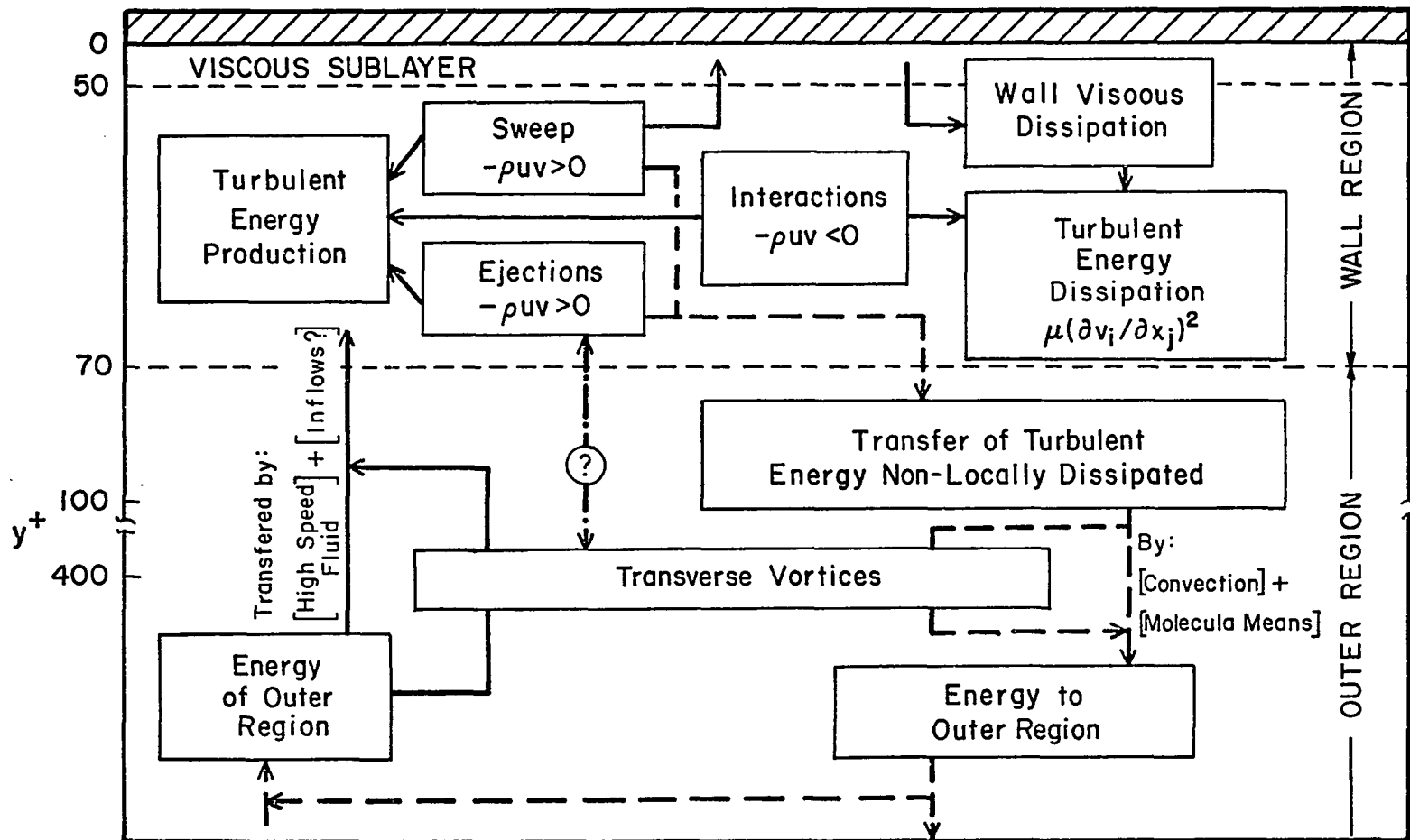


FIGURE 47. TURBULENT ENERGY PRODUCTION, DISSIPATION AND EXCHANGE

(positive $-\rho uv$) and their interactions (negative $-\rho uv$); moreover the interactions of ejections and sweeps are responsible for high rates of viscous dissipation [positive $\mu(\partial U_i/\partial x_j)^2$]. The turbulent energy generated and not locally dissipated is partly transferred by molecular means and convected (by the sweeps) towards the sublayer region, thus contributing to this region's small velocity fluctuations and viscous dissipation at the wall. The rest of the non-dissipated energy is transferred outwards mainly by convection. The balance of energy must be provided by the outer flow and the event mainly responsible for this transport is the accelerated flow. The transverse vortices act as an exchange mechanism for energy transfer from and to the wall region.

One of the most important deductions of the present visual observations and velocity measurements is a new insight to the puzzling questions concerning the connection and interaction of the wall and the outer regions in a turbulent boundary layer. The breaking down of the turbulent shear flow field into individual identifiable events and their interactions allows an answer based solely on a pure physical picture.

Connected fluid motions between the wall and outer regions or throughout the extent of a region do occur, but only in the context of an individual event. Most important

of all, the character of connected movements changes in the streamwise direction. It is to be emphasized at this point that connected or non-connected fluid motions between the wall and the outer regions do not occur all the time; they manifest themselves only during some of the events, i.e., they exhibit an intermittent character.

DISCUSSION AND COMPARISON WITH OTHER WORK

For the sake of simplicity of presentation, the visual studies of other investigators will be first discussed and compared with the present work. Then the measurements and observations obtained by other means will be considered.

Visual Studies

Corino and Brodkey (7,8) made visual studies of the wall region of a turbulent pipe flow. The basic principle of their experimental technique was essentially the same as the present one. They dispersed submicron magnesium oxide particles in trichlorethylene and studied the motions with a high speed motion picture camera moving with the flow. However, the field of view was much smaller than the present one. They employed a magnification of about 4.3X versus a (1/18)X magnification of the present work. The experimental problems associated with the photographing of such a small field of view (8) are entirely different than in the present case. Another difference between the two works is that the visual study of Corino and Brodkey was restricted to the wall region. A valid comparison between the two must be restricted to the wall region only. The

different geometrical configuration (pipe versus flat plate flow) imposes different implications on the nature of the fluid motions occurring in the outer regions. This is associated with the intermittent character of the flat plate turbulent boundary layer and the absence of such intermittency phenomena in the outer region of turbulent pipe flow. They observed in the wall region in turbulent pipe flow the intermittent ejections of fluid elements away from the wall. These ejections were part of a deterministic sequence of events which was observed to occur randomly in space and time.

The first event of this sequence was a deceleration of the axial velocity. It occurred in a localized radial region of $0 \leq y^+ \leq 30$, while its axial extent could not be estimated because of the limited dimensions of their field of view. This decelerated fluid moved nearly as a plug flow and velocity deficiencies as high as 50 percent of the local mean were observed. While the decelerated fluid was still in view the second event occurred. This was a mass of fluid entering from upstream with a velocity almost equal to the local mean. It usually extended as close as a $y^+ = 15$ and moved toward the wall at angles of 5 degrees to 15 degrees. This event was called acceleration; its dimensions were usually larger than the field of view. The accelerated fluid displaced and accelerated the retarded

fluid above a particular y^+ position. A shear layer was formed between the accelerated and retarded flow regions, which was then followed by the ejection event. This event was an abrupt outward movement of decelerated fluid. It was observed to be localized and random in space and time. Ejection angles were from 1.5 degrees to 21 degrees with an average value of 8.5 degrees. These angles were independent of Reynolds number, but the ejection frequency did depend on this number. The cycle ended with the sweep event, which was a flow of accelerated fluid from upstream. The event swept the entire picture from the field of view. Whenever an interaction between accelerated and decelerated fluid was observed, it produced a chaotic motion relative to the laminar-like character of the events themselves.

There is a striking similarity between the observations and measurements of Corino and Brodkey and the present ones. A one-to-one correspondence between the events occurring in the wall region can be immediately recognized in the two works. The acceleration event of Corino and Brodkey is the same as the wall zone of the accelerated fluid of the present work. Since their field of view was much smaller than the present one, they had no way of observing its y^+ -extent. Their visual observations and measurements of wallward angles of the accelerated fluid elements are in perfect agreement with the present ones.

The order of the sequence of events in the wall region is exactly the same. Although they did conclude that the streamwise extent of the decelerated fluid was larger than their field of view, they did report that its y^+ -extent was usually of the order of $30y^+$ units. In the present work it was observed that the deceleration extended up to the far outer region. A reinspection of Corino's movies showed that the decelerated region did at times cover the entire field of view, but at the time of ejection was generally limited. Apparently their observations of the deceleration were near the "tail end" of the wall zone of low speed fluid observed in the present work, where the radial extent was limited by the encroaching high speed fluid. No association or relation of the wall region ejections with events of the outer region (transverse vortices) could be observed by them because of their limited field of view.

Corino did take a few movies of the outer region of his turbulent pipe flow. These movies were not analyzed as a part of his thesis, since Corino's thesis problem was concerned only with the wall region. In one of these outer-region movies, there is a large scale rotating motion, reminiscent of a forward transverse vortex. It occurred at a $y^+ = 390$ and had an approximate diameter of $80y^+$ units. Since the y^+ -extent of the whole field of view was only

$90y^+$ units ($N_{Re} = 40,000$), it was impossible to suggest the source of the vortex, nor could an association with wall region events be observed during its occurrence. It is emphasized that this movie is not discussed in Corino's thesis nor is it in the reel of Corino's film available for loan (7).

Corino (7) suggested that the character of wall region ejections was basically dependent on local conditions. He further observed that their frequency of occurrence and velocity of ejection was dependent on mean flow parameters. To this end he suggested that some large scale motion of the outer flow might have provided favorable conditions for the wall ejections.

Corino and Brodkey observed that most of the ejections occurred in a region $5 \leq y^+ \leq 15$ and that the region of most intense interactions was $7 \leq y^+ \leq 30$. They estimated that about 70 percent of the positive contributions to the Reynolds stress comes from the ejections and the remaining 30 percent was attributed to the sweeps.

The visual observations and qualitative conclusions of the work of Corino and Brodkey are in excellent agreement with the ones of the present work. Because of their magnified view, their observations concerning the events and the areas inside the wall region where they occur are more complete than the present ones. On the other hand their concentration on the wall region did not permit them to

link those events with the ones of the outer region. The small dimensions of their field of view did not provide for identification and observation of the large scale motions and events of the outer flow. In the present work both the wall and the outer regions were in view at the same time; the events and nature of the wall region could be easily identified. Most important their relation to the outer region could be observed. To this extent the two works complement each other.

The frequency of wall region ejections as a function of Reynolds number was compared with the measurements of Corino and Brodkey (8). A very good agreement was found when both sets of the data were compared on the same friction velocity U^* . Because of the limited range of Reynolds numbers in the present study a frequency of events as a function of Reynolds number could not be established. The above mentioned comparison was made only for one value of Reynolds number.

Kline et al. (20) and Kim et al. (18) have performed extensive visual studies of a flat plate turbulent boundary layer. They developed and used a combined time-streak hydrogen bubble method which permitted measurements of instantaneous velocity profiles; dye injection techniques were also used in their flow visualizations. They divided the turbulent boundary layer into inner ($y^+ < 40$) and outer

($y^+ > 40$) zones. A distinct structure was observed in the inner zones different from the one suggested by long time averaging procedures. The most important element of this wall structure was a regular flow pattern distributed in the spanwise direction. It consisted of alternating low and high \bar{u}_x velocity streaks. They originated in the zone $0 \leq y^+ \leq 10$ and their spacing in the transverse direction was found to be a function of Reynolds number; the correlation, $76.5 = \lambda^+ = (\lambda U^*)/\nu$, for the spacing, λ , and the mean flow parameters was reported. The streamwise dimension of the streaks was much larger than the other two dimensions. The low speed streaks while moving downstream developed a wavy motion. This actually was part of a flow model consisting of a chain of events which was called "bursting." The process of "bursting" is composed of the following three stages:

- (1) Slow lifting of a low-speed streak accumulates until a shift occurs involving more rapid outward motion of the low-speed streak; at this time, an inflexional instantaneous velocity profile is observed.
- (2) Downstream from the inflexional zone rapid growth of an oscillatory motion is observed; it continues for a few cycles.
- (3) The oscillation is terminated by the onset of a more chaotic fluctuation called "breakup." This completes the cycle, and the velocity profile returns to a form generally like the mean profile shape. These general processes are observed in all cases studied; the details are uniform up to the end of the first stage, low-speed-streak lifting, but the

second and third stages vary from case to case in structural detail [Kim et al. (18)]¹

The process of "bursting" was observed to be of an intermittent character. The inflexional velocity profile was the result of a perturbation created by the lifting up of the low-speed streak; in addition the inflexion point occurred at the point of maximum streamwise vorticity.

Kim et al. (18) observed that the most characteristic fluid motion of the oscillatory growth of the lifted low-speed streak was a streamwise vortex motion. Two other less common fluid motions were observed during the second stage of "bursting"; there were (i) a transverse vortex (relatively rare) and (ii) a "wavy motion" (more common). They reported that more than two-thirds of the cases studied involved a streamwise vortex. In Figures 48(a) and 48(b) a schematic illustration of the formation of streamwise and transverse vortex is given as reported by Kim et al. (18). Increase in the scales of fluid motion by at least one order of magnitude were observed during the oscillatory growth; they were observed to be about $240y^+$ units, i.e., half the boundary layer thickness.² Kim et al.

¹Kim et al. (18), p. 144.

²There is a discrepancy in Kim et al. between the boundary layer thickness $\delta = 800y^+$ reported and the calculated $\delta = 540y^+$ from the data given. The correct value is the calculated $\delta = 540y^+$. (Private communication with Prof. S. J. Kline.)

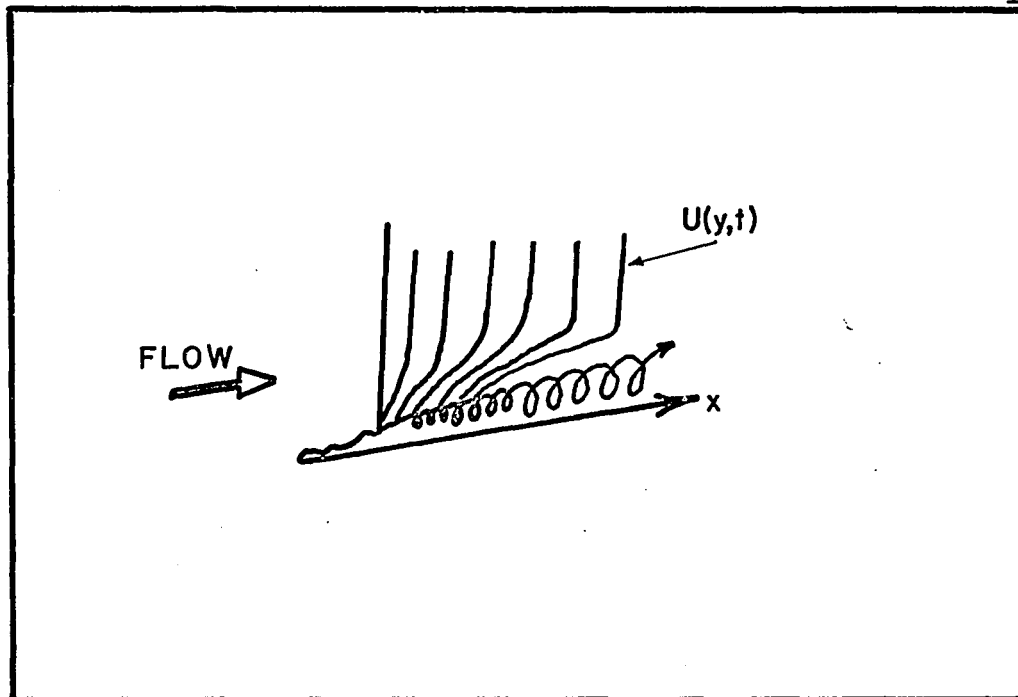


FIGURE 48(a). A STREAMWISE VORTEX MOTION

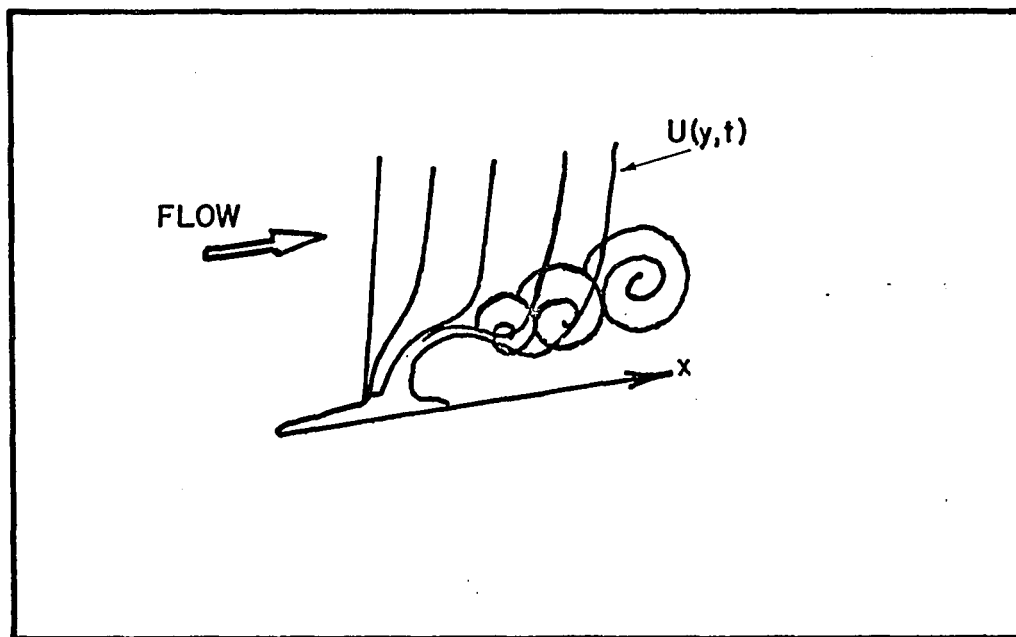


FIGURE 48(b). FORMATION OF A TRANSVERSE VORTEX [adapted from Kim et al. (18)]

excluded the possibility that such a picture could have been the result of entrainment of the lifted low-speed streak by a large scale motion. The arguments offered against such an entrainment process were the intermittent character of the process and the fact that such an increase in the scale of fluid motions was the result only of an inflexional velocity profile.

Essentially all the turbulent energy production according to the data of Kim et al. occurs during "bursting" in the region $0 < y^+ < 100$. Specifically they suggested that the oscillatory growth of stage (2) be associated with the turbulence production whereas the breakup of stage (3) with wave-number transfer.

For a comparison of the observations and measurements of Kline et al. (20) and Kim et al. (18) with the present work, one should keep in mind some of the differences in the experimental techniques. Their camera was stationary and the filming speed was considerably slower. In the present work the view of travelling camera permitted the observations of developing flow events for longer times. This resulted in a more complete observation of a sequence of events per se. In spite of the different point of view and terminology used, a general agreement between the two works can be recognized. In both cases a deterministic sequence of flow events occurring randomly in space and

time was observed. In the wall region, the lifting up of low-speed streaks corresponds to the ejections of the decelerated fluid in the present work. The region $10 \leq y^+ \leq 40$ where most of these streaks originated and their outward angles (from a maximum of 26 degrees to 0 degree) are in excellent agreement with the present observations.

Kline et al. and Kim et al. did not report any deceleration or acceleration events as such. This is apparently due to the limitations of their experimental technique. It can be recalled that the convected view of the camera greatly facilitated the observation of regions having velocity gradients by visually identifying their differences in velocity. Low speed streaks as such were not observed in the present work; instead decelerated regions extending from the wall to the far outer region occurred. This is due to differences in observations; the present experimental technique did not permit observations in the spanwise direction.

A disagreement exists as far as the causative factors that give rise to an inflection point in the velocity profile. In the present work a strongly inflexional velocity profile appeared in the shear region between decelerated and accelerated fluid. But it was the result of the gradual displacement of low speed fluid by the much faster moving accelerated one. At the time of this displacement the

decelerated fluid extended nearly throughout the whole boundary layer.

In Figure 49 is illustrated the wall zone of a decelerated region and an ejection originating in it. The shape of this region close to the interface at the time of ejection can be viewed as a lifted up low-speed streak. The ejected fluid element does create an instantaneous inflexional velocity profile; but in the present observations, as already has been stated it was not this instantaneous velocity profile which caused the formation of a transverse vortex. Moreover the transverse vortex of the present work was not the result of growth of smaller scale fluid motions (e.g., ejections); neither was its occurrence as rare as in Kim et al. More important it was the outer accelerated fluid which caused its formation and not the "triggering" action of the lifted low-speed streak. The higher frequency of occurrence of transverse vortices in the present work and the mechanism of their formation do not exclude them from being one of the mechanism of entrainment of higher speed fluid towards the inner zones.

Kim et al. did not report any observation of a reverse transverse vortex. On the other hand, no "wavy motion" of the decelerated fluid was observed in the present work.

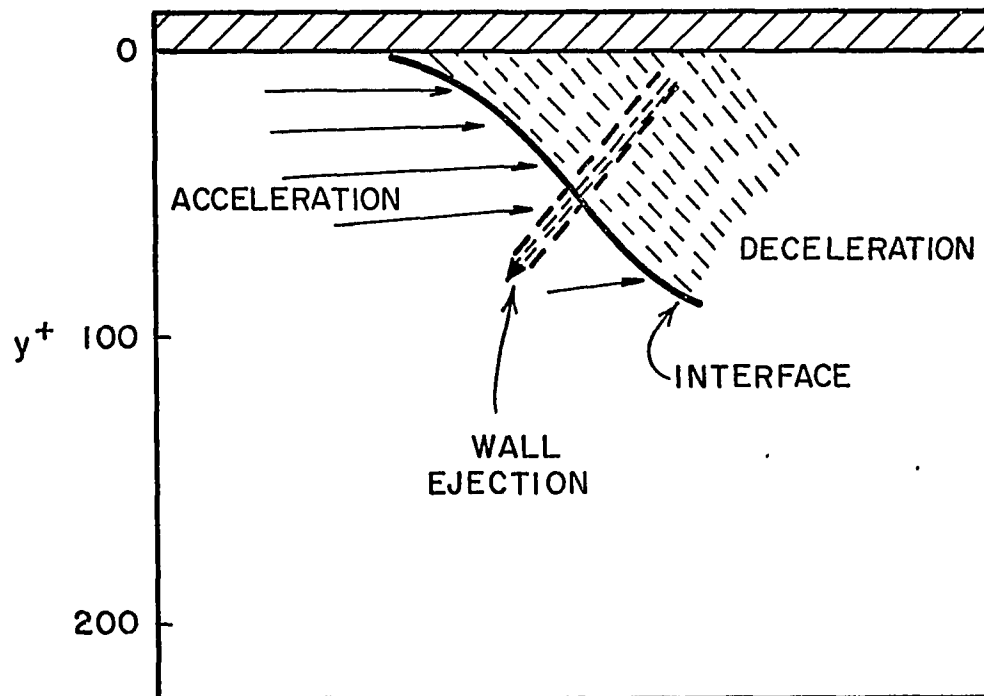


FIGURE 49. DECELERATED FLUID REGION AND WALL EJECTION CONSIDERED AS LIFTED UP "LOW-SPEED STREAK" (CONVECTED VIEW)

Streamwise vortices as such were not observed in the present work. The failure of observing them might be due to limitations of the experimental technique but this is questionable. A streamwise vortex in the present observations should appear as a sequence of alternating inflows and outflows of comparable scale. Although in the present work usually inflows followed outflows and vice versa, they were of much larger scale. Moreover they occurred as rather isolated fluid motions in several cases. Very rarely, small scale fluid elements were observed to make one complete loop in the wall region; their scale did not grow any further. No definite conclusion can be drawn from the observation of these motions as being part of streamwise vortices. The width of the light beam, which dictated the depth of field, was 0.75 inches at the flat plate wall. This is equivalent to a $Z^+ = ZU^*/\nu = 200$ in the transverse direction. At half the boundary layer thickness the depth of field is equivalent to $Z^+ = 167$. According to Kim et al. the scales of streamwise vortices grow up to one-half the boundary layer thickness (i.e., $\delta/2 = 270y^+$ units). Such fluid motions could not be completely identified in the present work, even if the axis of these vortices coincided with the center plane of the light beam. Since the streamwise vortices of Kim et al. occurred randomly in the transverse direction, the probability of such a coincidence was very small.

Kim et al. concluded that essentially all turbulent energy production in the area $0 \leq y^+ \leq 100$ occurs during bursting periods. The energy produced during non-bursting was either zero or very small. In the present work both ejections and sweeps contributed (positive contribution) to the instantaneous Reynolds stress. Their interactions contribute negatively to the instantaneous $-\rho uv$. This can be seen from the Tables 1 through 5 where an interaction would correspond to u positive, v positive, i.e., accelerated fluid reflected away from the wall.

Other Studies

Wallace, Eckelmann and Brodkey (37) in their hot-film measurements classified the instantaneous, uv , product according to the sign of its components, u and v , in four groups. These correspond to ejections (u negative, v positive), sweeps (u positive, v negative) and their interactions: u positive, v positive (high speed fluid reflected away from the wall) and u negative, v negative (low speed fluid deflected toward the wall). They then averaged these classified groups to obtain their contribution to the Reynolds stress, $-\rho uv$. Their measurements over the region $3.5 \leq y^+ \leq 100$ showed that the ejections and sweeps contributed positively more than 100 percent to the $-\rho uv$. The balance of 100 percent of the Reynolds stress came from the interactions of ejections and sweeps since their contribution to the $-\rho uv$ was negative.

The limited measurements of the present work do not form a statistical sample and hence they don't permit assigning a percent contribution to the $-\rho uv$ from the various events (i.e., ejections, sweeps and their interactions). Nevertheless the qualitative conclusions drawn from these measurements are in agreement with the work of Wallace, Eckelman and Brodkey (see Tables 1 through 5).

The work of Grass (12) is in excellent agreement with the present observations and measurements. Although he estimated that the intrushes (sweeps) should make the same positive contributions to the Reynolds stress as the ejections, he did not realize the negative contribution to this stress from their interactions.

In the same context the work of Willmarth and Lu (38) is in agreement with the present one. They did suggest that positive contributions to the Reynolds stress $-\rho uv$ should be attributed not only to the ejections but also to the sweeps. In excellent agreement with the present data are their measurements of individual contributions to the instantaneous Reynolds stress, $-\rho uv$. Values as large as 62-times higher than the local mean were identified.

Kovaszny et al. (18) studied the intermittent region of a turbulent boundary layer using conditional sampling and averaging techniques. They measured conditional

averages of the streamwise and normal velocity components U and V as a function of the distance from the wall. In addition space-time auto-correlations of the streamwise velocity fluctuation R_{uu} , of the normal velocity fluctuation R_{vv} , as well as cross-correlations R_{uv} at different intermittency levels were measured. From their experimental results they concluded that a large scale motion exists which is strongly correlated with the shape and motion of the turbulent non-turbulent interface. These large scale motions appear as individual "bulges" or "bursts," and they are elongated in the streamwise direction with a typical streamwise length between $\delta/2$ and δ . They regard the structure of turbulent non-turbulent interface as being composed of these individual bursts occurring at random.

The following model was suggested by Kovaszny et al.:¹

A new burst begins with a violent outward motion from the interior of a lump of turbulent fluid having a typical diameter of $\delta/2$. Arriving in the new environment, this lump has both a momentum defect relative to the local average velocity of the non-turbulent fluid and in addition it has also an angular momentum proportional to $(\partial\bar{U}/\partial y)$, characteristic of the average conditions at the level of its origin. If one could fix the co-ordinate system so that the lump at the moment of its arrival would appear as stationary, the flow of the surrounding fluid would be quite similar to the flow around a sphere. A turbulent

¹Kovaszny et al. (22), p. 322.

wake would develop rapidly and it would become more and more extended in the downstream direction. This phase is of short duration, but at the same time the lump loses its momentum defect through turbulent mixing and gradually becomes the observed turbulent burst. By spreading the angular momentum over a large region, a constant $(\partial \bar{U} / \partial y)$ is reached within the turbulent fluid. . . .

There is an apparent similarity between the results of Kovaszny et al. and the present work. The outward movement of a lump of fluid and its scale correspond in part to a forward transverse vortex. Observation by a moving coordinate system corresponds to the convected view of the travelling camera. The angular momentum proportional to $(\partial \bar{U}_x / \partial y)$ corresponds to the direction of rotation of a forward transverse vortex. In spite of this apparent similarity, there are differences in the two works which are based on the fact that in the present work only individual events were sought and no averages of any kind regarding the events were conducted.

A reinterpretation of the results of Kovaszny et al. is possible in the light of individual events observed in the present work. It will be recalled that the occurrence of forward transverse vortices was more frequent than the one of reverse transverse vortices. Moreover that for most of the cases the transverse vortices were transported downstream on a small outward angle. The low speed fluid during the time of its participation in a forward transverse vortex moved away from the wall. Most of the wall

region ejections (low speed fluid) were closely associated with the transverse vortices. If one would conduct a conditional sampling and averaging during these events, one would arrive at a picture of a lump of fluid being ejected and rotating with an angular momentum compatible with the gradient ($\partial \bar{U}_x / \partial y$). The combined effect of a transverse vortex and a large scale outflow would intensify the picture of a lump of fluid moving outward in such an averaging process. Kovaszny et al. suggested that the lump of fluid rotated because of the influence of an average velocity gradient characteristic of the local average conditions of its origin. In contrast, in the present work the forward transverse vortex had such a rotation because of the mechanism of Helmholtz instability involved in its formation. Kovaszny et al. failed to observe a reverse transverse vortex; this fact can be attributed to their averaging process. They did conclude that the flow in the "Fronts" (downstream) of the bulges is toward the wall, while in the "Backs" (upstream), the flow is directed outwards. This is in agreement with the present observations. The wallward flow in the "Fronts" correspond to the wallward bending of the high speed fluid during the formation of a forward transverse vortex.

Kaplan and Laufer (16) used a conditional sampling technique to study the structure of the turbulent non-

turbulent interface and its relation to the entrainment process. Their measurements confirmed the results of Kovaszny et al. and complemented the observations concerning the behavior of the bulges of the interface. They found a small velocity defect between the trailing edge and leading edge of the bulges, with the leading edge having a higher velocity. They concluded that the entrainment of non-turbulent fluid occurs mainly along the trailing edge. In the present work it was proposed that the transverse vortices are one of the mechanisms for the entrainment of non-turbulent fluid. An agreement between the two works should be viewed only in the context that in their conditional averaging process at least one of the events included was the transverse vortex.

Narahari et al. (25) concluded that the mean frequency of "bursts" scales with the variables of the outer flow instead of the inner variables. Laufer and Narayanan (16) showed in addition that the convection time for an average wavelength of the turbulent-laminar interface (period of bulges) was of the same order of the average period of the production cycle, \bar{T} . The argument used to support this scaling with the variables of the outer flow is the fact that the nondimensional period $(U_0 \bar{T} / \delta)$, is independent of the Reynolds Number R_θ .

In the present work a picture of connected and non-connected regions was given in the content of the individual events. According to this picture a mixed scaling of inner and outer variables would be physically meaningful. It can be observed though that the range of R_θ (between 10^3 and 10^4) for the most of the experimental points is limited. There is only one experimental point at $R_\theta = 5 \times 10^4$ by Willmarth and Tu (39) which extends the range of the Reynolds number R_θ ; this point though involves experimental uncertainties rendering it unsuitable for the argument in question.*

Summary

The nature of the fluid motions in the wall and outer regions of a turbulent boundary layer as reported in this study is compatible with the results reported by other investigators who used different methods of study. In several cases where a comparison of specific features or measurements was possible, there was good agreement. It is important to notice that different investigators, using different techniques, often found similar observations and measurements for the same feature of the turbulent process.

In some cases though, the difference in the method of investigation resulted in disagreement regarding the nature

*Private communication with Professor W. W. Willmarth.

of some of the fluid motions. Thus, e.g., regarding the formation of transverse vortices a disagreement exists between the work of Kim et al. and the present study. Certain aspects of fluid motions studied by entirely different experimental techniques were found consistent with the present work after a reinterpretation was made to those measurements and observations (e.g., the work of Kovasznay et al.).

CONCLUSIONS

The following accomplishments and conclusions were reached as a result of this experimental investigation.

1) An experimental technique was developed which permitted qualitative and semi-quantitative observations for a basic physical understanding of the fluid motions occurring in the wall and outer regions of a flat plate turbulent boundary layer. This technique does not require the introduction of any measurement or injection device in the flow.

2) In turbulent boundary layer flow the fluid motions have a distinct character which manifests itself by the occurrence of a sequence of well-defined events. Although the events occur randomly in space and time, their sequence is deterministic.

3) The most important events of the wall region ($0 \leq y^+ \leq 70$) are the ejections, sweeps and their interactions. The ejections are small scale three-dimensional disturbances. Although they occur as localized events, they are closely associated with events of the outer region ($y^+ \geq 70$). The sweeps are the wall zone part of an accelerated fluid which extends up to the far outer region.

4) The single most important event observed in the outer region was the transverse vortex. It is the result of an instability interaction (Helmholtz instability) between accelerated and decelerated fluid. Two kinds of transverse vortices were observed and they were distinguished by the opposite sign of their rotation. These were: forward and reverse transverse vortices. The transverse vortices are closely associated with the wall region ejections and they are believed to be one of the mechanisms which cause these ejections to occur. In addition, the transverse vortices appear to be one of the mechanisms of turbulent energy exchange between the wall and the outer region; they also are part of the entrainment process of higher speed fluid.

5) Both ejections and sweeps contribute positively to the instantaneous Reynolds stress, $-\rho uv$, while their interactions give negative contributions to $-\rho uv$. In addition the interactions are associated with high rates of viscous dissipation. The process of turbulent energy production appears highly intermittent. Estimated positive and negative contributions to the instantaneous Reynolds stress, $-\rho uv$, are two orders of magnitude higher than the local mean averages.

6) A basic physical picture in terms of individual events is presented as an answer to the questions concerning

the connection and interaction of the wall and the outer region. Connected motions (fluid motions which move as a whole) from this viewpoint occur only during events extending from the wall to the outer region and as such they occur intermittently.

RECOMMENDATIONS

1) Using the established experimental technique research efforts should be directed towards photographing the three-dimensional character of the flow. This could be accomplished by illuminating a flow region with narrow beams of colored light and using color film in the high speed camera.

2) Obtain further experimental information on factors causing the wall ejections. Theoretical model studies could be undertaken towards studying the pressure field during a transverse vortex.

3) Using as guide the present and similar visual observations, investigations should be directed towards analyzing the whole turbulent signal from hot-film anemometry measurements. An adequate quantitative characterization of the events and their interactions could be one of the major steps towards a fundamental understanding of the processes involved in turbulent shear flows.

4) From the present visual picture and the detailed information obtained from recommendation (3), a direct numerical calculation of heat and mass transfer could be

undertaken now in the well-known (knowledge of velocity correlations, cross-correlations, spectra and the descriptive parameters from these i.e., microscales and macroscales of turbulence) turbulent field.

APPENDIX I

SAMPLE CALCULATIONS

The individual instantaneous particle velocities were calculated from the distance they traveled during a measured period of time. From the projected movies and known magnification, trajectories of particles were traced. Since the camera is moving with the flow, the traced trajectories are referred to as "apparent," i.e., the trajectories of particles as seen by an observer moving with the camera velocity U_c . Such an apparent trajectory is shown in Figure 50.

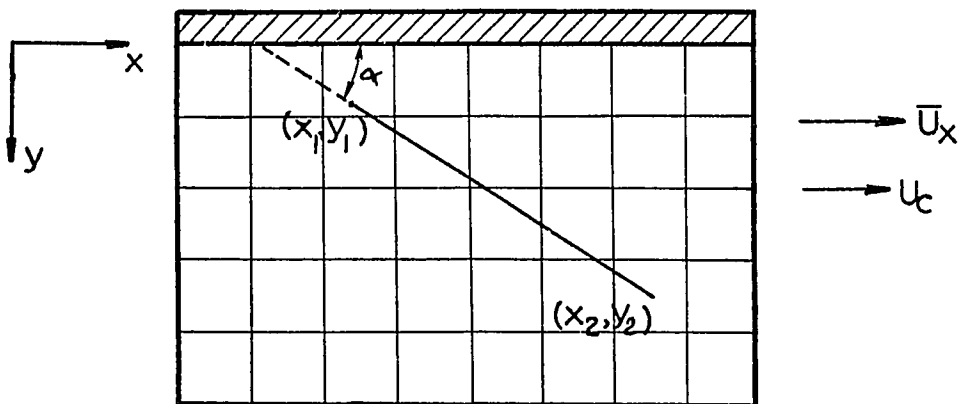


Figure 50. Analysis Grid.

The line marked (x_1, y_1) , (x_2, y_2) represents the apparent particle trajectory. Let:

α = apparent angle of ejection measured from wall

e = apparent length of travel of particle

t = time of travel

U_g = apparent ejection velocity

U_c = carriage velocity, same direction as \bar{U}_x

U_t = actual ejection velocity

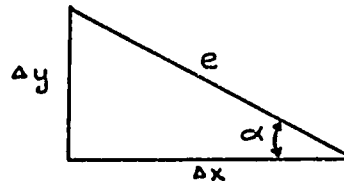
ϕ_e = actual ejection angle

As a sample calculation an ejection from Figure 27 is considered.

The measurements taken are:

$$\Delta x = 0.62 \text{ cm}$$

$$\Delta y = 0.44 \text{ cm}$$



$$\therefore \tan \alpha = \frac{\Delta y}{\Delta x} = \frac{0.44}{0.62} = 0.710$$

$$\text{and } \sin \alpha = 0.575; \cos \alpha = 0.85; \alpha = 35^\circ 23'.$$

$$\text{Frames elapsed} = 530 - 487 = 43$$

$$\text{Framing speed} = 264 \text{ frames/sec.}$$

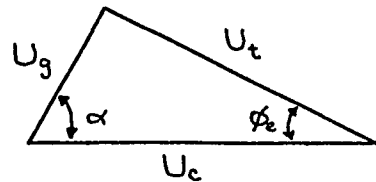
$$\therefore \text{Time elapsed} = \frac{\text{frames elapsed}}{\text{frames/sec}} = \frac{43}{264} = 0.163 \text{ sec.}$$

$$e = \frac{\Delta x}{\cos \alpha} = \frac{0.62}{0.815} = 0.76 \text{ cm}$$

$$U_g = \frac{e}{t} = \frac{0.76}{0.163} = 4.67 \text{ cm/sec}$$

$$U_c = 8.50 \text{ cm/sec.}$$

In order to determine the actual velocity and ejection angle the following vector diagram taking into account the motion of the camera



From trigonometry, $U_t^2 = U_c^2 + U_g^2 - 2U_c U_g \cos \alpha$

$$U_t^2 = (8.50)^2 + (4.67)^2 - 2(8.50)(4.67)(0.815) = 28.88$$

$$U_t = 5.37 \text{ cm/sec.}$$

$$\sin \phi_e = \frac{U_g \sin \alpha}{U_t} = \frac{(4.67)(0.575)}{5.37} = 0.502$$

$$\phi_e = 30^\circ 10'$$

It can be noted that the apparent angle of ejection was larger than the actual ejection angle. This enhancement is due to the moving camera which permitted small deviations to be observed more precisely.

APPENDIX II

ADDITIONAL EXPERIMENTAL DATA

In this appendix additional experimental data are presented. They were obtained from the whole set of the motion picture runs. They show the same qualitative and quantitative features as the data already presented in the experimental part. The information contained in these additional data does not alter the conclusions reached in the present investigation; therefore they were not analyzed in detail.

In the following figures the numbers next to the particle paths, represent times in seconds relative to the same zero starting time. The tic marks along the particle paths represent time intervals equal to 0.10 seconds.

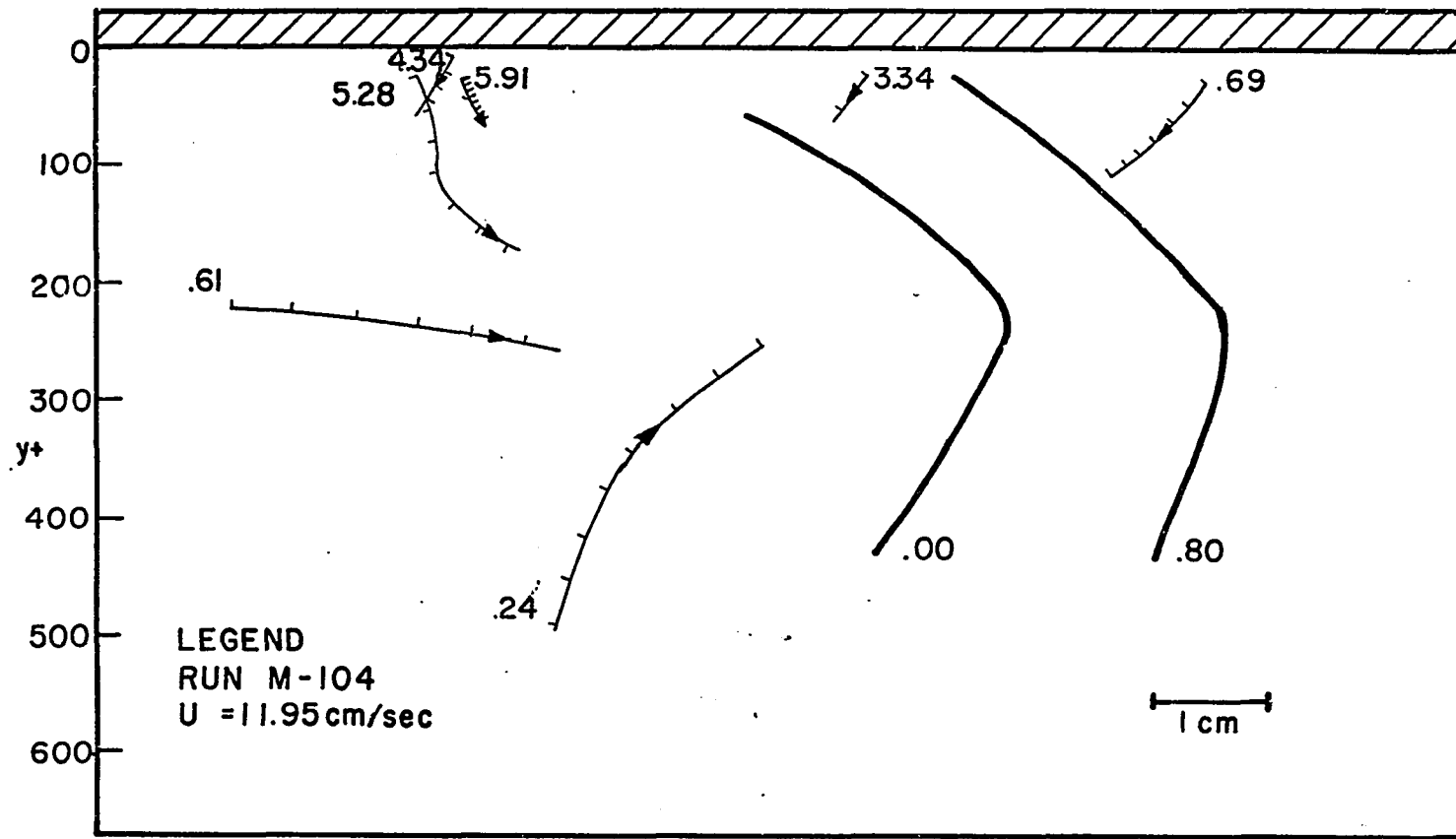


FIGURE 51. EJECTIONS AND ACCELERATION (CONVECTED VIEW)

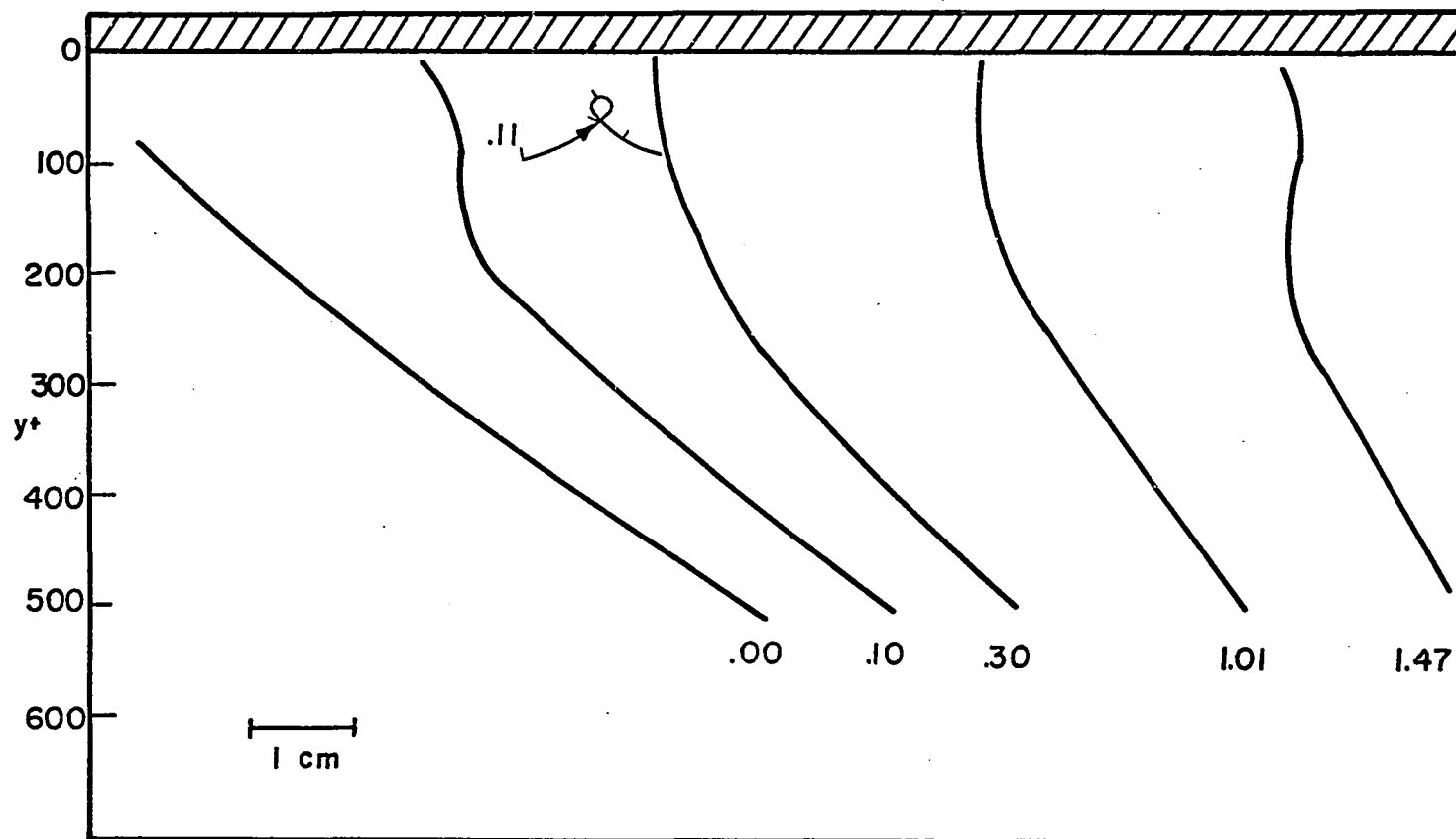


FIGURE 52. ACCELERATION (CONVECTED VIEW)

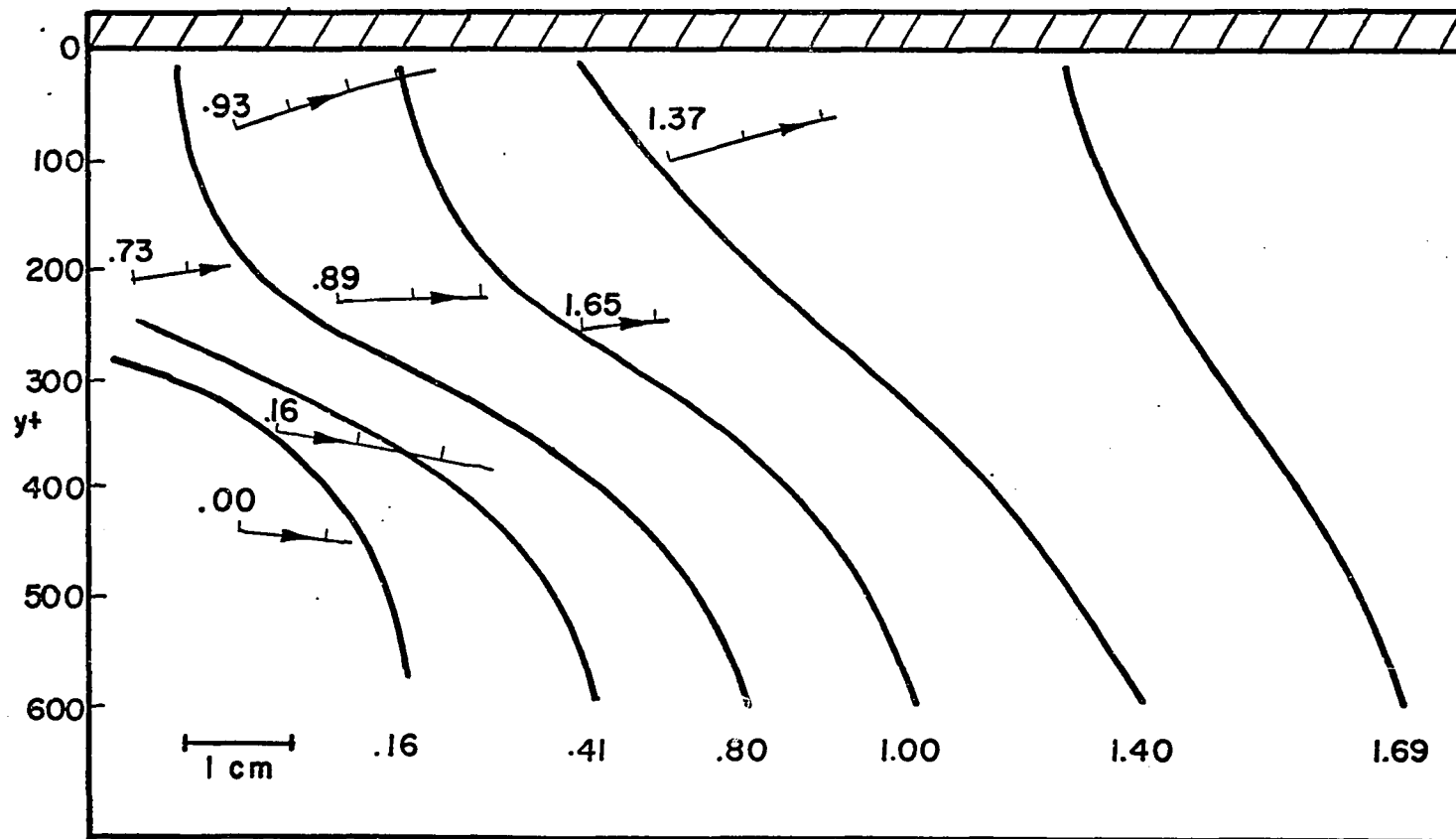


FIGURE 53. ACCELERATION (CONVECTED VIEW)

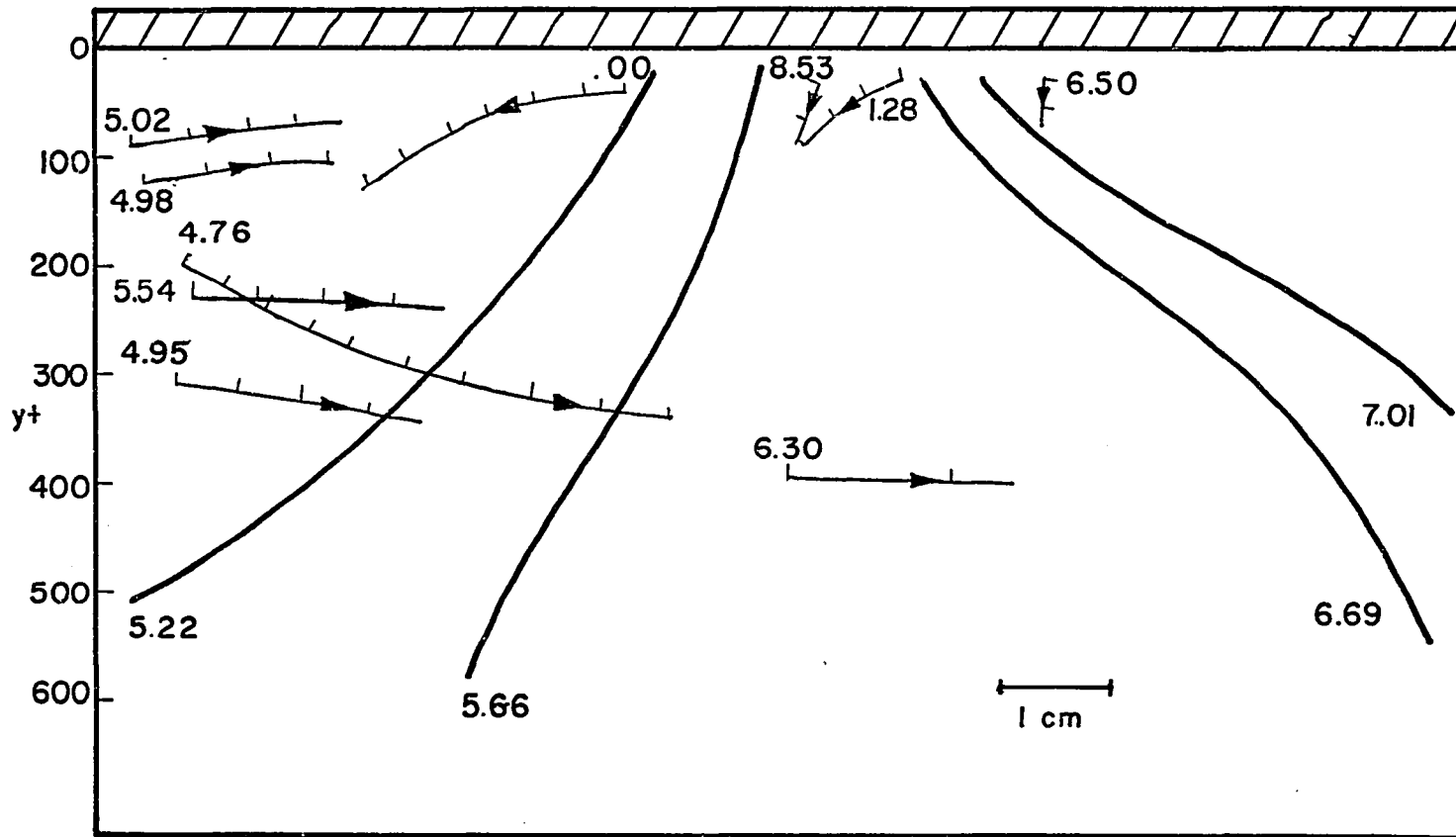


FIGURE 54. EJECTIONS AND ACCELERATION (CONVECTED VIEW)

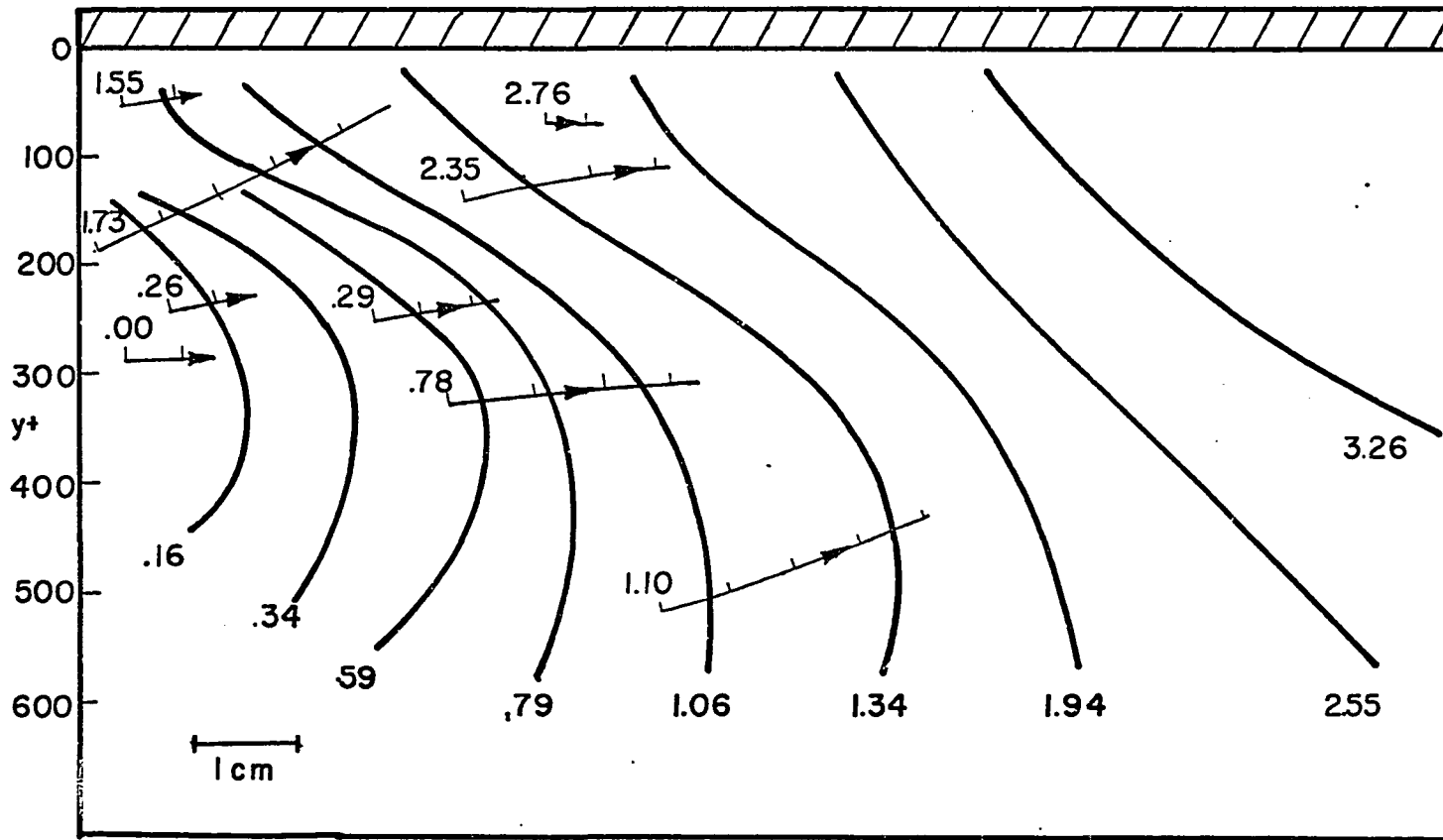


FIGURE 55. ACCELERATION (CONVECTED VIEW)

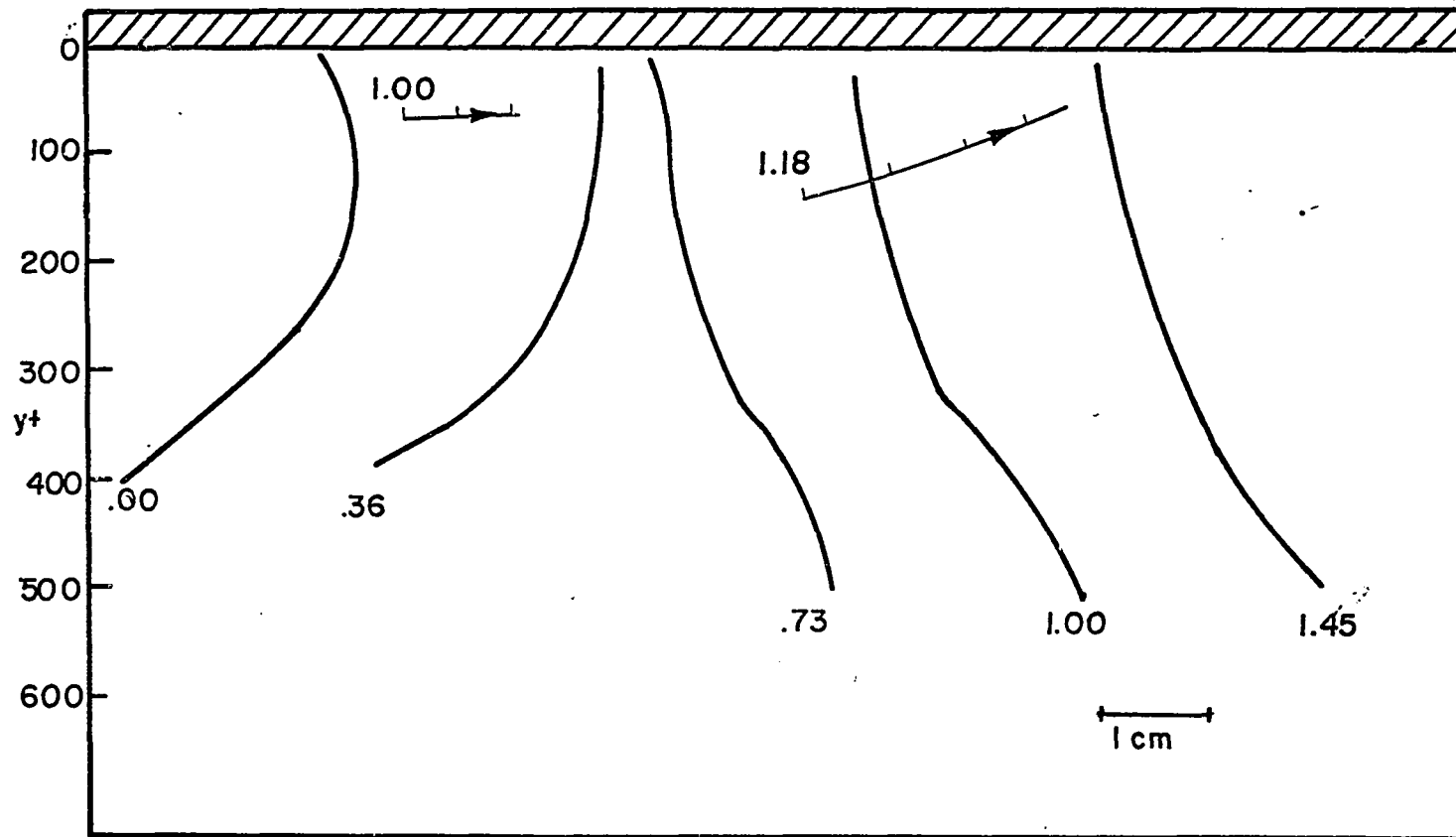


FIGURE 56. ACCELERATION (CONVECTED VIEW)

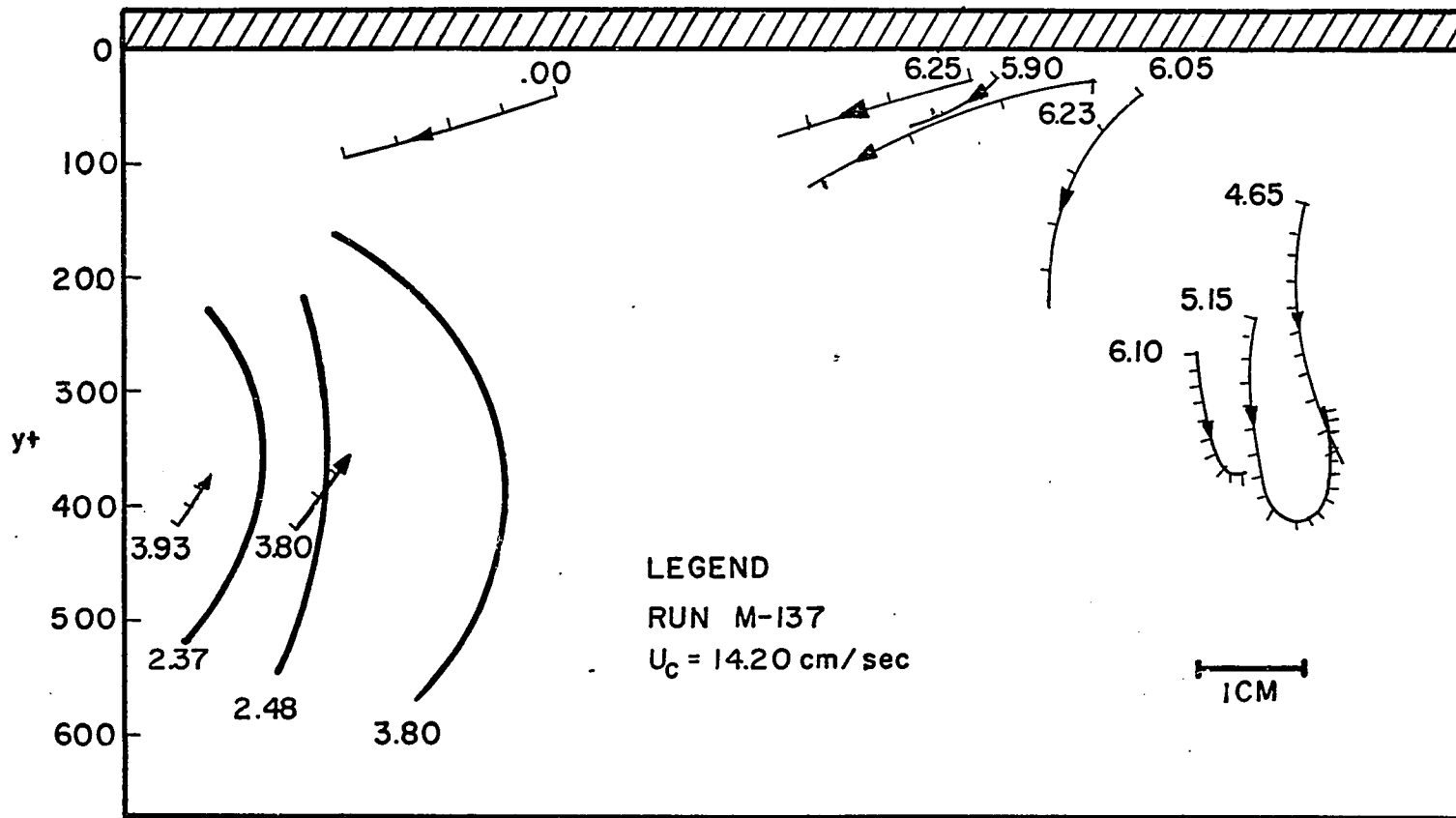


FIGURE 57. EJECTIONS AND ACCELERATION (CONVECTED VIEW)

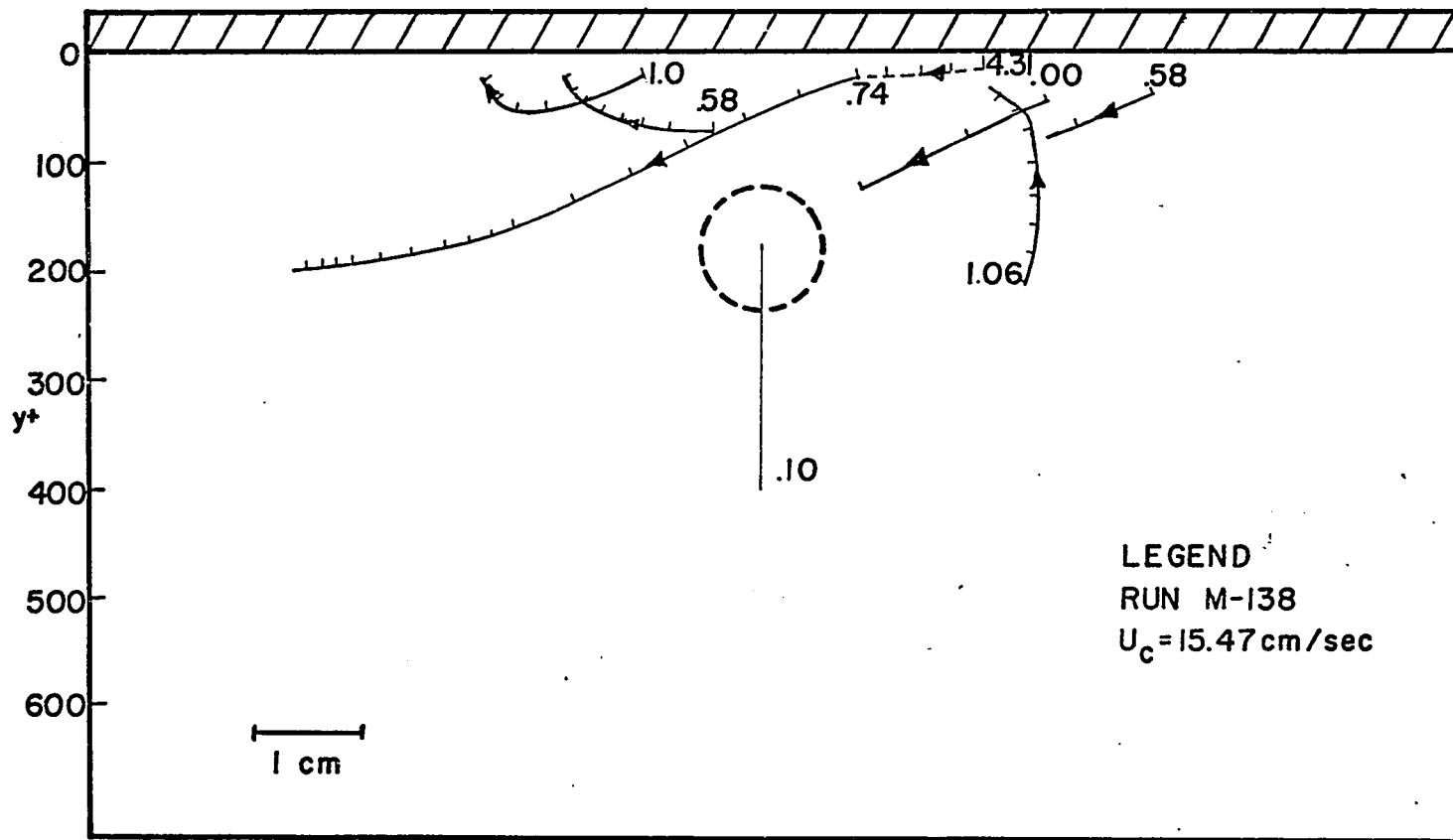


FIGURE 58. EJECTIONS AND FORWARD TRANSVERSE VORTEX (CONVECTED VIEW)

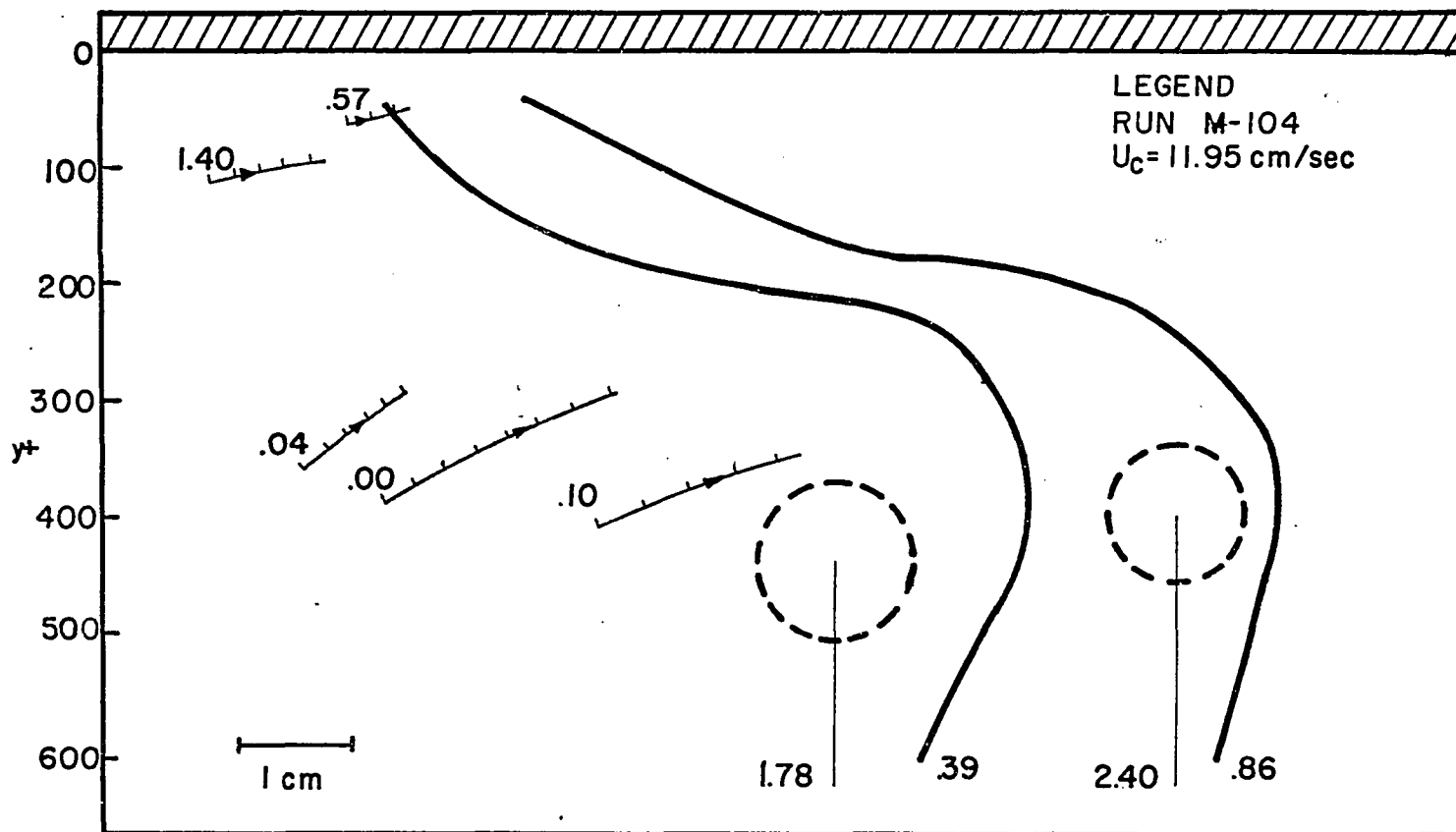


FIGURE 59. ACCELERATION AND FORWARD TRANSVERSE VORTEX (CONVECTED VIEW)

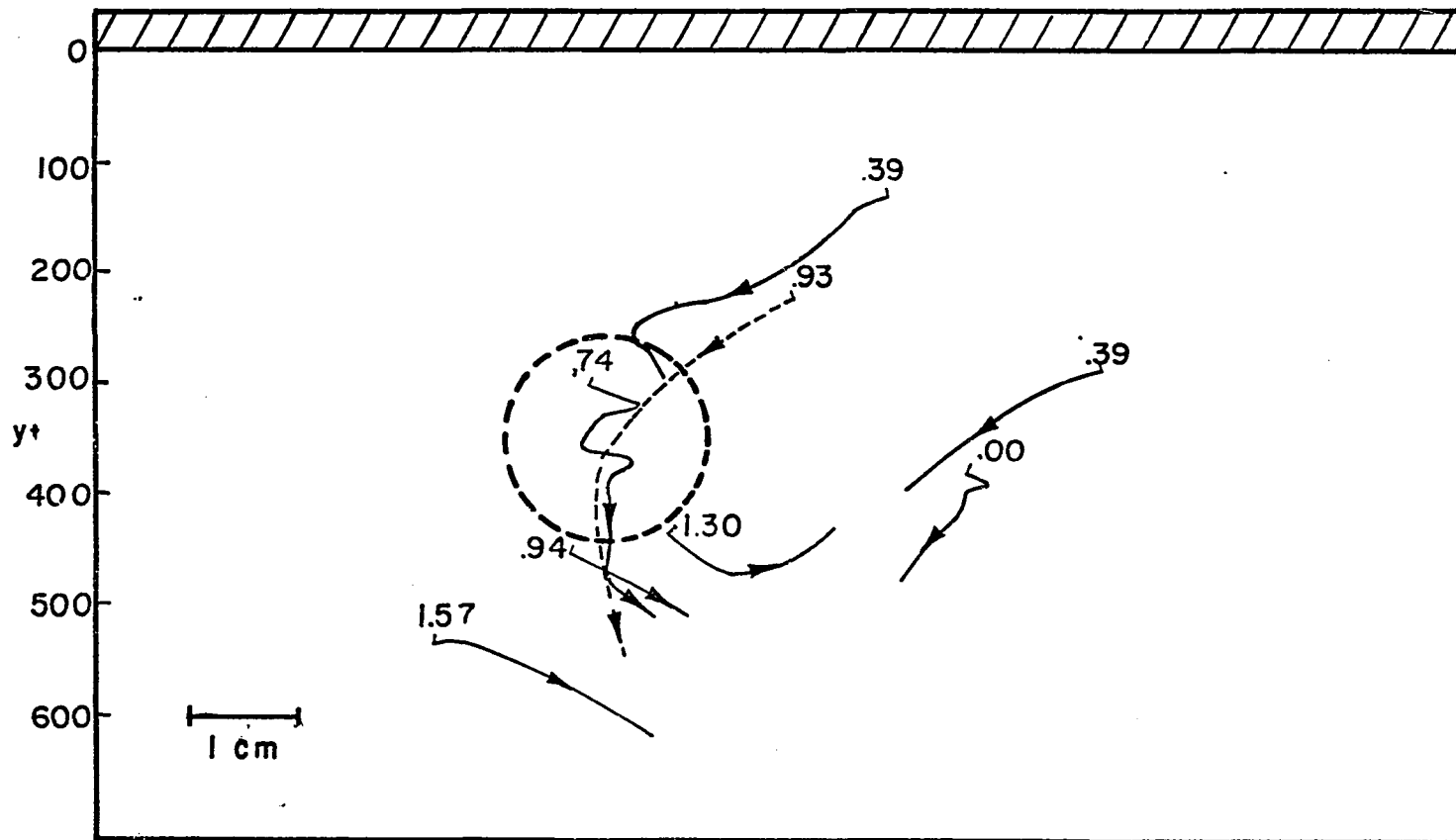


FIGURE 60. CONVICTED (STATIONARY VORTEX) VIEW OF A FORWARD TRANSVERSE VORTEX

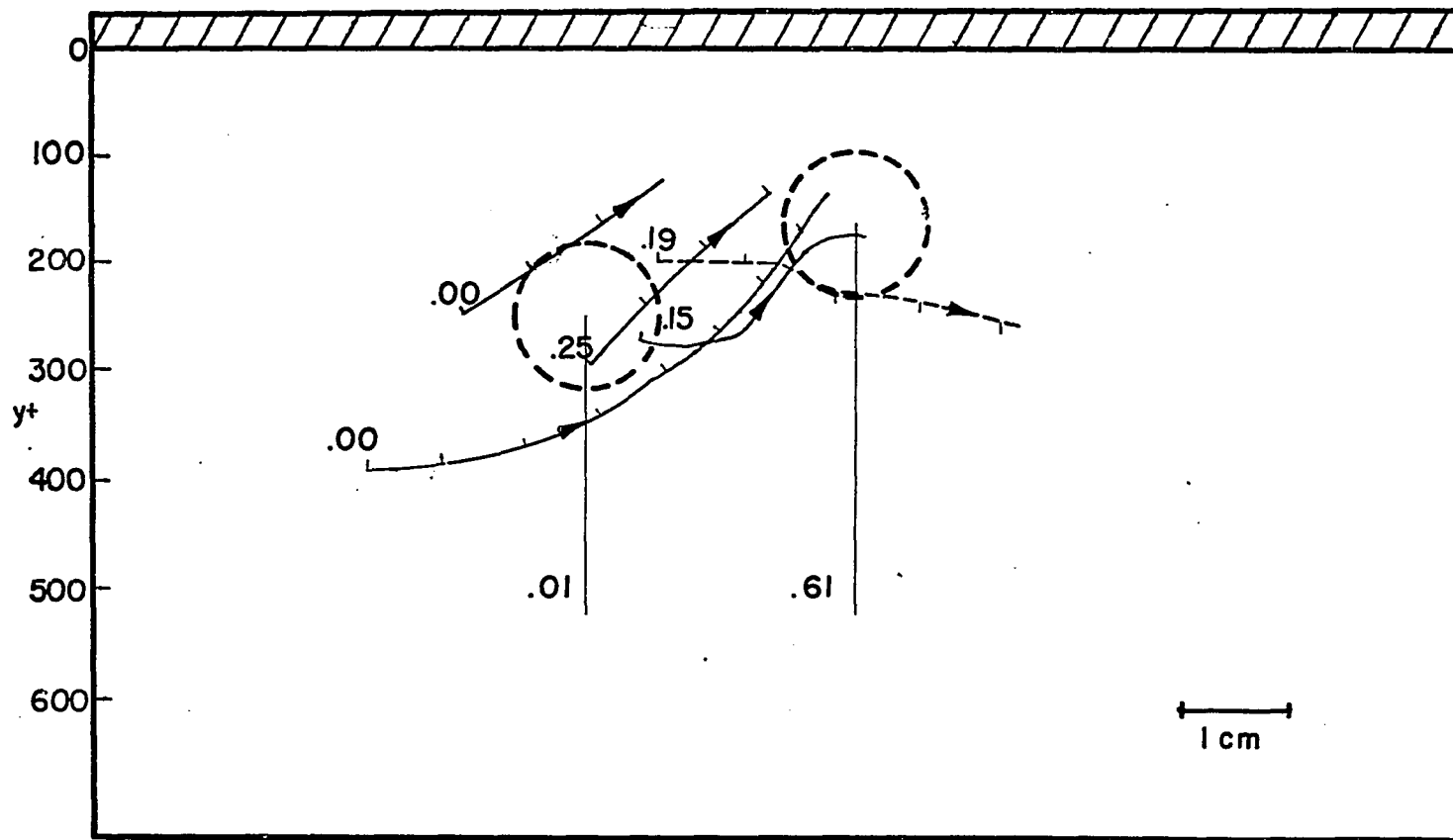


FIGURE 61. INDIVIDUAL PARTICLE PATHS DURING A REVERSE TRANSVERSE VORTEX (CONVECTED VIEW)

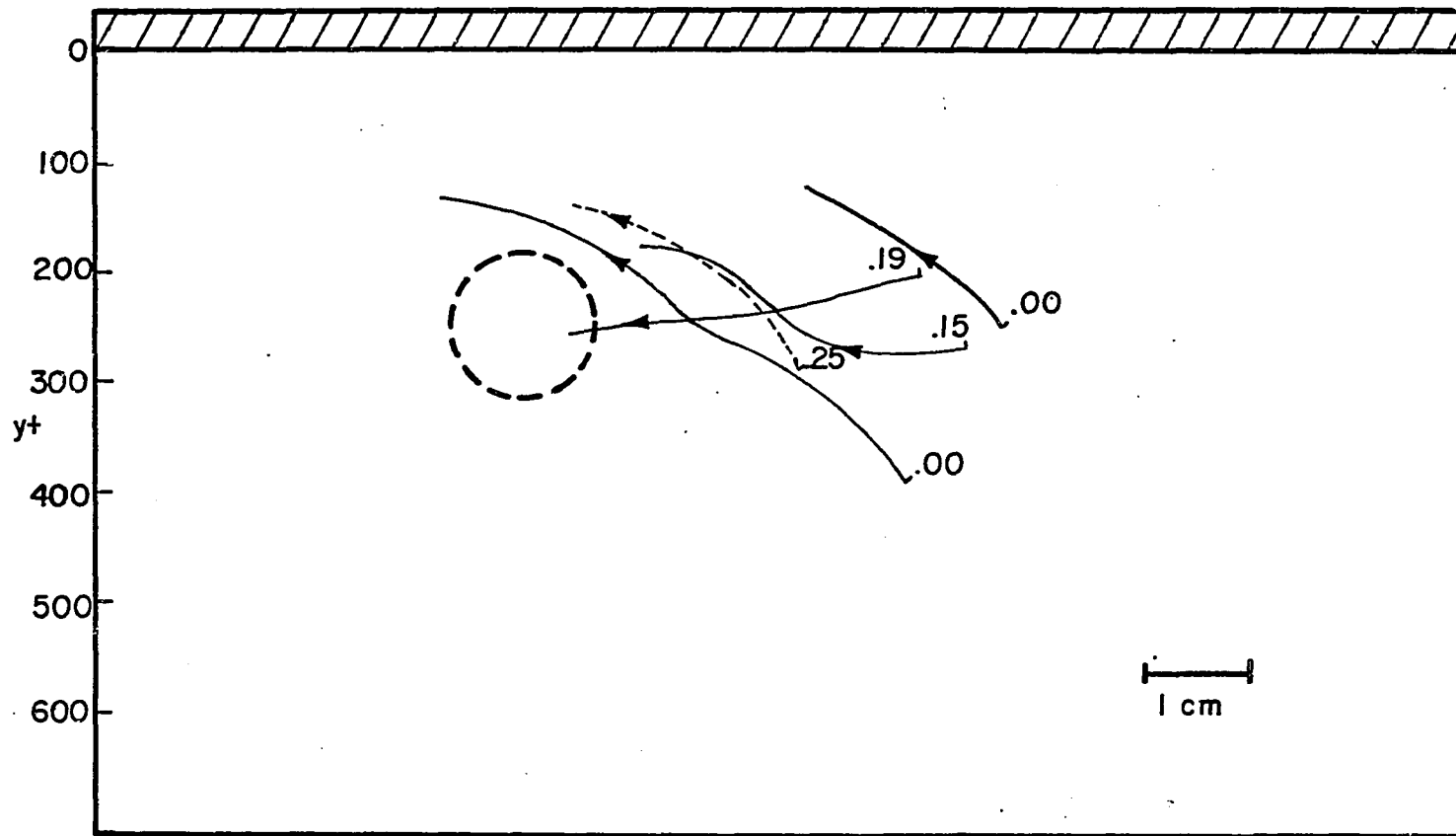


FIGURE 62. CONVECTED (STATIONARY VORTEX VIEW) CORRESPONDING TO FIGURE 60

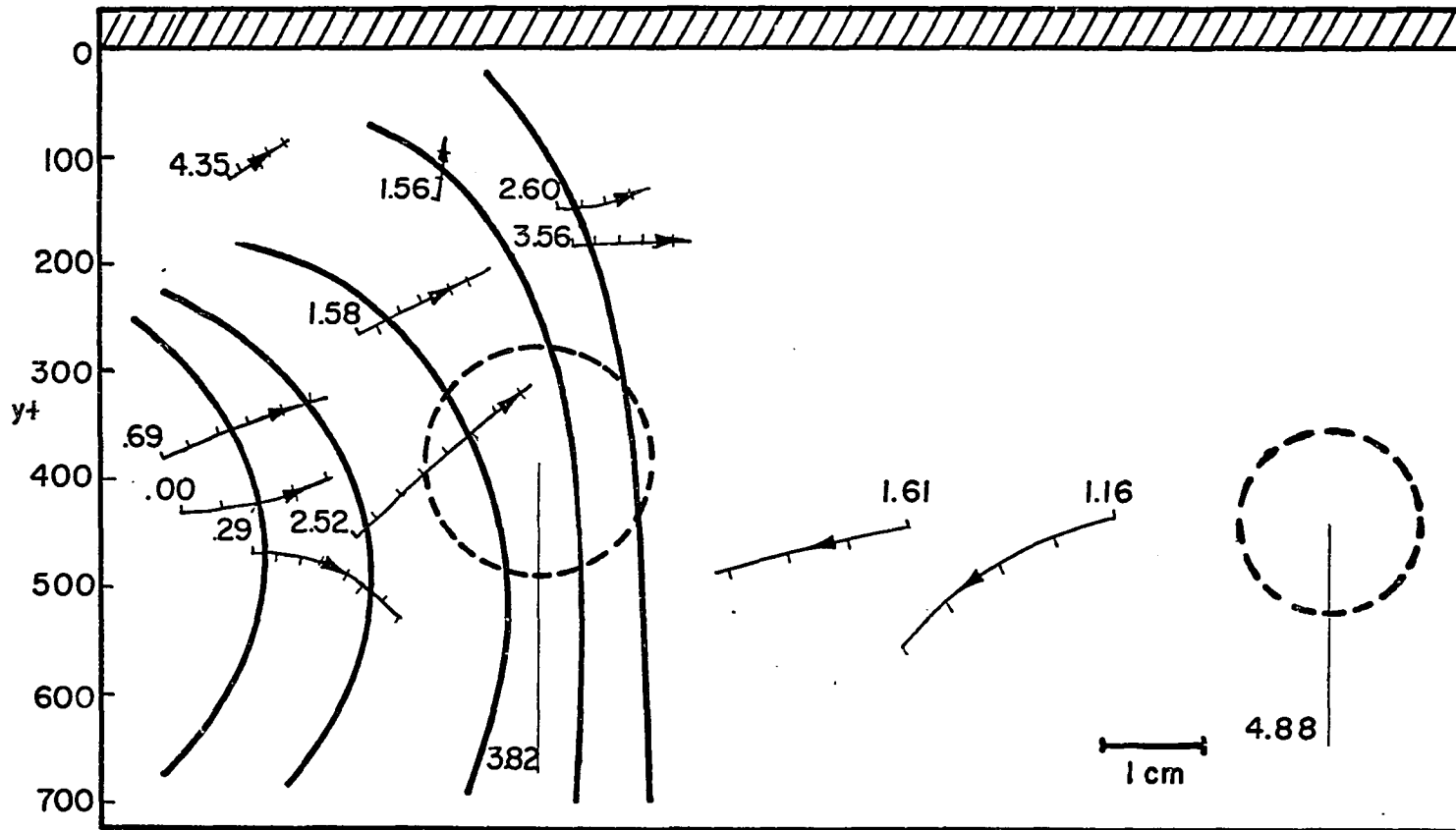


FIGURE 63. ACCELERATION AND REVERSE TRANSVERSE VORTEX (CONVECTED VIEW)

BIBLIOGRAPHY

1. Bakewell, H. P. and J. L. Lumley, *Phys. Fluids*, 10, 1880 (1967).
2. Batchelor, G. K., "Theory of Homogeneous Turbulence," Cambridge University Press, Cambridge, 1967.
3. Blackwelder, R. F. and R. E. Kaplan, paper presented at AGARD Meeting on "Structure of Turbulent Shear Flows," London (1971).
4. Blackwelder, R. F. and L. S. G. Lovasznay, "Large Scale Motion of a Turbulent Boundary Layer with a Zero and a Favorable Pressure Gradient," Report DA-31-124-ARO-D-313. U.S. Army Research Office--Durham Box CM, Duke Station. Durham, N. Carolina 27706. July 1970.
5. Brodkey, R. S., "The Phenomena of Fluid Motions," Addison-Wesley, Reading, Massachusetts, 1967.
6. Brodkey, R. S., H. C. Hershey, and E. R. Corino, "An Experimental Facility for the Visual Study of Turbulent Flows," from "Turbulence Measurements in Liquids." (G. K. Patterson and J. L. Zakin, editors), p. 127. University of Missouri-Rolla, Department of Chemical Engineering Continuing Education Series, 1971.
7. Corino, E. R., Ph.D. thesis, The Ohio State University, (1965).
8. Corino, E. R. and R. S. Brodkey, *J. Fluid Mech.*, 37, 1 (1969).
9. Corrsin, S. and A. L. Kistler, NACA Report 1244 (1955); supersedes NACA TN 3133 and Wartime Report W-94 (1946).
10. Fiedler, H. and M. R. Head, *J. Fluid Mech.*, 25, 719 (1966).
11. Grant, H. L., *J. Fluid Mech.*, 4, 149 (1958).

12. Grass, A. J., J. Fluid Mech., 50, 2 (1971).
13. Gupta, A. K., J. Laufer, and R. E. Kaplan, J. Fluid Mech., 50, 493 (1971).
14. Hama, F. R., J. Aero Sci., 24, 236 (1957).
15. Hinze, J. O., "Turbulence," McGraw-Hill, New York, 1959.
16. Kaplan, R. E. and J. Laufer, "The Intermittently Turbulent Region of the Boundary Layer," University of Southern California, Department of Aerospace Engineering, Report USCAE 110, November 1968.
17. Kibens, V. and L. S. G. Kovaszny, "The Intermittent Region of a Turbulent Boundary Layer," Report DA-31-124-ARO-D-313. U.S. Army Research Office--Durham Box CM, Duke Station. Durham, N. Carolina 27706, January 1969.
18. Kim, H. T., S. J. Kline, and W. C. Reynolds, J. Fluid Mech., 50, 133 (1971).
19. Klebanoff, P. S., NACA Report 1247 (1955); Supersedes NACA TN 3178.
20. Kline, S. J., W. C. Reynolds, F. A. Schraub, and P. W. Rundstadler, J. Fluid Mech., 30, 741 (1967).
21. Kovaszny, L. S. G., "The Turbulent Boundary Layer," in "Annual Review of Fluid Mechanics," Volume 3, p. 95. Annual Reviews Inc., Palo Alto, California, 1970.
22. Kovaszny, L. S. G., V. Kibens and R. F. Blackwelder, J. Fluid Mech., 41, 283 (1970).
23. J. Laufer and M. A. B. Narayanan, Phys. Fluids, 14, 182 (1971).
24. Mollo-Christensen, E., AISS Journal, 9, 1217 (1971).
25. Narahari, R. K., R. Narasimha, and B.M.A. Narayanan, J. Fluid Mech., 48, 339 (1971).
26. Prandtl, L., Verhandlg. d. III, Intern. Mathe. Kongr., Heidelberg (1904); NACA TM 452 (1928) translation.

27. Rundstadler, P. W., S. J. Kline, and W. C. Reynolds, "An Experimental Investigation of the Flow Structure of the Turbulent Boundary Layer," Stanford University, Department of Mechanical Engineering, Report MD-8, 1963.
28. Sandborn, V. A., J. Fluid Mech., 6, 221 (1959).
29. Schlichting, H., "Boundary Layer Theory," McGraw-Hill, New York (1960).
30. Schraub, F. A. and S. J. Kline, "A Study of the Structure of the Turbulent Boundary Layer with and without Longitudinal Pressure Gradients," Stanford University, Department of Mechanical Engineering, Report MD-12, 1965.
31. Schubert, G. and G. M. Corcos, J. Fluid Mech., 29, 113 (1967).
32. Taylor, G. I., Proc. Roy. Soc. (London) 151A, 421 (1935).
33. Townsend, A. A., Australian J. Sci. Res., 1A, 161 (1948).
34. Townsend, A. A., Australian J. Sci. Res., 2A, 451 (1949).
35. Townsend, A. A., "Structure of Turbulent Shear Flow," Cambridge University Press, Cambridge, 1956.
36. Townsend, A. A., J. Fluid Mech., 26, 689 (1966).
37. Wallace, J. M., H. Eckelmann, and R. S. Brodkey, "The Wall Region in Turbulent Shear Flow," J. Fluid Mech., (in press).
38. Willmarth, W. W. and S. S. Lu, paper presented at AGARD Meeting on "Structure of Turbulent Shear Flows," London (1971).
39. Willmarth, W. W. and B. J. Tu, Phys. Fluids, 10, S134 (1967).